Master Thesis, Department of Geosciences

Composition and trace-element geochemistry of clays of the Upper Cretaceous to Paleogene Kilwa Group, Tanzania: A provenance study

Orhan Mahmic

UNIVERSITY OF OSLO

FACULTY OF MATHEMATICS AND NATURAL SCIENCES

Composition and trace-element geochemistry of clays of the Upper Cretaceous to Paleogene Kilwa Group, Tanzania: A provenance study

Orhan Mahmic

Master Thesis in Geosciences

Discipline: Geology

Department of Geosciences

Faculty of Mathematics and Natural Sciences

University of Oslo

June 2nd, 2014

ACKNOWLEDGMENTS

First and foremost I would like to express my deepest thanks to my supervisor, professor Henning Dypvik, at the Department of Geoscience, UiO. He has been supportive since the day I began working on this project, and has encouraged and shared his valuable time and knowledge through the rough road to finish this thesis. You have been a great inspiration to me since the first lecture in Gel2120. Asante!

My gratitude has to be addressed to co-supervisor Arild Andresen (UiO) for the interesting insights into the structural geology of the Mandawa Basin during the group meetings. PhD-student Katrine Fossum deserves big thanks for her support and company during the field trip and further more for her helpful assistance during my master thesis. I also want to thank everyone else who precipitated and made the field trip in Tanzania educational and safe.

I would like to thank Statoil ASA for founding this project and making it possible. I wish to extend my sincere gratitude to Erik Holter (Statoil Tanzania) for the welcome and help in Tanzania, and Mogens Ramm (Statoil International) for all the assistance in Oslo.

I owe particular thanks to Maarten Aerts (UiO), for helping me through the laboratory techniques and XRD interpretations. Thanks to Berit Løken Berg (UiO) for assisting me during electron microscope analysis. I also want to thank Lars Magne Kirksæter from the Petrological Service, who did an outstanding job on preparing the thin sections. Thanks to PhD-student Lars Riber for teaching Siroquant and valuable inputs about clay minerals, Erik Zakariassen for making the geological maps for the Mandawa Basin Project, and Imran Ali for helping with the proofreading.

I would like to give a special gratitude to Ray Ferrell (Louisiana State University) for his inspiring lectures about clay mineralogy and saving me of getting lost in the endless labyrinth of clay minerals. Thanks to Christopher J. Nicholas (Trinity College) for informative lecture about the Mandawa Basin and the helpful discussions.

This master thesis would not have been as enjoyable and fun without the company of Kristine Nerbråten and Ellen Gundersveen. Thank you for all the support and the cheerful moments during our field trip to Tanzania and thereafter.

My dearest appreciation goes to my family, especially to my sister Irma for all the love, patience, and for always being supportive. Thank you for being there.

ABSTRACT

The abundance of specific clay minerals have been used to reconstruct the origin of the Kilwa Group clays, and to determine the relative changes in diagenesis, weathering and climate conditions. Late Cretaceous to Early Oligocene fine-grained sediments from the Kilwa Group in southern coastal Tanzania have been analysed. The Kilwa Group is composed of four formations; the Nagurukuru, Kivinje, Masoko and Pande Formations. This study comprises detailed petrographical, mineralogical (thin section, XRD and SEM) and geochemical (trace and REE) analyses to infer the nature of the adjacent source rocks and provide insight regarding to the depositional environment. Two main lithologies were observed in the Kilwa Group, calcareous rich marine-clays are dominant, and limestones.

The Kilwa Group clays variation variations in the clay mineral assemblages, which were based on abundant changes of nine clay minerals determined by fitting simulated with experimental diffraction patterns. The deposition of these clays took place across a passive margin, in a mid to outer shelf environment, with periodically influx of shallow shelf detritus transported by density currents. The broadly homogeneous appearance of the Kilwa Group clays indicate that the sediments were repeatedly homogenized before the final deposition. The uppermost Pande Formation, however, reflects a shift from deep- to more shallow-marine facies compare to the underlying formations. This could be attributed by a substantial regional uplift or eustatic sea level drop during Early Oligocene.

The trace element data of the Kilwa Group clays were compared with North American Shale Composite (NASC), Post Archean average Australian shales (PAAS), and the upper continental crust (UCC). Chondrite normalized REE patterns are comparable to the UCC, and indicate a felsic average provenance and a relatively severe weathering regime. Various dicrimination diagrams and ratios revealed minor contribution from mafic volcanic rocks. However, these signals may have been smoothed by transitional storage before the final deposition.

The XRD-bulk and trace elements results of the four Statoil offshore clay samples (Cenomanian and Paleocene) were compared with Kilwa Groups clays of same age, and the data suggest comparable depositional conditions and source areas.

CONTENTS

1. INTRODUCTION

The Mandawa Basin is located in southern coastal Tanzania as part of a mainly stable African plate (Figure 1.1). In the recent years, an international research team, the Tanzania Drilling Project (TDP), have undertaken many shallow land borings of the Upper Cretaceous-Paleogene sediments in the coastal zones. The goal was to get a better understanding of the complex geological history by studying stratigraphy, micropaleontology and paleoclimate (e.g. Person et al., 2004; Person et al., 2006; Nicholas et al., 2006; Jeménez Berrocoso et al., 2010). The paleoclimate studies were especially emphasized due to the excellent preserved microfossils in the area.

In terms of hydrocarbon potential, Tanzania has gained increased economic interest lately, especially in the offshore regions. The recent discoveries (Block 2) by BG, Statoil and co-venture ExxonMobil, highlights offshore Tanzania as an emerging world-class petroleum provenance. How these prospective reservoirs reflects in the onshore Mandawa Basin will be of major interest during this and other studies ahead.

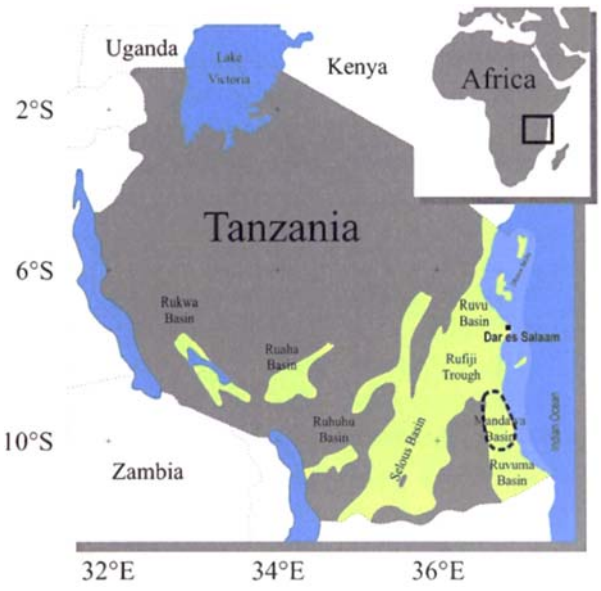

Figure 1.1 *- Map showing the location of the Mandawa basin in Tanzania. Green color represents the sedimentary basins and the grey color represents the metamorphic and igneous rocks. From Hudson, (2011).*

This thesis is part of a larger international research project funded by Statoil. Project chairman and main supervisor for this thesis is Prof. Henning Dypvik (UiO). The Mandawa Basin Project (MBP) further consists of co-supervisor Prof. Arild Andresen (UiO), five master students and two PhDs from Norway and Tanzania. The aim of the MBP is to better understand the history and the evolution of the Mandawa Basin, from break up of Gondwana to Eocene deposits. These studies will discuss various properties of main stratigraphic formations, as e.g. depositional environment, reservoir quality, diagenetic changes and sediment transportation from source to sink.

No reference on detailed trace element geochemistry and clay fraction (< 2 μm) mineral assemblage exist of the Kilwa Group clays (Late Cretaceous – Early Oligocene). Sedimentological and trace element geochemical analysis of the Kilwa Group clays are compiled to identify and characterize possible processes effecting the deposition of the clays.

The specific objectives of this thesis are:

i. Study the stratigraphical variations in the XRD-determined abundances of major clay-mineral groups and mixed-layered clays. The aim is to shed light on relative contributions of weathering and source rock changes to the origin of the clay minerals in the Kilwa Group clays.

ii. Study the distribution and concentrations of trace elements to deduce signatures of provenance and depositional environment, and to compare these signatures to Statoil offshore clay samples.

iii. Establish the possible source of the Kilwa Group clays.

The results presented in this master's thesis are based on sedimentological analyses of the core logs, different mineralogical (XRD, thin sections, SEM) and trace-element geochemical analyses. Clay samples from Statoil Block 2, approximately 80 km off the coast of Tanzania in the offshore region were also compared with onshore samples (Fig. 1.2).

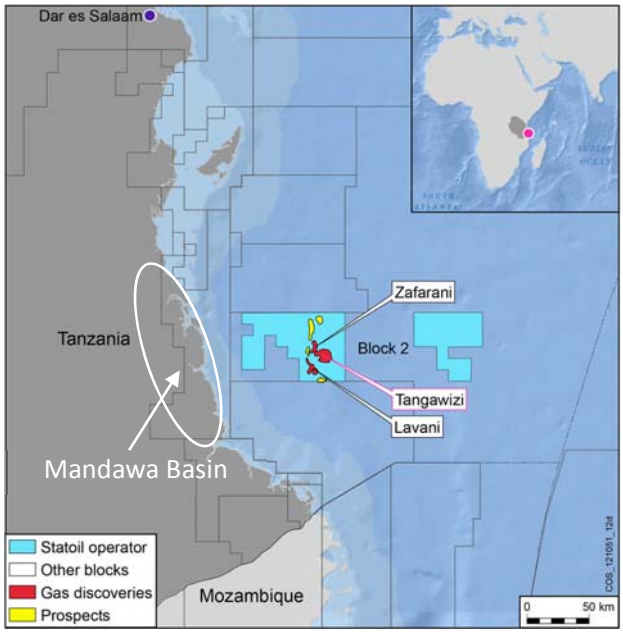

Figure 1.2 *– Map showing the location of the Statoil Block 2 off the coast of Tanzania. From Statoil (2014).*

2. REGIONAL SETTING

This chapter presents the tectonic development of the Mandawa Basin and the lithostratigraphical setting of the Kilwa Group located with this basin. The Mandawa Basin represents one of four different basins types recognized in Tanzania; the coastal basins (i.e. Mandawa Basin), the Karoo rift basins, East African Rift valley and the cratonic sag basins (Mbede, 1991) (Fig. 2.1). The coastal basin of Tanzania is located along the passive continental margins of the western Indian Ocean, and is characterized by an extensional style (Mpanda, 1997).

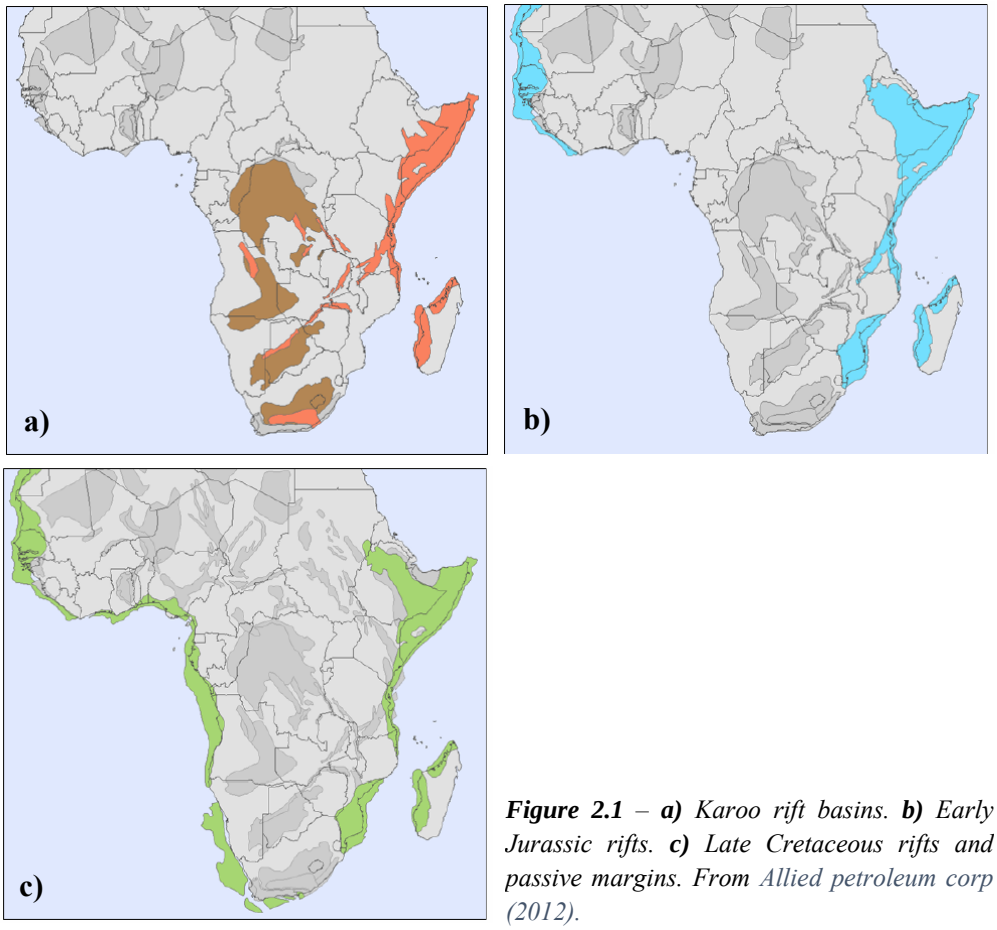

Figure 2.1 *– **a)** Karoo rift basins. **b)** Early Jurassic rifts. **c)** Late Cretaceous rifts and passive margins. From Allied petroleum corp (2012).*

2.1. GEOLOGICAL SETTING

The geological history of the Mandawa Basin has its roots back when the initial rifting (i.e. late-Gondwana stage) of Gondwana Supercontinent was initiated in Permian and ended 157 Ma. The deposits from that period are recognized as the Karoo Group (Salman and Abdula, 1995). The post-Gondwana rifting phase took place from 157 Ma to recent, and is marked by the break-up of

Gondwana, separating it into eastern (Africa) and western blocks (India and Madagascar) (Salman and Abdula, 1995). In Early Jurassic, rift basins formed along what is now the Indian Ocean margin of Africa (e.g. the coastal Mandawa Basin of Tanzania). During Late Jurassic major dextral strike-slip movement took place, and Madagascar and India rifted away from Africa along the David Ridge transform zone (Fig. 2.1.1a). During mid-Cretaceous the rifting jumped east if Madagascar. Due to this shift of tectonic activity away from East Africa, a passive-margin in the Tanzanian coastal region developed with deposition of thick sedimentary packages (Jiménez Berrocoso et al., 2010). A major transgression accompanied the quiet period which lasted from Late Cretaceous to Early Miocene, dominated by thick outer shelf marine clays (Fig. 2.1.1b). This was a period of uniform subsidence across margin. During the post-Miocene period, Mandawa Basin has undergone compression and strike-slip deformation, with high-angle reverse faults, thrusts and 'pop-up' structures (Nicholas et al., 2007).

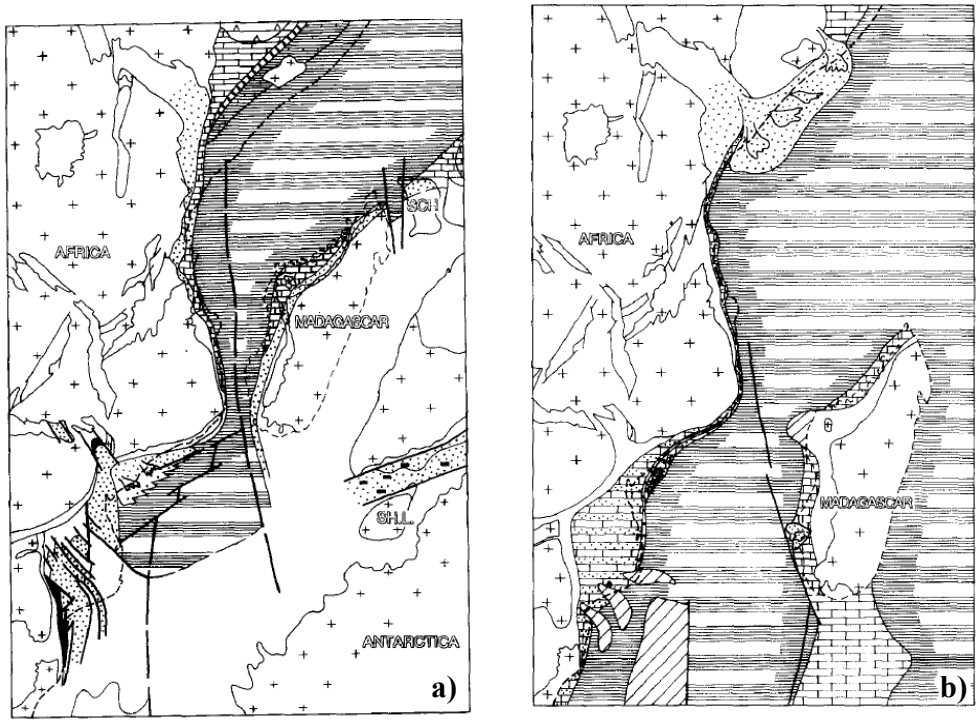

Figure 2.1.1 *– **a)** Post-Gondwana stage 157-118 Ma. Drifting of Madagascar and India away from East Africa **b)** The quite period (65-35 Ma) with deposition of the Kilwa Group in the coastal Tanzania (From Salman and Abdula (1995)).*

Provenances

The geology of Tanzania is dominated by the ancient Archean cratonic shield and metamorphosed Proterozoic systems (Fig. 2.1.2). The Archean rocks in Tanzania consists of Archean Tanzania

Craton, Dodoma complex, greenstone belt, and some small areas of anorthosite. The craton in the central part of Tanzania consists generally of granitic complexes. Gneisses, schists, magmatites, intrusive ultramafic to felsic rocks are also present in this central plateau. The Dodoma System (Fig. 2.1.2) occurs as an elongated belt trending WNW. The system comprises of metasediments and metavolcanics (Kilimajaro Mining Company, 2008). This system also contains intrusive mafic and felsic rocks.

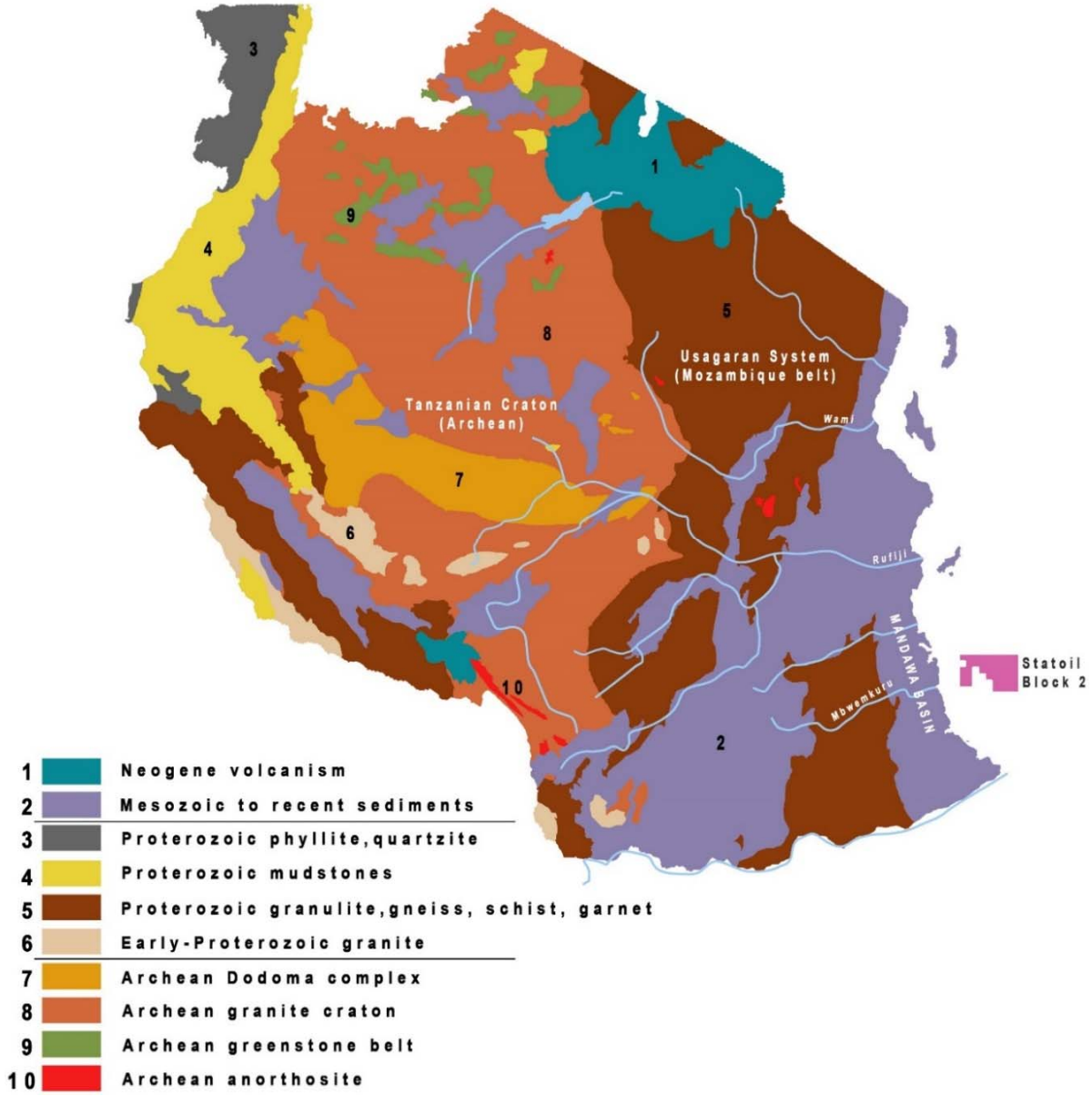

Figure 2.1.2 *– Geological map of Tanzania. Modified from Geological Map of Tanzania.*

The Proterozoic rocks are identified as ancient orogenic belts, e.g. Usagaran System. The Usagaran System comprises of sedimentary, metamorphosed gneisses and volcanics rocks (Schlüter and Hampton, 1997; Hudson, 2011). Masjority of exposed Usagaran System surrounds the Tanzanian craton to the east (Mozambique Belt), but is also exposed west of Mandawa Basin (Masasi basement spur). These older complexes were subsequently rifted to produce Karoo and younger sedimentary basins, such as the Mandawa Basin. The Lower Jurassic to Quaternary alternating continental and marine sedimentary rocks dominate the coastal area of Tanzania. For more information about the Karoo and pre-Paleocene sedimentary deposits in the Mandawa Basin, see Fossum (2012), Nerbråten (2014) and Gundersveen, (2014).

2.2. LITHOSTRATEGRAPHICAL SETTING OF THE KILWA GROUP

Outer shelf deposits dominate the Kilwa Group of the Mandawa Basin, dominated by homogenous clays from Late Cretaceous to Early Oligocene. Nicholas et al. (2006) divided the Kilwa Group into four formations, the Nangurukuru, the Kivinje, the Masoko and Pande formation (Fig. 2.2.1). The base of this (about ~1 km) thick clay succession, lies disconformably on Albian marls (Fig. 2.2.2). On which the top of the group is possibly unconformably covered by shallow marine Miocene clays (Nicholas et al., 2006, Hudson, 2011) (Figure 2.2.1). The base of the Kilwa Group displays an increase of clay-dominated lithologies compared to the older lithologies, reflecting the transgressive trend (Nicholas et al., 2006). The Paleogene deposition took place generally during steady subsidence along the passive margin (Hudson, 2011).

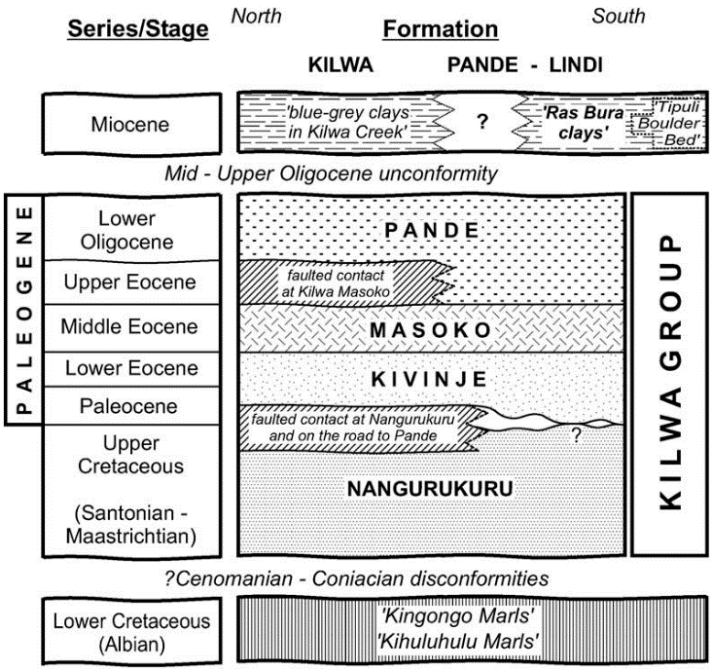

Figure 2.2.1 *- Stratigraphy scheme of costal Mandawa, Kilwa and Lindi area. From Nicholas et al. (2006).*

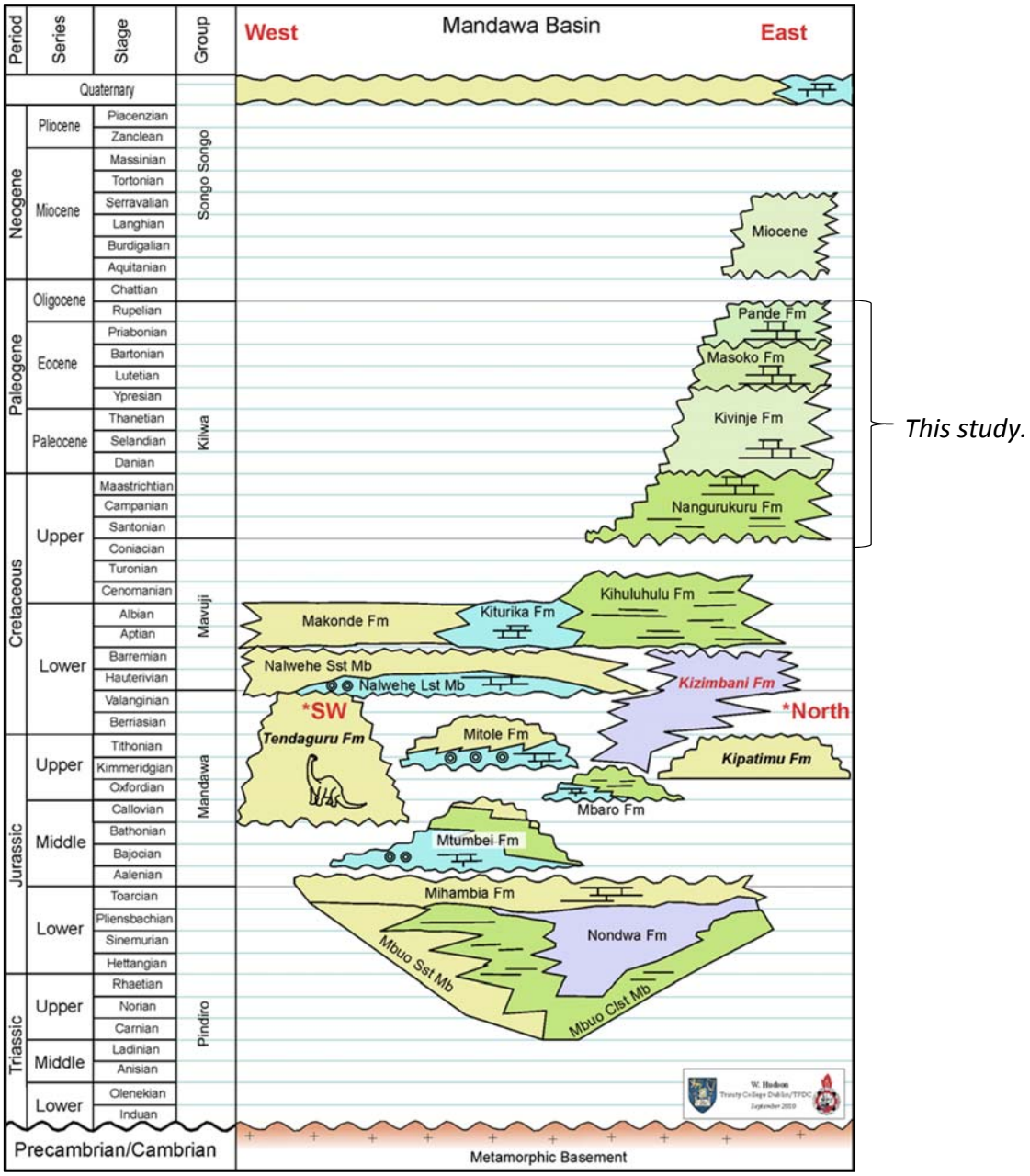

Figure 2.2.2 *– Lithostratigraphical scheme for the Mandawa Basin (from Hudson, 2011).*

The Nangurukuru Formation

Green-grey clays are the dominant lithologies of the Nangurukuru Formation. These clays lies disconformably across the shelf on top of Albian marls. The clays are interbedded with thin turbiditic, hard, carbonate-cemented fine to coarse sandstones (Nicholas et al., 2006, Hudson, 2011). These thin sandstone units show high level of bioturbation in their upper parts, with different

sole marks at their base. The trace fossils found at the base of these sandstones represents the Nereites ichnofacies, as suggested by Nicholas et al. (2006). These same thin 'Nereites sandstones' are found by Pearson et al. (2006) in TDP 9 (Fig. 4.1.2). Pyrite nodules are found in the clay sections of the formation. Inoceremid beds (Nicholas et al., 2006) define the top marker horizon of the formation.

The Kivinje Formation

The Kivinje Formation exhibit two kind of lithologies; a more silty clay in the lower two thirds of the core, and a greenish-clay with fine quartz sandy partings in the upper on third of the core (Figure 5.1.1). The fine to very fine sandy partings, with occasionally cross-lamination, can range from a few mm and up to 10 cm. The base of the formation is composed of large benthic foraminiferal limestones (i.e. slump breccia) as described by Nicholas et al. (2006). Lower Paleocene has not yet been recovered in the Kilwa Group. The surface between Nagurukuru and Kivinje formation could therefore represent an unconformity across the shelf area. The dipping of the laminated beds can indicate a fault present (Hudson, 2011). Comparable dips of laminated beds from Paleocene - lower Eocene was found by Pearson et al. (2004) at TDP 3 (Fig. 4.1.2). One characteristic that is distinct for the Kivinje Fm. is the fibrous calcite veining ('beef') (Fig. 5.1.1).

The Masoko Formation

The light olive grey clay sediments of the Masoko Fm. show a softer nature than the underlying two formations, with dispersed calcite giving the clays a 'sugary' texture (Pearson et al., 2006). The main distinguishing lithology of this formation is the sparry calcite cemented limestone beds enriched in large Nummulites. The rounded quartz grains present in the fine carbonate matrix of the limestone beds decrease in number towards the top, displaying normal grading (Pearson et al., 2006). Both Nicholas et al. (2006) and Pearson et al. (2006) recognized two of these limestone horizons, with rip-up clay clasts and some cross-lamination at the top of the beds.

The Pande Formation

The clays and claystones of the Pande Formation shows a darker shade of green than the underlying formations. Quartz partings in the upper section are found throughout the clays with thin carbonate cement beds. The occurrence of creamy micritic limestone is considered by Nicholas et al. (2006) to be a very good marker for recognizing the Pande Fm. in the field. The limestone beds often contain clay rip-up clasts (up to 5 cm) and occasionally balls of micrite. There is also evidence of normal grading in some of the limestone beds. In the upper part of the formation (i.e. lower Oligocene), plant debris and benthic foraminifera are abundant, especially shallow-marine species (Pearson et al., 2006).

3. CLAY MINERALS

Clay minerals refer to a larger class of silicates within the phyllosilicates. These consist predominately of oxygen, silicon, aluminum, magnesium, iron or hydroxyl (OH), with different cations in the structure (Chamley, 1989). The grain size of clay minerals is often very small, normally less than 0.002 mm in diameter.

The phyllosilicates have large specific surface area compared to their thickness. These layers consists of alternating sheets of SiO_4 tetrahedra (T) and octahedral (O) (Fig. 3.1). Two main types of layers are recognized;

- The *1:1 layer* (T.O.), which consists of one tetrahedral and one octahedral sheet, e.g. kaolinite (Fig. 3.1.1).
- The *2:1 layer* (T.O.T.), where two tetrahedra sheet are bonded to one octahedral sheet, e.g. illite and the smectite group.

The latter is often referred to as swelling clays, since they may swell up from 14 - 17 Å due to wetting.

The chlorite family is the exception to this. It has one extra octahedral layer (brucite-like layer), giving it a 2:1:1 (T.O.T.O.) structure (14 Å) (Figure 3.1).

The interlayer site (i.e. the space between two layers), may contain different cations (e.g. K, Na, Mg, Ca) if the successive layers have a negative charge (Fig. 3.1). The ionic bonding between the

two successive layers are much weaker compared to the bonding of tetrahedral and octahedral layers. This makes the minerals cleaves easily along this plane. The thickness of the different clay minerals is a sum of a layer plus the interlayer. For example, mica has 2:1 structure + interlayer, which gives it a basic repeat distance near the 10 Å value (Fig. 3.1).

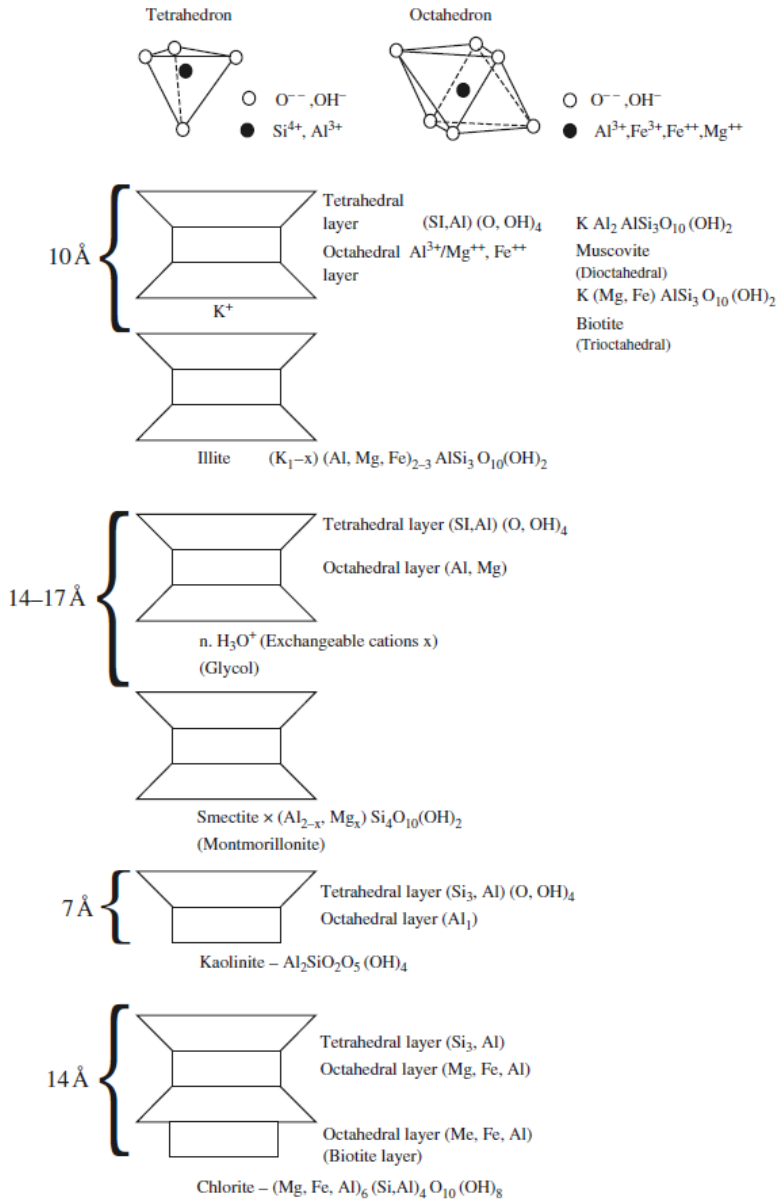

Figure 3.1 *- Illustration of the different clay minerals structures together with interlayers. (From Bjørlykke, 2010).*

4. METHODS AND MATERIAL

4.1. CORE LOGGING

The logging of cores TDP 1, 2 and 7B was carried out in September 2013, from 18.09-24.09, in Tanzania at TDP storage facility. The work was done in a group of three students; Ellen Gundersveen, Kristine Nerbråten and the author, under the supervision of Professor Henning Dypvik (UiO). The cores TDP 9, 21 and 24 was logged by PhD students, Katrine Fossum (UiO) and Justina Saroni (UDSM) during the same period.

Each core box contains three pieces of core with length of one meter each (Figure 4.1.1). Many of the cores were not complete, in some places even whole sections were missing. Each box was carefully opened, measured and visually inspected before the logging started. The sections were logged on standard logging sheets (Appendix 1) in scale of 1:50.

Figure 4.1.1 *- Example of a core box containing three core sections. The bottom section (3) is statigraphically deeper then section 1.*

Samples collected for XRD, lithology, thin section and geochemical analyses where brought back to UiO. A total of 79 samples were collected, each were ca. 1 cm thick section of the core. The sample identifiers are referring to the site, core number, and section number. E.g., TDP2/19/1, 50.20 – 50.21 cm indicates TDP site 2 in core 19, section 1 at 50.20 – 50.21 m from bottom of the deepest core in the well. The location of TDP well sites is shown in Figure 4.1.2.

In this thesis, the samples have been renamed. For example, TDP2/19/1, 50.20 – 50.21 m is renamed to c2_50.20. See Figure 5.1.1 and 5.1.2 for overview over the logs and sample sites.

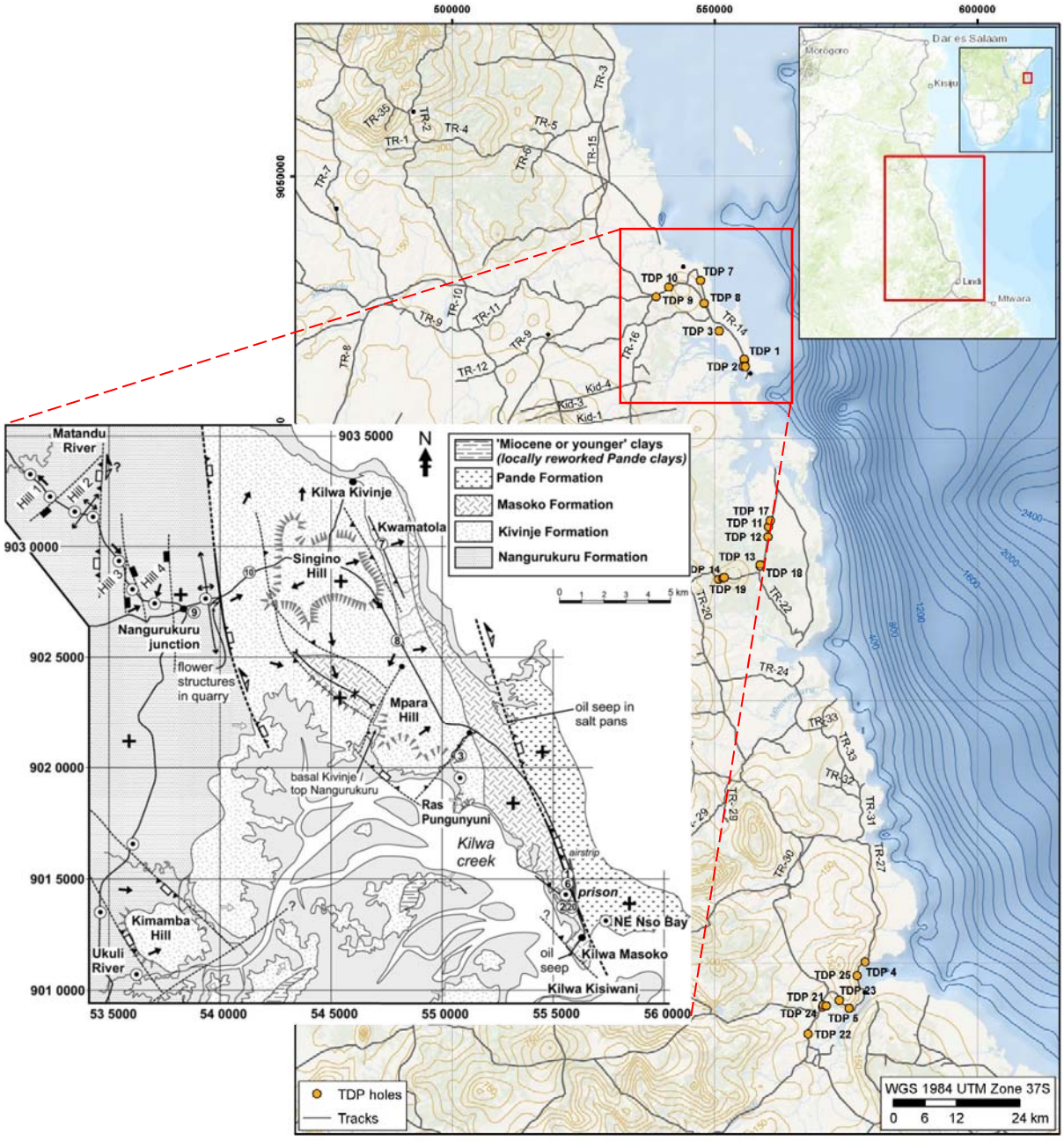

Figure 4.1.2 *– Map of localities of TDP wells (Modified by Zakariassen (2014) from ESRI (2014)). In this study cores from wells TDP 1, 2, 7B and 9 have been studied. The simplified geological map of the Kilwa peninsula from Nicholas et al., 2006.*

4.2. FACIES DESCRIPTION AND FACIES ASSOCIATIONS

In this thesis, the Wentworth grain-size classification (Wentworth, 1922) will be used (Table 4.3.1). Shales are defined as rocks with more than 50 percent grain size less than 0.062 mm. The shales can be further divided into siltstone or claystone based on the percentage of clay-size constituents; ***Claystone*** (66-100% clay-size constituents), ***Siltstone*** (< 33% clay-size constituents) (Boggs, 2006).

Definition of the sedimentary facies is based on lithology, texture and structures from core logs, thin sections analyses and photos. The respective facies are then grouped together in facies associations, reflecting a specific depositional environment.

Table 4.3.1 - *Wentworth (1922) grain-size classification scale of terrigenous sediments.*

Millimeters (mm)	Micrometers (μm)	Phi (ϕ)	Wentworth size class		Rock type
4096		-12.0	Boulder	Gravel	Conglomerate/ Breccia
256		-8.0	Cobble		
64		-6.0	Pebble		
4		-2.0	Granule		
2.00		-1.0	Very coarse sand	Sand	Sandstone
1.00		0.0	Coarse sand		
1/2 0.50	500	1.0	Medium sand		
1/4 0.25	250	2.0	Fine sand		
1/8 0.125	125	3.0	Very fine sand		
1/16 0.0625	63	4.0	Coarse silt	Silt	Siltstone
1/32 0.031	31	5.0	Medium silt		
1/64 0.0156	15.6	6.0	Fine silt		
1/128 0.0078	7.8	7.0	Very fine silt		
1/256 0.0039	3.9	8.0			
0.00006	0.06	14.0	Clay	Mud	Claystone

4.4. MINERALOGICAL AND PETROGRAPHICAL ANALYSES

The mineralogical and petrographical analyses has been performed by using different approaches, such as thin section observations, scanning electron microscope (SEM) and X-ray diffractometry (XRD) analysis. The used laboratory techniques and petrological analysis were conducted under the guidance and supervision of Prof. Henning Dypvik, Head Engineer Maarten Aerts (XRD and sediment laboratory), Senior Engineer Berit Løken Berg (SEM), and P.hd student Katrine Fossum (UiO).

Thin sections

Lars Magne Kirksæter at the Petrological Section Service (Petro-Sec) prepared the thin sections of selected samples. The rocks were impregnated in blue epoxy before they were glued onto 2.5 cm x 4.5 cm glass plates and polished down to 30 µm.

Detailed observations of the thin sections were performed on 13 samples (see Table 5.3.1). A *Nikon Labophot-Pol* petrographical microscope has been used for the analysis. The optical analysis has been conducted to yield textural, sorting, qualitative and quantitative information of the coarser (i.e. silt to sandstone) parts of the formations. All samples have been studied under plain polarized light (ppl) for distinguishing mineral characteristics, e.g. relief and pleochroism. Cross polarized light (xpl) was used for the observation of zoning, twinning and the degree of feldspar weathering (Figure 4.4.1).

Category	1	2	3	4	5
Description	Fresh, has not been subjected to weathering	Show some evidence of weathering, but twins are almost fully preserved	Intermediate. Twins start to look blurry and grain surfaces show roughness	Very rough surface. Twinning might be hard to recognize	Twins are absent or bearly identified. Hard to identify plagiocalse from microcline. Grain surfaces show extensive dissolution and has extreme rough surface.
Example	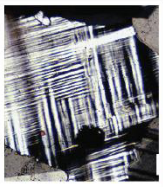	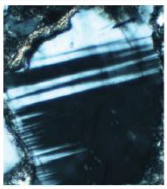		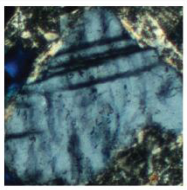	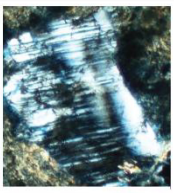

Figure 4.4.1 – *Feldspar weathering/ preservation based on categories 1-5. Figure from Fossum (2012).*

4.5. X-RAY DIFFRACTION ANALYSIS (XRD)

The X-ray diffractometry (XRD) was executed to gain qualitative and quantitative information over the bulk mineralogical composition. The qualitative peak interpretation was carried out with help of *Bruker* software EVA.

Bulk XRD Analysis

Maarten Aerts carried out 53 bulk XRD analysis at the Department of Geoscience at UiO. The selected samples were quickly crushed to rock powder by the author with help of a swing mill for about 2 min to a size of 1-2 mm. The same moment of torsion (40Nm) was used on every sample. Due to the hardness of some samples, they had to be crushed two to three times longer. The powderized fraction was then divided into two parts; one part was used for bulk XRD and the other for future clay separation and trace-elements analysis.

To achieve an average particle size of < 10 μm, approximately 3 g of the powderized sampled for bulk XRD was further powderized by McCrone micronizer. The sample was added to a plastic container with small agate cylinders. 7 ml of ethanol was added before the sample was grounded for 10 min. The finished micronized sample was then transferred to a plastic cup and left to dry overnight in an oven at 50^{o}C.

The dry micronized samples were placed in plastic holders for XRD analysis. The data was collected on a *Bruker* D8 Advance, equipped With Lynxeye linear PSD detector, 2 kW Cu anode X-ray tube, operated at 40 kV and 40mA variable divergence slit, sample length 15mm Ni Kbeta filter 2.5 degrees soller slits (both primary and secondary), and sample rotation at 30 RPM.

The detection limit is on the order of 1-2% in multiphase geological mixtures. However, this may be much lower for certain cases, since the detection limit is of a phase in a multi-mixture is highly dependent on the mixture itself. For example, a tiny amount of quartz in an otherwise pure calcite powder will have a much lower detection limit than, for example, a tiny amount of pyrite in a very clay-rich and partly amorphous sample with 10+ phases. Longer counting time will also increase the intensity of the different phases, separating small peaks from the background noise.

Qualitative Analysis of Bulk XRD

The qualitative analysis of the bulk XRD-samples was done using the analytical *Bruker* software EVA. Mineral identification was estimated by reading the distinct peak position based of utilized d-spacing (Table 4.5.1) in the diffractograms (Fig. 4.5.2). The search and match function in the Eva software was also utilized for the minor mineral phases.

Table 4.5.1 *- The peak positions of d-values utilized for the qualitative analysis of the bulk XRD samples.*

Mineral	d-value (Å)	Reflection
Quartz	4.25	001
Plagioclase	3.19	003
K-feldspar	3.24	003
Calcite	3.04	001
Dolomite	2.89	001
Siderite	2.79	001
Pyrite	2.71	001
Ilmenite	2.75	001
Illite and biotite	10	001
Kaolinite	3.58	002
Gypsum	7.56	001
Mixed layer	10-13	001
Chlorite/smectite	14	001

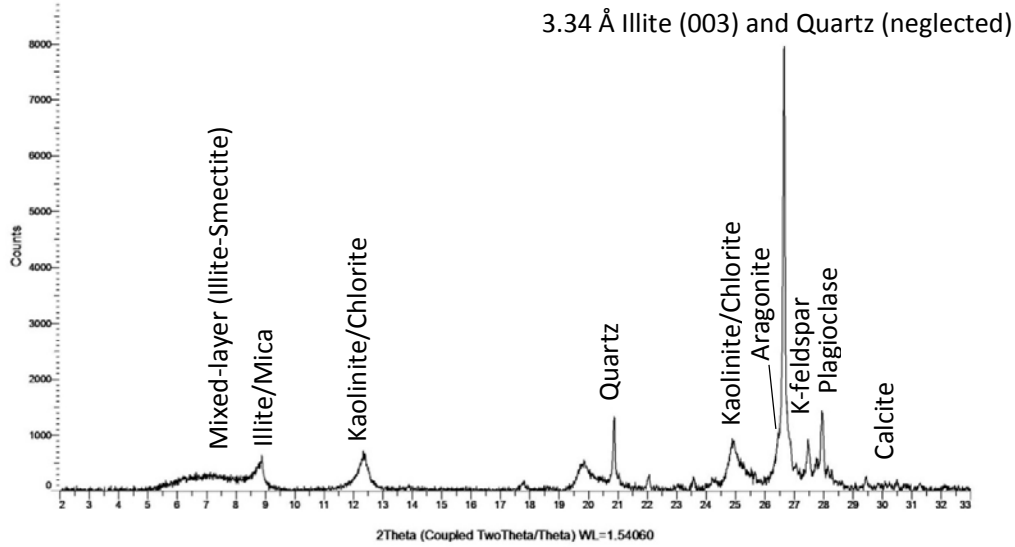

Figure 4.5.2 *– Example XRD curve with primary constituents illustrated according to their d-value position. The 060-positions are not illustrated, due to the main emphasis on the range between 0º2θ-30º2θ.*

Semi-Quantitative Analysis of Bulk XRD

The semi-quantitative analysis was done using the software EVA as before. Maximum peak intensities for the different minerals was used after <Peak search> command was utilized. This gave counts values of the peaks in the diffractograms. The approximated values of the different minerals were later used as a guideline for the quantitative analysis.

Quantitative Analysis of Bulk XRD

The quantification of crystalline components was performed using Siroquant v4 software on the same XRD samples as for the semi-quantification analysis. This was done in order to get a fully quantitative representation (Rietveld method) of the different minerals in samples. The Chi Squared value, which the program calculates, should be as low as possible (< 6) to get most accurate results. It is important to note that chi values should only be considered as a guide, and not base the results on it alone. At the end, the visual inspection is most important, i.e. where the experimental diffractograms matches the theoretical diffractograms as best as possible.

For some of the clay samples from the Pande Formation, the quantification could not be done. This was either be due to incorrectly sample preparation before XRD run, or that the sample contained some minerals which was not correctly identified by the software.

4.6. CLAY FRACTION (< 2 µm) SEPARATION

For the clay fraction analysis, 24 samples were separated. The separation was done in two stages;

Stage 1 – Separation by gravity*:* Samples were crushed in the swing mill to a size of 1-2 mm. Approximately 3-5 g of sample were then suspended in ca. 350 ml distilled water mixed with sodium carbonate Na_2CO_3 (0.125g x l^{-1}) to prevent flocculation. The suspended sample mixture inside laboratory beaker went through disaggregation for 10 min in VWR Ultrasonic Bath. This was done to accelerate the dispersion of the clay particles. After the ultrasonic treatment, the suspended material was transferred to cylindrical beakers, which were filled with approximately 1.2 L with the same mixture of distilled water and sodium carbonate. This was then left for 24 hours. For separating the clay fraction from the coarser siliciclastic material at the bottom of the cylinder, a hose was injected into the cylinder and the upper 30 cm (1 L) of the clay suspended

material was filled into laboratory beakers for preservation. The remaining coarser material was thrown away.

Stage 2 – Millipore filter: The clay fraction (< 2 mm) was run through a Millipore filter by using the Millipore vacuum technique. After filtering the material was flushed with 1M Magnesium-Chlorite ($MgCl_2$) to induce cation exchange. The sample was then inverted onto round Pyrex glass platform and placed in aluminum holders for future analysis in the Bruker D8 XRD instrument. All the samples went through four different treatments:

1. The samples were left to air dry in rom temperature for 12 hours before they were analyzed.
2. After the air dried samples have been processed, they were placed in a glass exsiccator, filled with ethylene glycol at the bottom and put in oven for 12 hours at 60^{o}C. This treatment was done in order to detect swelling clays, e.g. smectite. When treated, the smectite will expand from 14 Å (air-dry) to ~17 Å in ethylene glycol.
3. Samples were heated to 350^{o}C in an oven for about 2 hours in order to destroy the smectite lattice and remove the diffraction pattern at ~17 Å.
4. The last step is heating the sample to 550^{o}C. This treatment, as well as the 350^{o}C, is irreversible. This was done to detect kaolinite, since it will become amorphous at this temperature and its diffraction pattern disappears (Moore and Reynolds, 1997).

Qualitative and Semi-Quantitative Analysis of Clay Fraction

In this study, five main principal clay minerals groups were identified: illite, smectite, kaolinite, chlorite and mixed-layer clays based on their X-ray diffraction maximum, called “peaks”. The identification of the mineral groups was done by methods described in (Biscaye, 1965, Moore and Reynolds, 1997). The qualitative analysis of the XRD clay fraction has been performed by the aid of the *Bruker* software EVA. Decomposition of the different peaks was done using Topas software to get a better understanding of the broad peaks, which guided the modeling process in NEWMOD for quantification of clay samples.

NEWMOD v.2.3 by Robert C. Reynolds, jr. and Robert C. Reynolds III was utilized for the semi-quantification of the clay portion of the samples. The software was used to simulate XRD models from a wide range of patterns both for single and mixed-layered clay minerals. The calculated patterns are very helpful when it comes to estimating the composition of the clay minerals. The limiting factor of the software is the amount of models possible to have (eight) at a given time. This give challenges fitting the simulated with experimental diffraction pattern. Another challenge is the influence of non-clay minerals in the samples, e.g. quartz and calcite, which can result in problems fitting the simulated XRD pattern accurately at higher 2-theta (Fig. 4.6.1). Thickness of the sample is also important. Too thin sample be disturbed by the amorphous glass influence in the diffractograms (Fig. 4.6.1).The parameters used in the simulation procedure to produce the synthetic pattern in NEWMOD (Figure 4.6.1 – yellow line) included; octahedral sheet Fe and K content, interlayer cations, stacking sequence and crystallite size distribution. The determined Fe

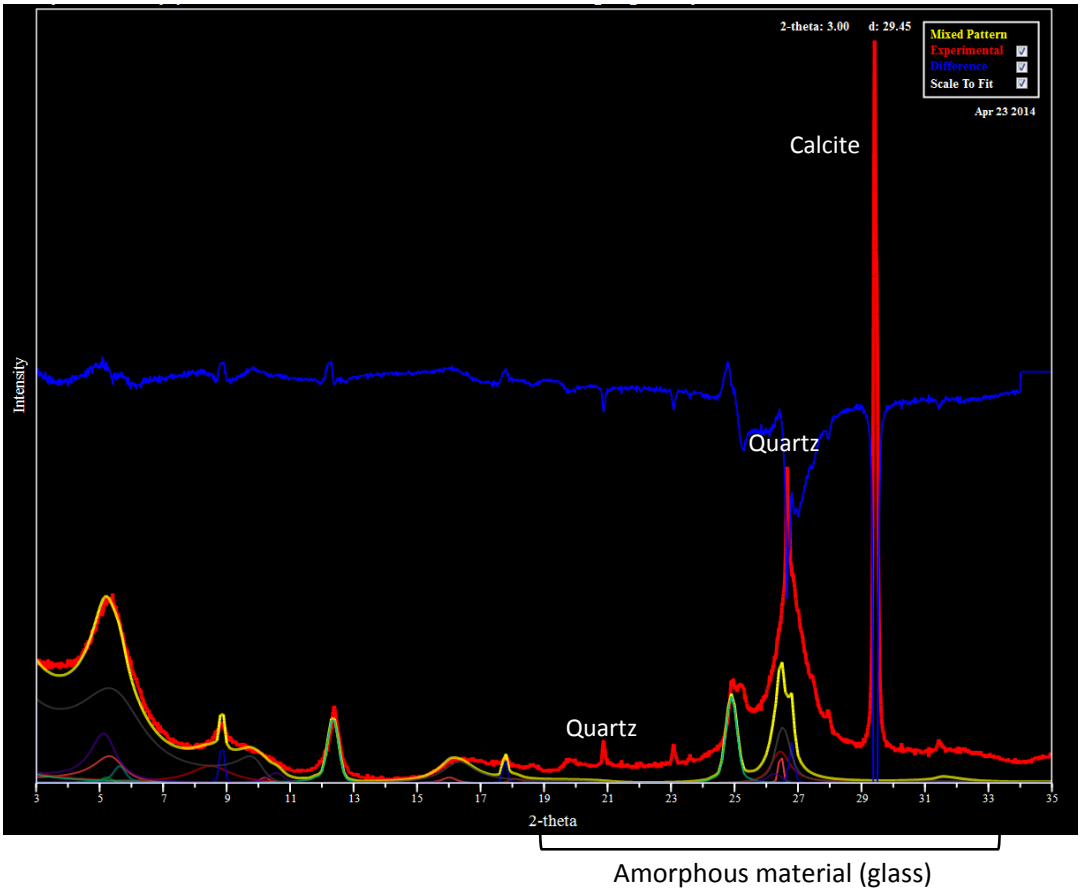

Figure 4.6.1 *– Figure showing an example of the EG-experimental (red line) and simulated (yellow line) diffractogram pattern in NEWMOD. The other colored lines are the different models used to produce the final theoretical diffractogram. The figure also illustrates the problems associated with non-clay minerals and amorphous material influencing the final result, which is shown in the difference line (blue).*

and K content in smectite (dioctahedral) and illite (dioctahedral) was by trial and error, with 0 - 1.7 Fe or K atoms in the octahedral sheet. All patterns were normalized to quartz intensity of 6000 counts.

4.7. GEOCHEMICAL ANALYSES

Twenty-eight crushed clay samples from Kilwa Group, and four clay samples from Statoil Block 2, were send to Activation Laboratories Ltd., Ancaster, Ontario, Canada, for trace-element geochemical analysis. The *Ultratrace 3 - Total Digestion - ICP and ICP/MS, INAA* method was used on approximately 1.3 g sample. The results are given in parts per million (ppm).

Rock-Eval analysis was also performed on eigsht samples (Appendix 7) to see if there is any drastically change in the TOC content. Robertson Geolab Nor AS, Trondheim, Norway, carried out the Rock-Eval analysis. For more results of the TOC in Pande (TDP 1) and Kivinje Formation (TDP 7B), see e.g. Pearson et al. (2004, 2006).

4.8. RAMAN SPECTROSCOPY

Raman spectroscopy is an inelastic light scattering technique used to observe vibrations, rotational, and other low frequency modes in a molecular system. Inelastic light means that the frequency of photons in monochromatic light changes upon interaction with a sample (Mukherjee, 2013). Typically, the technique involves shining a monochromatic light source or a laser beam, in the frequency range of visible, infrared or near-ultraviolet region and detecting the scattered light. Frequency of the reemitted photons in the sample is shifted up or down in comparison with original monochromatic frequency, which is called the Raman effect.

The purpose of utilizing this technique was to get information about the chemical and structural composition of the Kilwa Group clays, (e.g. differentiate the different clay minerals). Senior Engineer Niels Højmark Andersen at the Department of Chemistry, University of Oslo, tested two sample on Raman system. Both of samples produced very weak Raman signals due to high bioluminescence, i.e. high carbonate content in the samples.

5. RESULTS

5.1 FACIES DESCRIPTION

Table 5.1.1 – *The sedimentary facies of the Kilwa Group, as observed in cores, thin sections and pictures.*

Facies nr	Facies	Grain size	Description	Present in well	Figures
i-a	Claystone	Clay to silt	V.f. qtz sand partings (calcite cemented). Large benthic forams frequent. Burrows are rare to uncommon. Plant material and shell fragments. Usually reacts to HCl. May be well laminated. Fibrous calcite may also be present.	TDP 9, 7B, 2 and 1	Fig.5.1.3
i-b	Silty calcareous clay	Clay to silt	Same as i-a, but the lithology is slightly more silty.	TDP 7B (lower two thirds) TDP 9	Fig.5.1.3
ii	Clayey siltstone	Clay to silt	Reacts to HCl. Calcite cement in sandy partings. Large benthic forams present. Plant material. Some sand filled burrows. "Beef" veins may be present.	TDP 7B	Fig.5.1.1
iii	Highly fossiliferous, calcarenites	Medium / fine sand	Medium to fine sand with calcite cement. Reacts to HCl. Muddy partings may be evident. Fossiliferous, with plant and shell fragments throughout.	TDP 1	Fig.5.1.6
iv	Limestone (Calcarenite)	Medium to very coarse sand	Large fossil fragments (1-2 mm). Poorly sorted. Clay rip-up clasts may be present. Mixed with carbonate grains. Fining upwards sequences, with cross-lamination. Clay clasts evident.	TDP 7B TDP 2	Fig.5.1.4
v	Slump breccia	Very coarse sand	Matrix supported (light grey). Poorly sorted. Matrix consists of *Nummulites*, shell fragments and calcite cement. Breccia with 1-5 cm fragments, clay rip-up clasts and some pyrite nodules.	TDP 7B	Fig.5.1.4
vi	Fining upwards fine to medium qtz sand	Clay to medium sand	Dispersed fine to medium qtz sand in clay. Upwards fining units. Possible normal grading at some places. Parallel lamination. Sands grains are angular and dispersed in clay. Bioturbation is absent. Very low calcareous content.	TDP 1	Fig.5.1.6
vii	Silt to fine qtz sand horizons	Silt to fine sand	Thin cm size horizons within clay. Reacts to HCl. Soft sediment deformation structures are found.	TDP 1	Fig.5.1.6
viii	Clay with interbedded sandstone beds	Clay to fine sand	Sandstone beds with sharp bounding surface. Highly bioturbated. Flutes, grooves and prod marks at base. Nereites ichnofacies trace fossils.	TDP 9	Fig.5.1.5

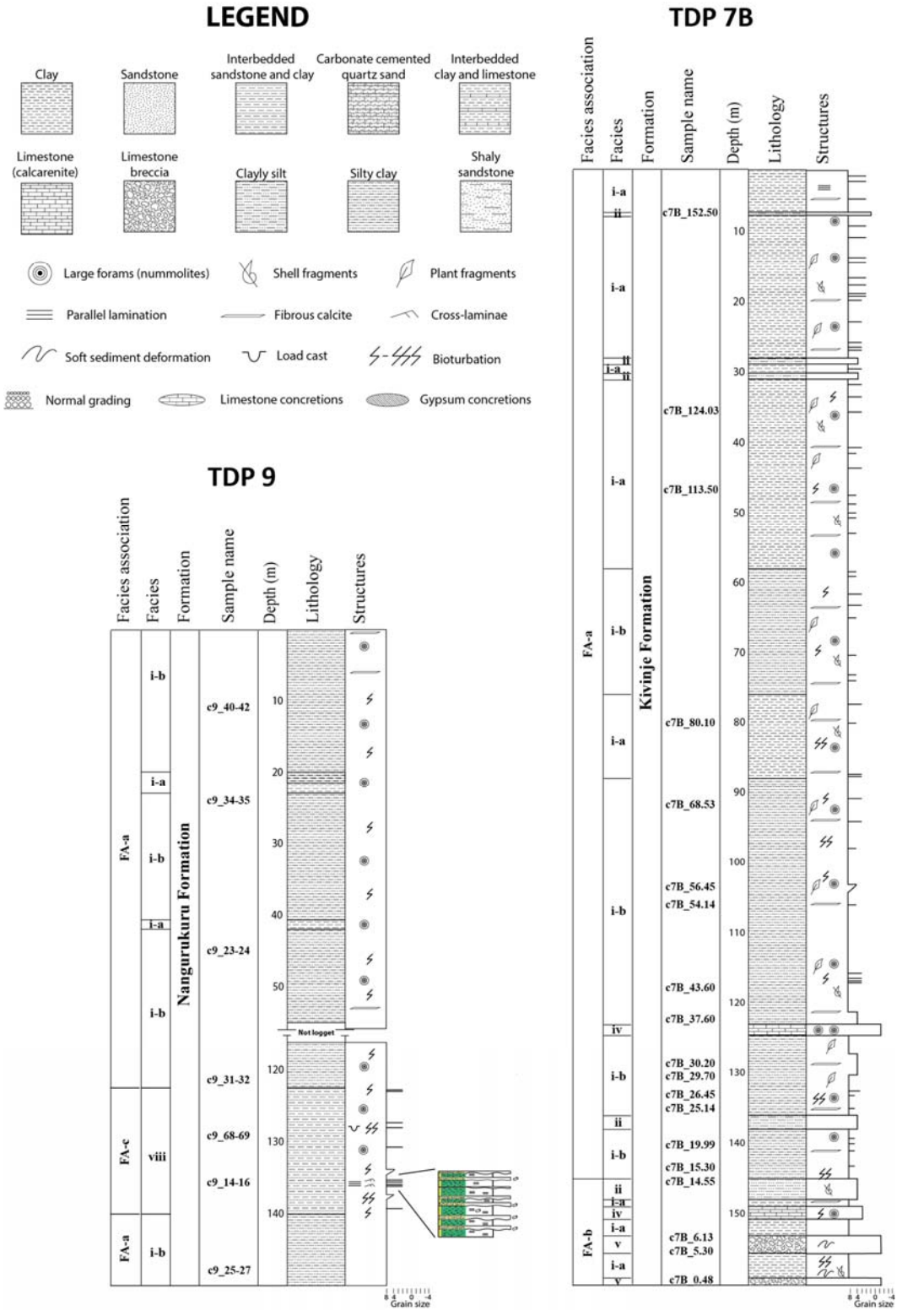

Figure 5.1.1 *– Facies and facies association of the Nangurukuru (TDP 9) and Kivinje (TDP 7B) formations. Nangurukuru Formation was logged by Katrine Fossum (UiO) and Justina Saroni (UDSM). Modified later by the author. The close up section in the lower part of the TDP 9 core, are the individual 'Nereites sandstone' layers with sharp boundaries. For borehole location, see map (Fig 4.1.2).*

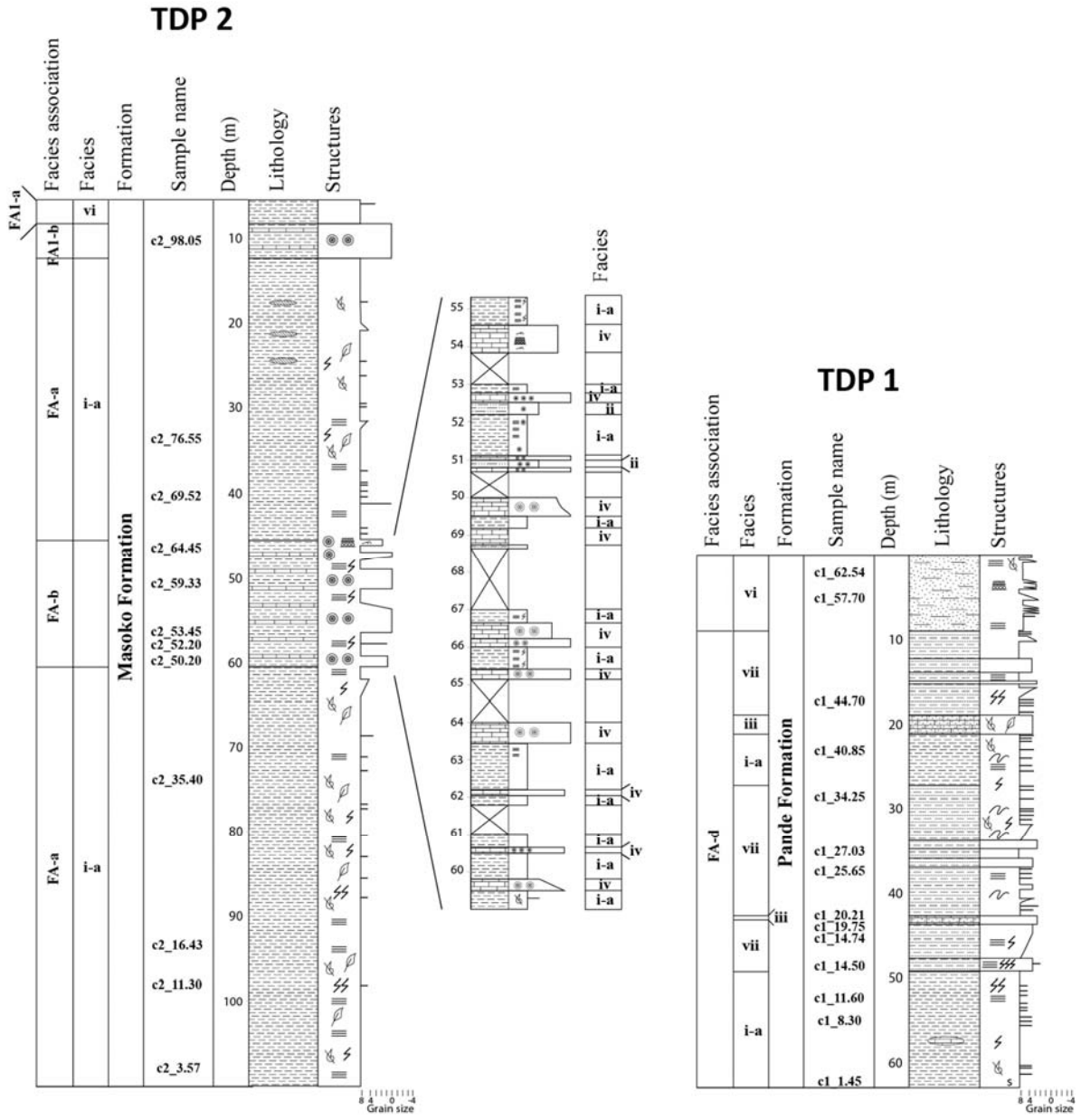

Figure 5.1.2 *– Facies and facies association of the Masoko (TDP 2) and Pande (TDP 1) Formation. A more detailed view of FA-b in Masoko Formation is shown to the right. For borehole location, see map (Fig 4.1.2)*

i.

a) **Claystone:** This facies is present in all the four formations. It contains very fine sand partings, which are usually calcite cemented. Calcite is also present in the clays as a combination of carbonate grains, including foraminifers and calcareous nannofossils, and reacts to HCl. Burrows are uncommon to rare. Small pieces of terrestrial plant material and shell fragments are present. In some sections, the clay can show well lamination. In core TDP 7B fibrous calcite is frequent in the clays (Fig. 5.1.1).

b) **Silty claystone:** Same as facies i-a, but the lithology is slightly more silty. This facies is present in TDP 9 and in the lower two thirds of core TDP 7B (Fig. 5.1.1).

ii. **Clayey siltstone:** This facies is only present in the lower one third of the core TDP 7B. Large benthic forams and plant material are often present in this dark greenish clayey siltstone. Some burrows are present, usually filled with either sand or pyrite. Sandy partings with calcite cements is also found in these clayey siltstones.

iii. **Highly fossiliferous calcarenites:** Two highly fossiliferous calcarenites horizon are found in TDP 1 (Fig. 5.1.2). It consists of medium to fine sand with calcite cements. Reacts vigorously to HCl. Terrestrial plant and shell fragments occur throughout these two units.

iv. **Limestone (calcarenite):** This facies is found in TDP 7B and TDP 2 (Fig. 5.1.1 and 5.1.2). This light grey fossiliferous limestone contains large amount of fossils and fossils fragments. Rip-up clay clasts occur in some places, consisting of dark greenish gray clay (Fig. 5.1.4b). These limestone beds are poorly sorted and highly cemented by sparry calcite. In some of these beds, cross-lamination and fining upwards sequences was found (Fig. 5.1.4a).

v. **Slump breccia**: This facies is only present at the bottom of the core TDP 7B (Fig. 5.1.1). Poorly sorted matrix supported breccia, with fragments ranging from 1-5 cm in size (5.1.4e). The color of matrix is light gray and medium light gray. It contains *Nummulites* and re-texturized shell fragments. Evidence of rip-up clasts and pyrite nodules.

vi. **Fining upwards fine to medium quartz sand:** Facies vi is present in the upper 10 m within Pande Formation (Fig. 5.1.2). It is characterized by dispersed fine to medium quartz sand in clay, lacks bioturbation and calcareous microfossils, and frequent upwards fining units. Possible crude normal grading at some places. Parallel lamination is also found (Fig. 5.1.6a).

vii. **Silt to fine quartz sand horizons:** Thin cm size quartz sand horizons within the clays are present in Pande Formation (Fig. 5.1.2). These thin sandstone units contain carbonate grains which reacts to HCl. Soft sediments structures can also occur in this facies (Fig. 5.1.6c).

viii. **Clay with interbedded sandstone beds:** 10-50 cm thick sandstone beds with sharp bounding surface, intensely grazed tops and Nereites ichnofacies trace fossils characterize this facies (Fig. 5.1.5). Bioturbation is moderate to high. Facies viii is found in lower part of core TDP 9 (Fig. 5.1.1).

5.2 FACIES ASSOCIATION

Facies Association 'a' (FA-a): These claystones (Figure 5.1.1 and 5.1.2), are present throughout the whole Kilwa Group and generally laminated, with occasional small burrows (i-a and b). The claystones usually contains dispersed granular carbonate, which reacts to HCl. Throughout the clay units, thin fine-grained sandy partings occur frequently. Relative to the benthic forams, planktonic forams are very common, which gives generally high P:B ratios (Pearson et al. 2004, 2006; Nicholas et al. 2006). Pyrite was observed in both the cores and XRD. Plant-, shell fragments and large foraminifers are frequent. FA-a is present in Nangurukuru, Kivinje and Masoko formations (Fig. 5.1.1 and 5.1.2).

Facies Association 'b' (FA-b): This facies association is composed of clay (facies i-a) with interbedded sparry calcite cemented beds containing large *Nummolites* (facies iv) and limestone breccia (facies v). Clay rip-up clasts, crude normal grading and cross-lamination is present in some of the limestone beds (Fig. 5.1.4). Parallel lamination can be seen in the clay units. FA-b is present in Kivinje and Masoko formation (Fig. 5.1.1 and 5.1.2).

Facies Association 'c' (FA-c): Facies association FA-c is composed of silty claystone interbedded with thin quartz-rich sandstones (facies viii). The sandstone beds show evidence of erosional base and ripples marks at the top. These sandstones are generally highly bioturbated. Nereites ichnofacies trace fossils are present (Fig. 5.1.5). FA-c is assigned to the lower portion of the Nangurukuru formation (Fig. 5.1.2).

Figure 5.1.3 – FA-a marine clays. **a)** Clay with what looks like a fragment of a coral. From Kivinje Formation (TDP 7B at ~83 m) **b)** Fibrous calcite "beef" in the clays, from Kivinje Formation at ca. 65 m. **c)** Facies i-b from core TDP 7B at ~96 m. **d)** *Nummulites* in the clay, TDP 7B at ~8 m. **e)** The bluish color of the shell fragment may possible be aragonite from Masoko Formation (TDP 2 at ~38 m). **f and g)** In picture f, the clays are from the upper one third of TDP2 with gypsum concretions, and picture g shows the clays from (~65-68 m) (Fig.5.1.2). Note the difference in color, where the lower is more grayish.

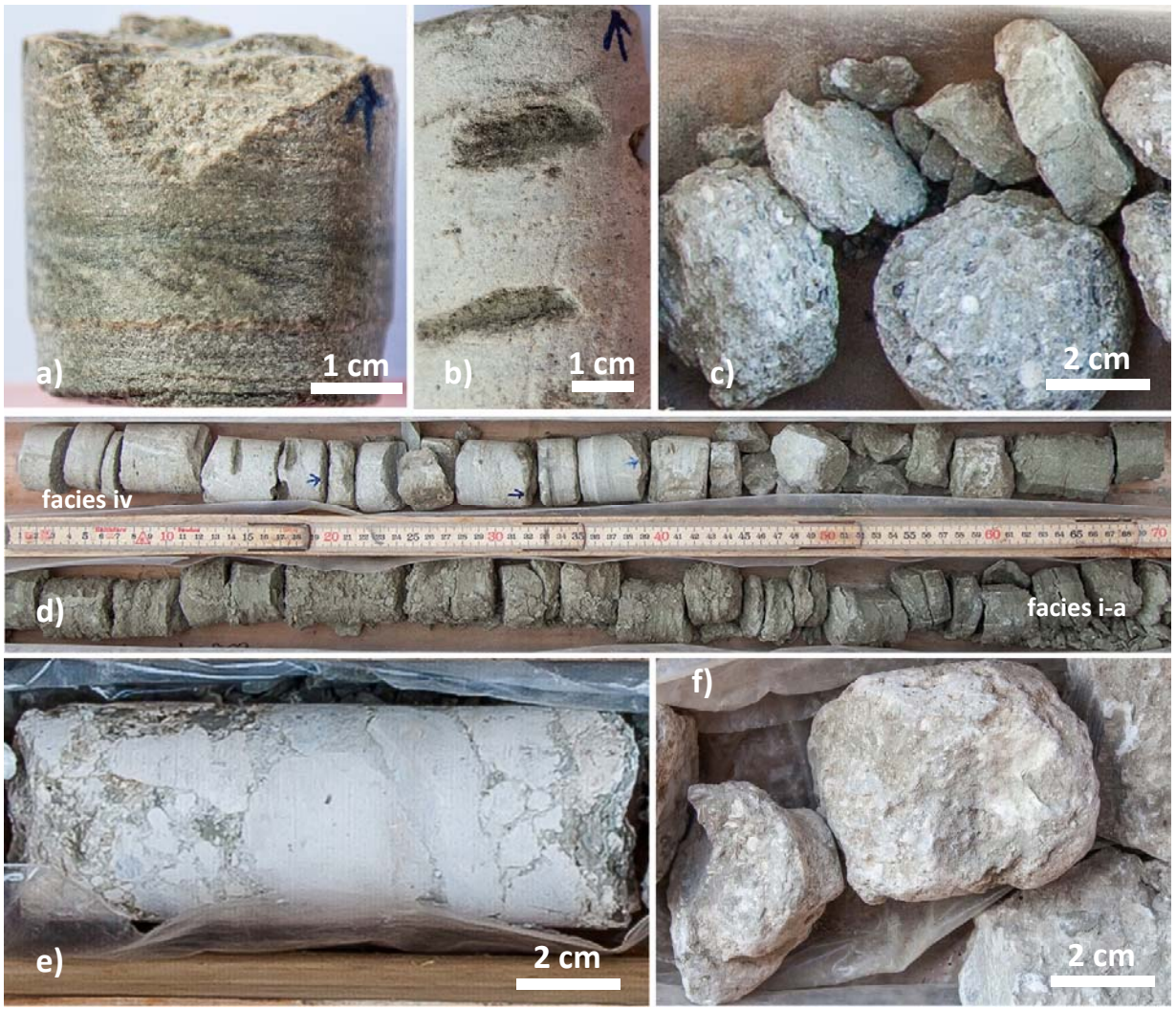

Figure 5.1.4 *– Pictures showing facies FA-b in Masoko (TDP 2) and Kivinje formation (TDP 7B) (Fig.5.1.1 and 5.1.2).* ***a)*** *Parallel- and cross-lamination. Upwards fining sequences from Masoko Formation at 46m* ***b)*** *Clay clasts found in TDP 2 at ca. 46 m.* ***c)*** *Large fossil fragments in core TDP 2 at ~54 m.* ***d)*** *In the upper part the facies iv is present, while in the lower part the facies i-a is shown (from TDP 2 at 44-46 m).* ***e)*** *Slump breccia at the bottom of TDP 7B (Fig. 5.1.1). The fragments consists of benthic foraminiferal limestone.* ***f)*** *Large benthic fossils in core TDP 7B at ~159 m (Fig. 5.1.1).*

Facies Association 'd' (FA-d): Facies association FA-d is composed of clays with fine quartz sand grains dispersed throughout (i-a and vii). Fine lamination is frequent. Calcareous microfossil and benthic forams are abundant, but bioturbation is rare. Highly fossiliferous, two calcarenites horizon with plant fragments and shell hash (coquina) is observed (facies iii). Soft sediment deformation, siderite bands and limestone concretions are also present. The FA-d is present in Pande Formation (Fig. 5.1.6).

Figure 5.1.5 *– FA-c in the lower part of the Nangurukuru Formation (TDP 9).* ***a and b)*** *Nereites ichnofacies at ~130m.* ***c and d)*** *Sharp (uneven, wavy) boundary between the thin cemented, sandstone beds and clay at ~135 m (Fig. 5.1.2).*

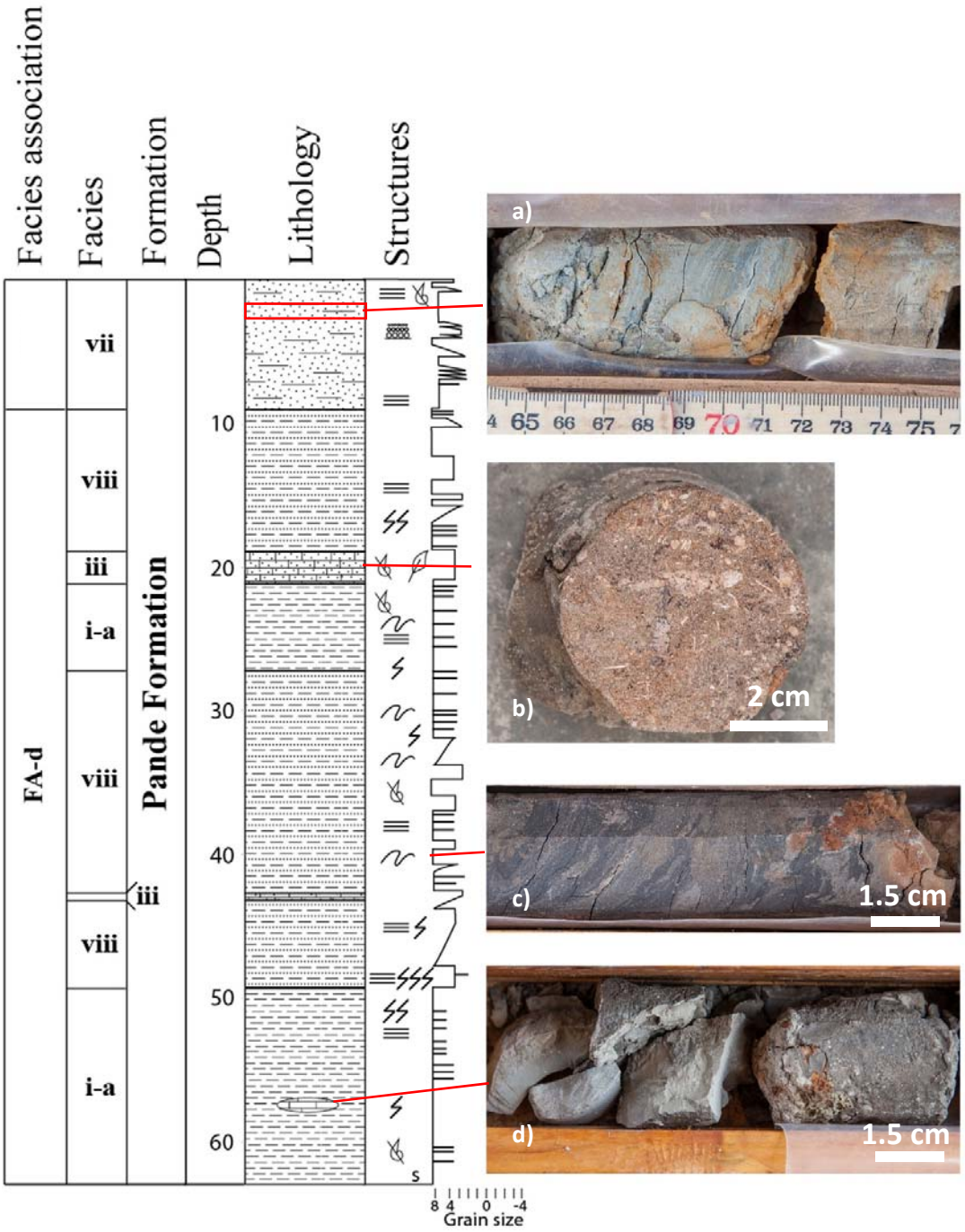

Figure 5.1.6 *– Facies and facies association of the Pande Formation (TDP 1).* ***a)*** *Lamination in clay.* ***b)*** *Coquina* ***c)*** *Soft-sediment deformation* ***d)*** *Limestone concretion.*

5.3 MINERALOGICAL AND PETROGRAPHICAL DESCRIPTION

The results presented in this chapter are based on thin sections, SEM and quantitative result of the XRD-bulk analyses. The petrographical analysis of the Kilwa Group presented here, were conducted to obtain mineral compositions of the sediment samples. For more detail on some of the thin sections, e.g. heavy-minerals and grain coatings of the Kilwa Group samples, see Nerbråten, (2014) and Gundersveen, (2014).

5.3.1. XRD-bulk results and thin sections

Nangurukuru Formation (Upper Cretaceous) –TDP 9

The lower most formation of the Kilwa Group, the Nangurukuru Formation, consists dominantly of dark greenish gray silty claystone (Fig. 5.1.1). The quantified XRD-bulk observation of the eight samples are shown in figure 5.3.1. Calcite is present in all the samples ~10-35%, with small amount of aragonite 3-5%. Ratio between plagioclase and K-feldspar show little variation throughout the samples, with an average ratio of 0.59. This indicates that the samples are slightly more enriched in plagioclase than K-feldspar (Fig. 5.3.2). Quartz/feldspar ratios yield an average of 0.45 (Fig. 5.3.1). The upper most sample, c9_40-42, show increase in feldspar content compared to the rest of the samples.

Major components of the samples are clay minerals and sheet silicates, which are estimated to about 50-60% of the total sample. Quantitative observation of samples c9_14-16 and c9_90-92, reveled higher abundance of quartz and feldspar compared to clays, 95% and 65% respectively (Fig. 5.3.1).

Thin sections

Thin section of three samples from the Nangurukuru Formation revealed two of the samples were poorly sorted siltstone and sandstone (c9_31-32 and c9_90-92), while the third sample was moderate sorted (Table 5.3.1). The grain size ranged from 49 – 88 µm. Felsic compartments show highest abundance of monocrystalline quartz, with small fraction of polycrystalline (< 2 %).

Plagioclase has highest abundance in sample c9_14-16, which is also found in XRD analysis (Fig. 5.3.1). The feldspar showed some degree of weathering alteration (1-3) (Fig. 4.4.1). Calcite, in form of cement, was recognized by its extremely high birefringence color of a higher order xpl. This carbonate cement might indicate post-depositional diagenetic precipitation.

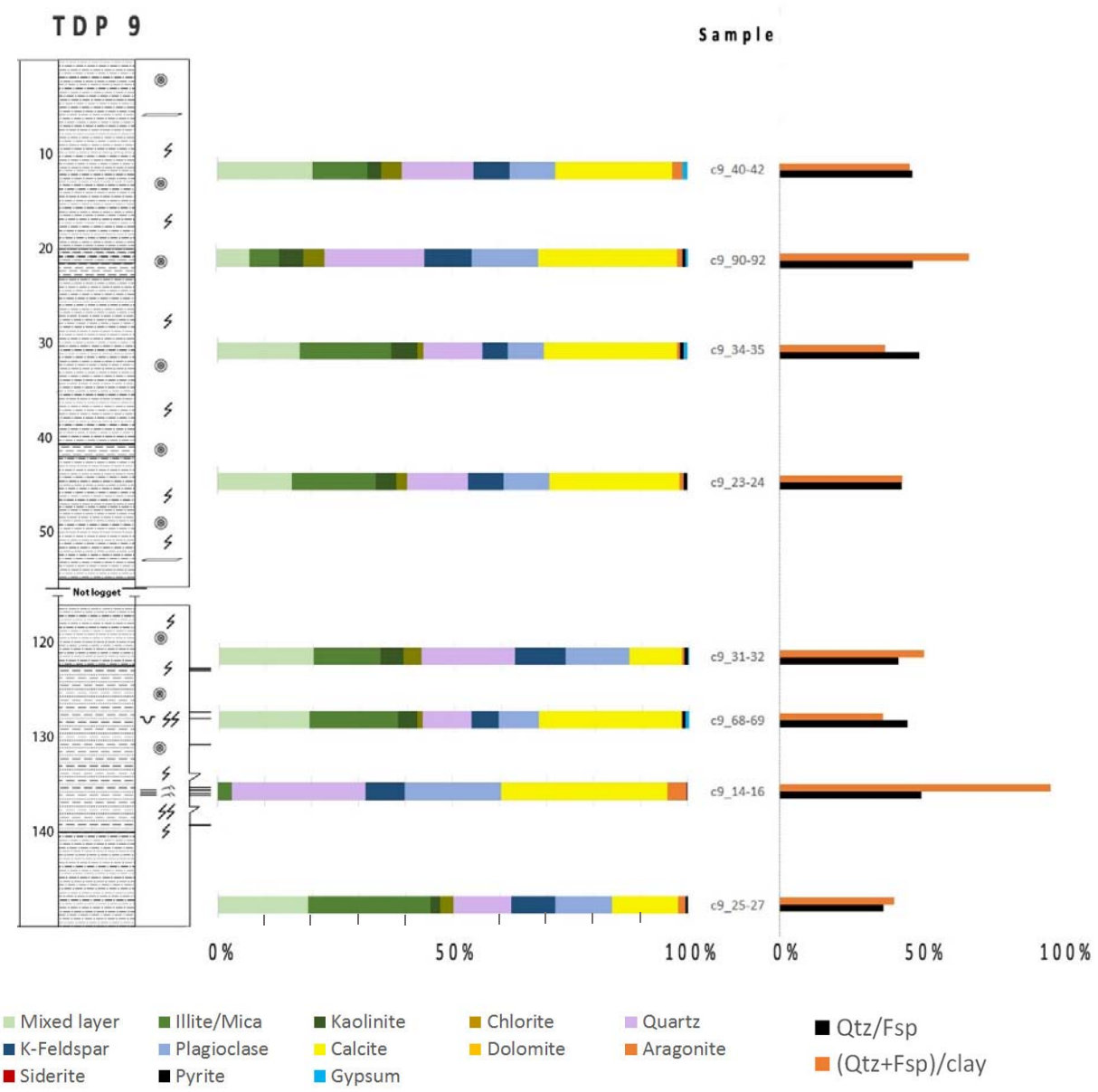

Figure 5.3.1 *– Quantified XRD results of the eight Nangurukuru Formation samples. Q/(Q+F)*100 (black lines) and (Q+F)/((Q+F)+clay)*100 (orange lines) ratios are shown on the right.*

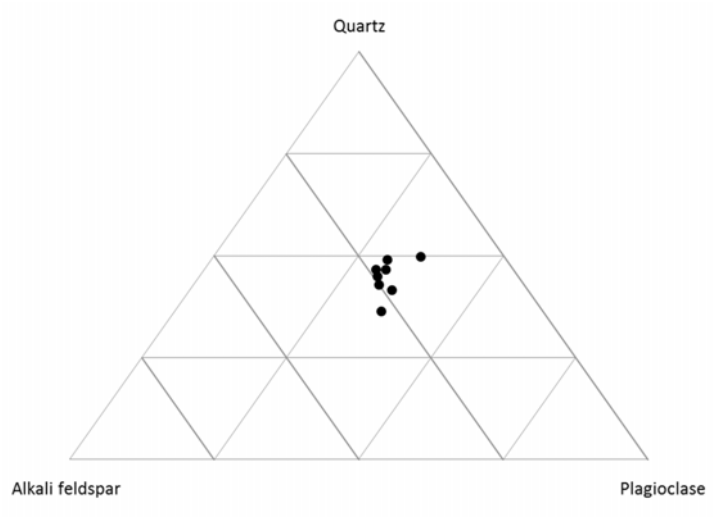

Figure 5.3.2 *– QAF (quartz-alkali feldspar-potassium feldspar) plot that shows ratio between quartz, alkali feldspar and plagioclase in Nangurukuru Formation.*

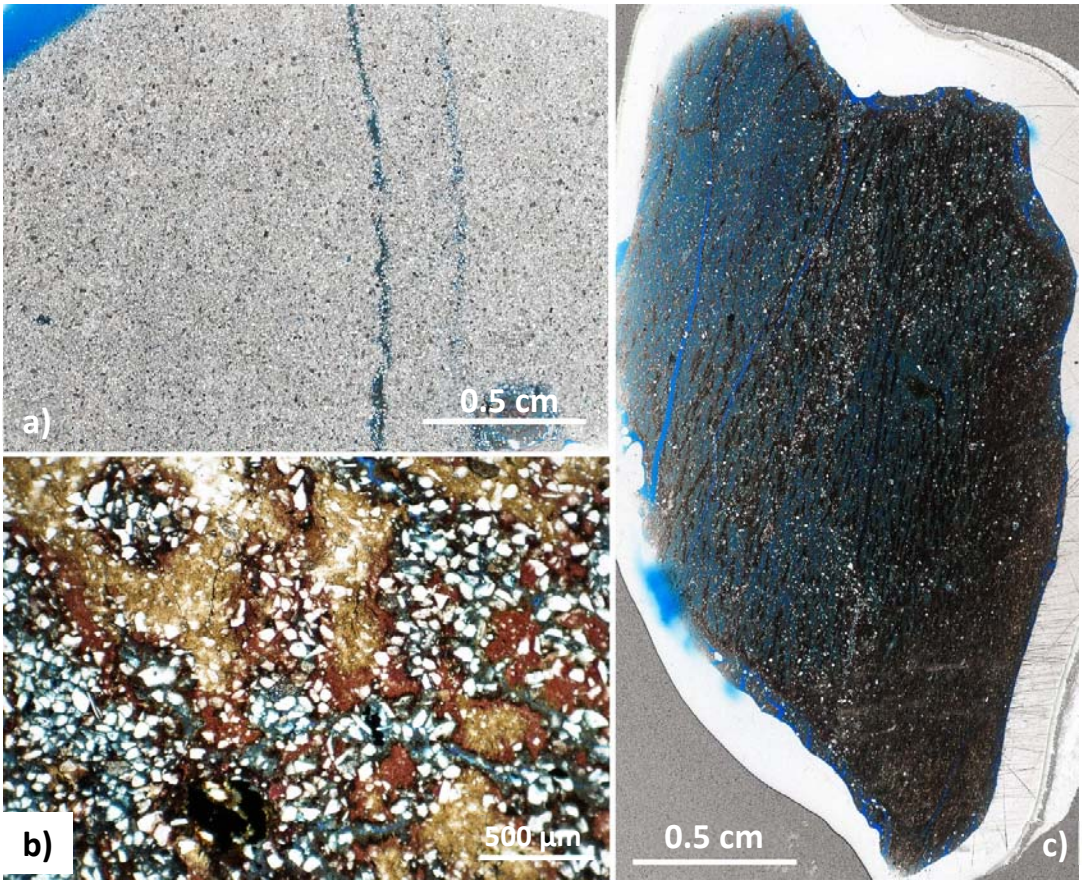

Figure 5.3.3 *– Scanned thin sections of two samples belonging to the Nagurukuru Formation.* ***a)*** *Highly cemented sandstone from sample c9_14-16 at ~136 m depth (Fig. 5.1.1).* ***b)*** *Sample c9_90-92 is composed of poorly sorted cemented sandstone/silt at ca. 22 m.* ***c)*** *Silty clay at ~122 m (Fig.5.1.1).*

Kivinje Formation (Paleocene – Lower Eocene) - TDP 7B

XRD analysis shows that calcite is dominant mineral in many of the intervals, ranging from 65% to 95%. This is most evident in the three first intervals (Fig. 5.3.4). In these same intervals, high abundance of dolomite is also present. In the rest of the samples the dolomite is either absent or very low (< 1%). Noticeable amount of gypsum is present in the upper two thirds of the core (Fig. 5.3.4). This is likely due to secondary gypsum growth on the outside of the cores during the storage.

On average, quartz constitutes 9.5% throughout the core, varying between 2 and 22%. The average quartz/feldspar ratio is 0.45 (Fig. 5.3.4). In generally, the increase in quartz/feldspar ratio relates somewhat with increase of calcite amount (Fig. 5.3.4). However, in the sample c7B_54.14 the quartz/feldspar ratio is 0.13. The K-feldspar/plagioclase ratio is also very low here, with a value of 0.20 (Fig. 5.3.5).

Quantitative XRD estimations of Kivinje Formation samples displays a larger heterogeneous character compared to the underlying Nangurukuru Formation (Fig. 5.3.1). The clay content increase and decrease upwards in the stratigraphy, ranging from 5% to 70%. In samples with highest clay content, the calcite abundance is considerably lower, 3-10%.

Thin sections

Three samples were analyzed under the microscope from the Kivinje Formation. Two of these were poorly sorted calcite cemented sandstones, the third sample was composed by calcareous silty clay (Table 5.3.1). In the XRD analysis, both sandstone samples (c7B_124.03 and c7B_152.50) contained high amount of calcite (Fig. 5.3.4).

Main characteristics found in the silty clay sample (c2_19.99) is the presence of fibrous calcite (Fig. 5.3.6a). This fibrous calcite was also observed in the other thin sections from the same formation (Appendix 9). In the same sample, siderite was found both during thin section and XRD analysis (Fig. 5.3.6b). It shows dark red staining along its margins, which can indicate oxidation conditions.

Quartz is present in all three samples, mostly as monocrystalline. K-feldspar is better preserved (scale of 1-2 – Fig. 4.4.1) compared to the higher altered stage of plagioclase (2-3). Calcite cements overgrowth was observed in sample c2_152.50.

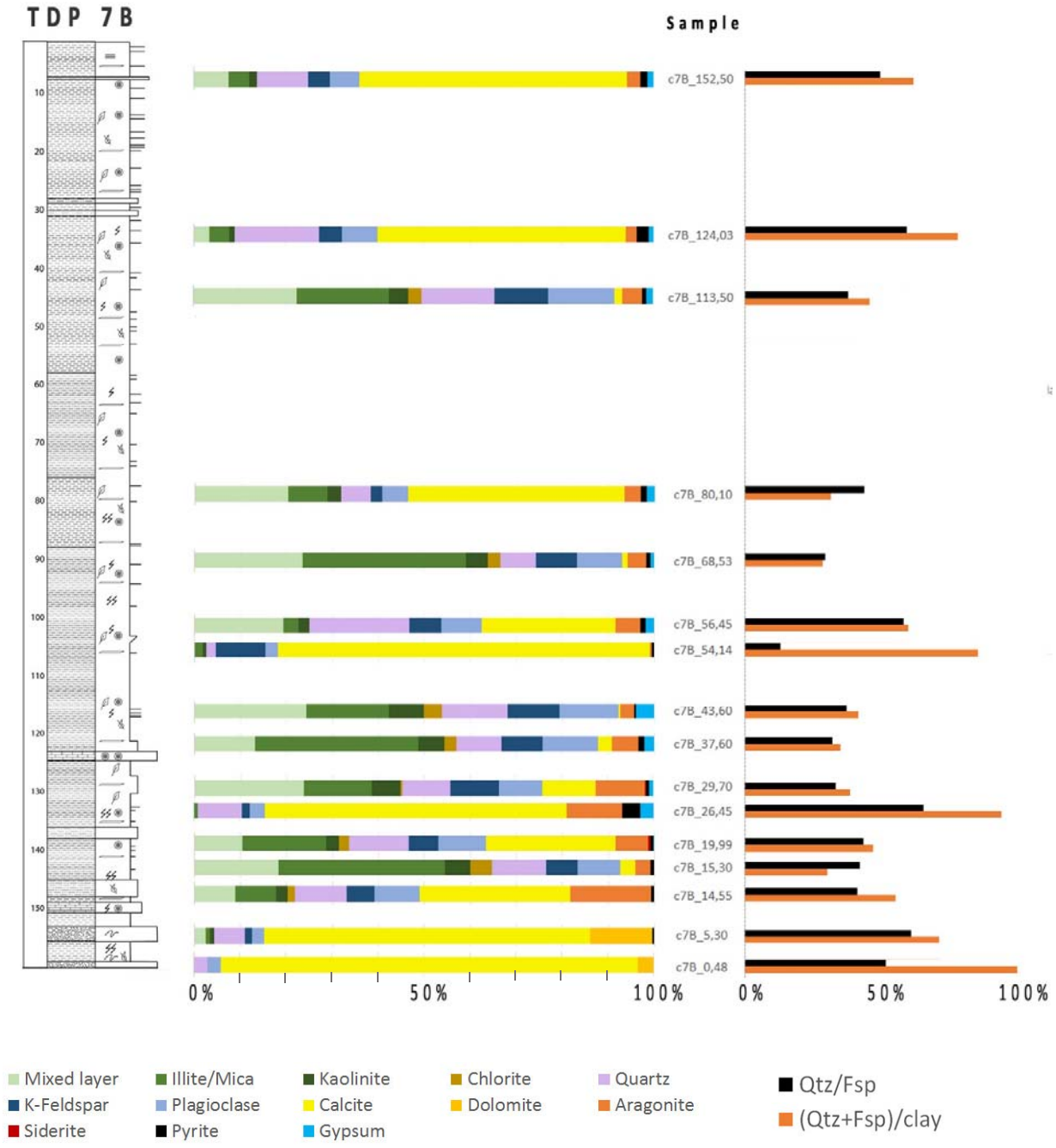

Figure 5.3.4 *– Quantified XRD results of the nineteen Kivinje Formation samples. Q/(Q+F)*100 (black lines) and (Q+F)/((Q+F)+clay)*100 (orange lines) ratios are shown on the right.*

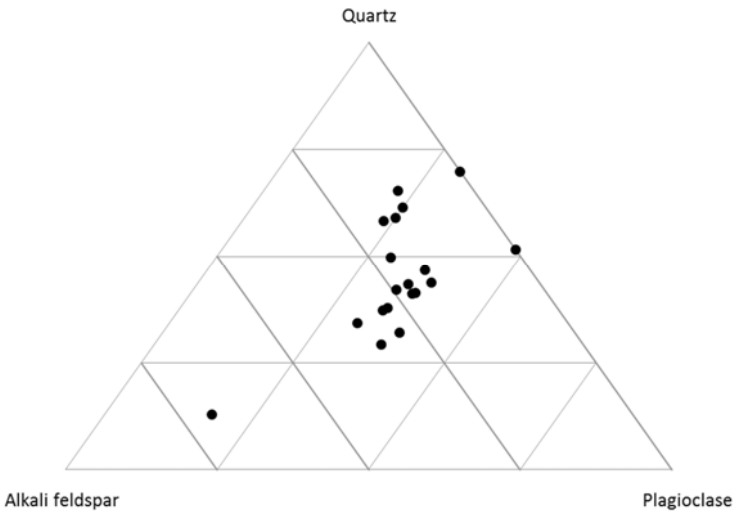

Figure 5.3.5 *– QAF (quartz-alkali feldspar-potassium feldspar) plot that shows ratio between quartz, alkali feldspar and plagioclase in Kivinje Formation.*

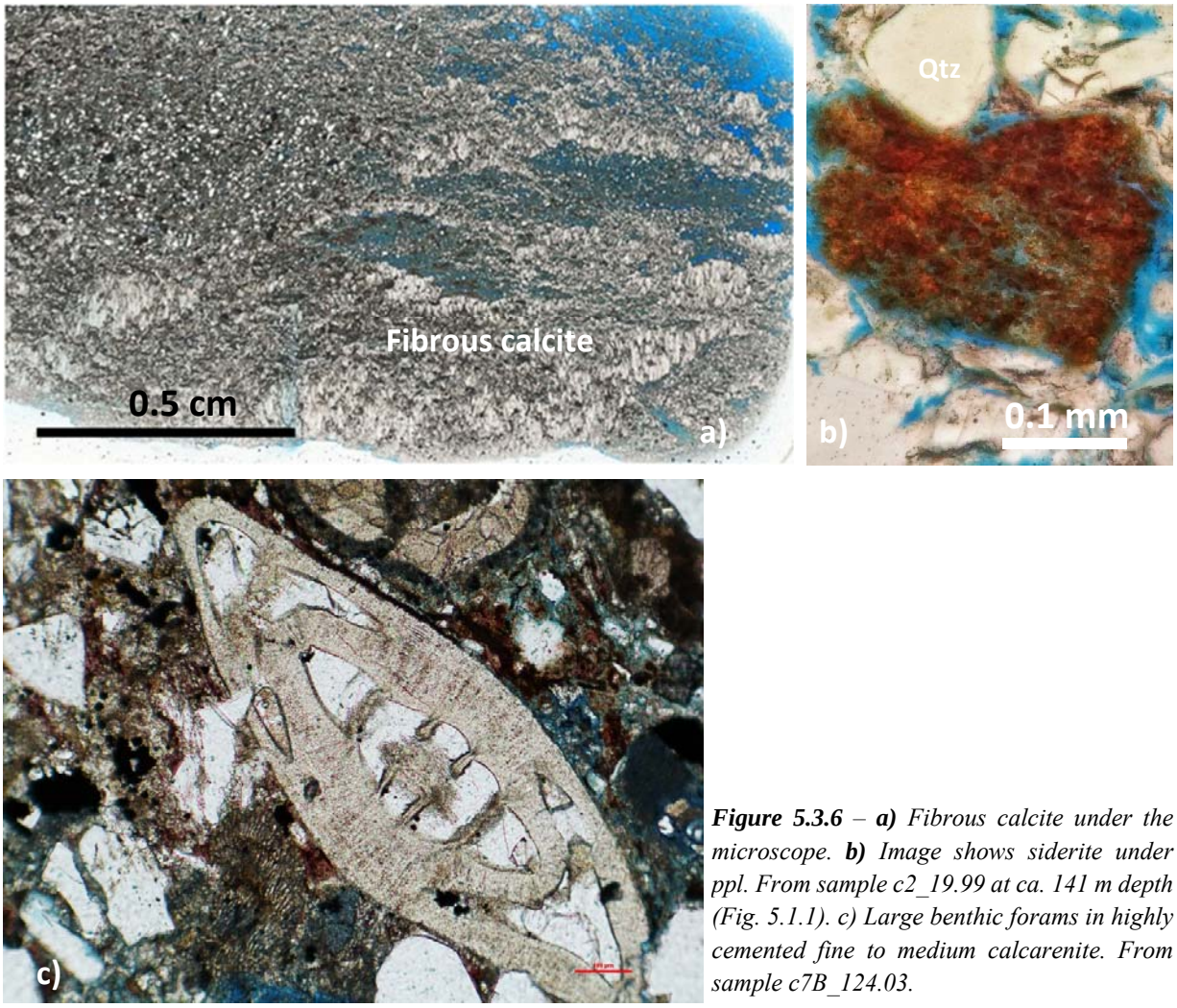

Figure 5.3.6 *– **a)** Fibrous calcite under the microscope. **b)** Image shows siderite under ppl. From sample c2_19.99 at ca. 141 m depth (Fig. 5.1.1). c) Large benthic forams in highly cemented fine to medium calcarenite. From sample c7B_124.03.*

Masoko Formation (Middle Eocene) - TDP 2

Clay minerals dominate the lower half of the Masoko Formation (Fig. 5.3.7). The clay constitute around 50-60 % of the total with little variations. The quartz to feldspar ratios are stable throughout this lower half, with an average of 0.31. Plagioclase is slightly higher throughout the whole Kivinje Formation compared to K-feldspar, averaging 9% and 7% respectively.

This relative homogenous lower part is abruptly changed to a calcite horizon (Fig. 5.3.7). From the log (Fig. 5.1.2) this represents facies association FA-b, which is interbedded clay and limestone. No feldspar or aragonite is present in the c2_53.45 sample, only small amounts of quartz. After this limestone horizon, clay minerals start to increase to around 35 % of the total. In the uppermost sample, c2_98.05, this limestone horizon is present again, with very little quartz and feldspar 2-3%, and no aragonite.

One of the samples (c2_53.45) contained no K-feldspar (Fig. 5.3.8).

Thin section

Two thin section from Masoko Formation were studied under the microscope (Table 5.3.1). One of the samples is highly cemented fine to medium sandstone (Fig. 5.3.9), the other is a silty clay. The degree of feldspar weathering is highest in the silty clay sample (3-4 scale – Fig. 4.4.1). Both samples are well sorted, matrix supported, and majority of the grains are sub-rounded. Monocrystalline quartz is the most dominant compare to the polycrystalline quartz (maximum 1-2 %).

Parallel bedding and upwards fining sequences going from darker to lighter color characterize sample c2_64.54 at 46 m depth (Fig. 5.1.2). These structures were also observed during the logging of the TDP 2 cores in the same section. Large benthic forams (1-2 mm) are also observed in the thin section.

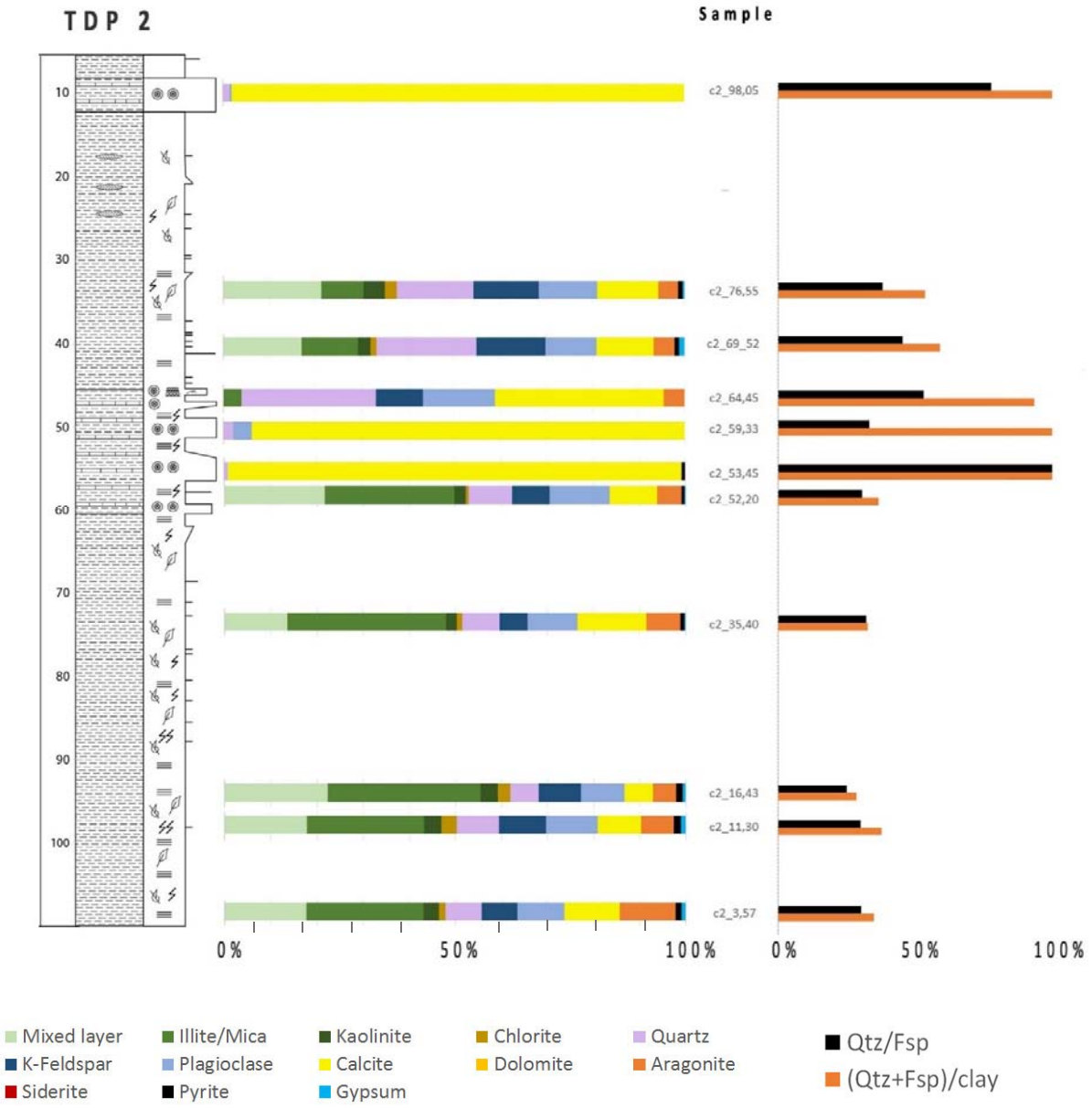

Figure 5.3.7 *– Quantified XRD-bulk results of the eleven Masoko Formation samples. Q/(Q+F)*100 (black lines) and (Q+F)/((Q+F)+clay)*100 (orange lines) ratios are shown on the right.*

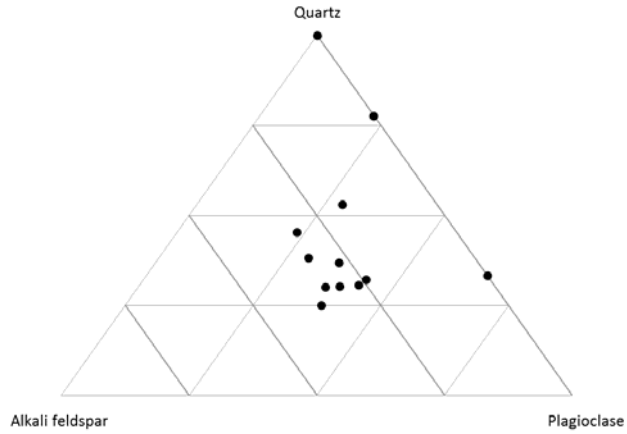

Figure 5.3.8 *– QAF (quartz-alkali feldspar-potassium feldspar) plot that shows ratio between quartz, alkali feldspar and plagioclase in Masoko Formation.*

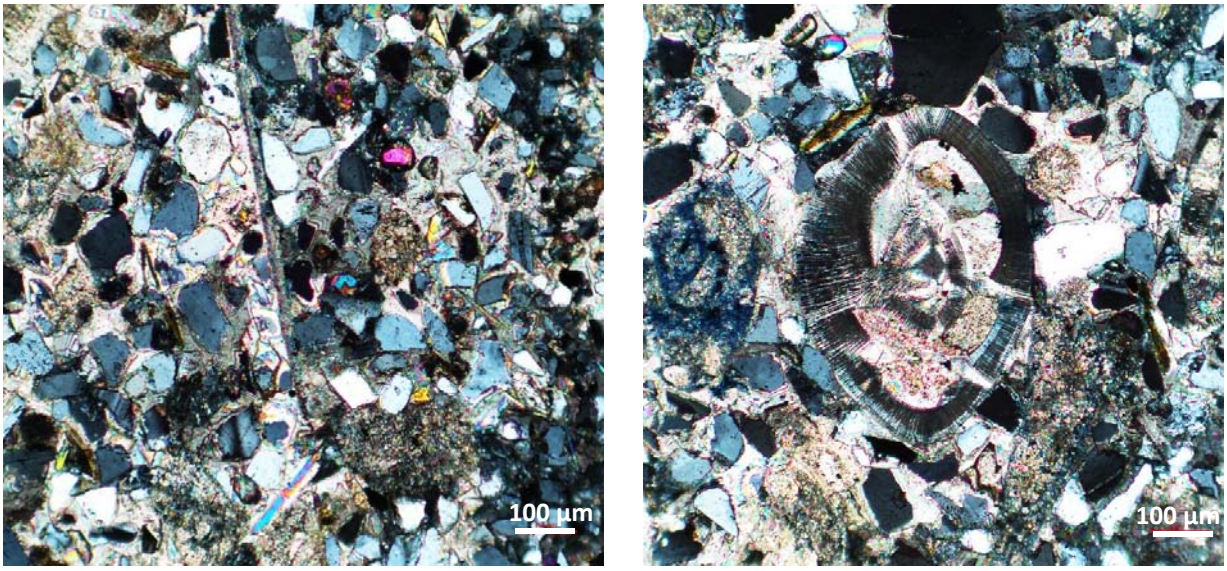

Figure 5.3.9 *– Highly cemented fine to medium calcarenite, with large benthic forams. From sample c2_64.45 (Fig. 5.1.2).*

Pande Formation (Upper Eocene – Lower Oligocene) - TDP 1

In this core, the quartz content is much higher when compare to the underlying cores, with an average of 33 % of the total. The quartz/feldspar ratios show generally higher values in samples with calcite present compared to the rest (Fig. 5.3.10). Siderite content is very high in the deepest sample c1_1.45, around 22% of the total. The average content of K-feldspar is 14.66% and plagioclase is only 6.73%. These higher values of K-feldspar can be seen in Figure 5.3.11.

The clay content varies severly throughout the core, but is generally lower realtiv to the other cores, ranging from 1-45 % of the total (5.3.11).

Thin section

From this formation four thin section were studied (Table. 5.3.1). Three of the samples are good to moderate sorted silt to silty clay, while the fourth is a poorly sorted sandstone (Fig. 5.3.12). Polycrystalline quartz is less frequent in this formation (< 1%) than in the underlying formations (~1-3 %). Based on microscopy and XRD analysis, K-feldspar show highest abundance and less pronounced weathering, compared to formerly presented formations. Quantitative XRD analysis of Pande Formation samples confirmed the predominance of K-feldspar over plagioclase (Fig. 5.3.10 and 5.3.11).

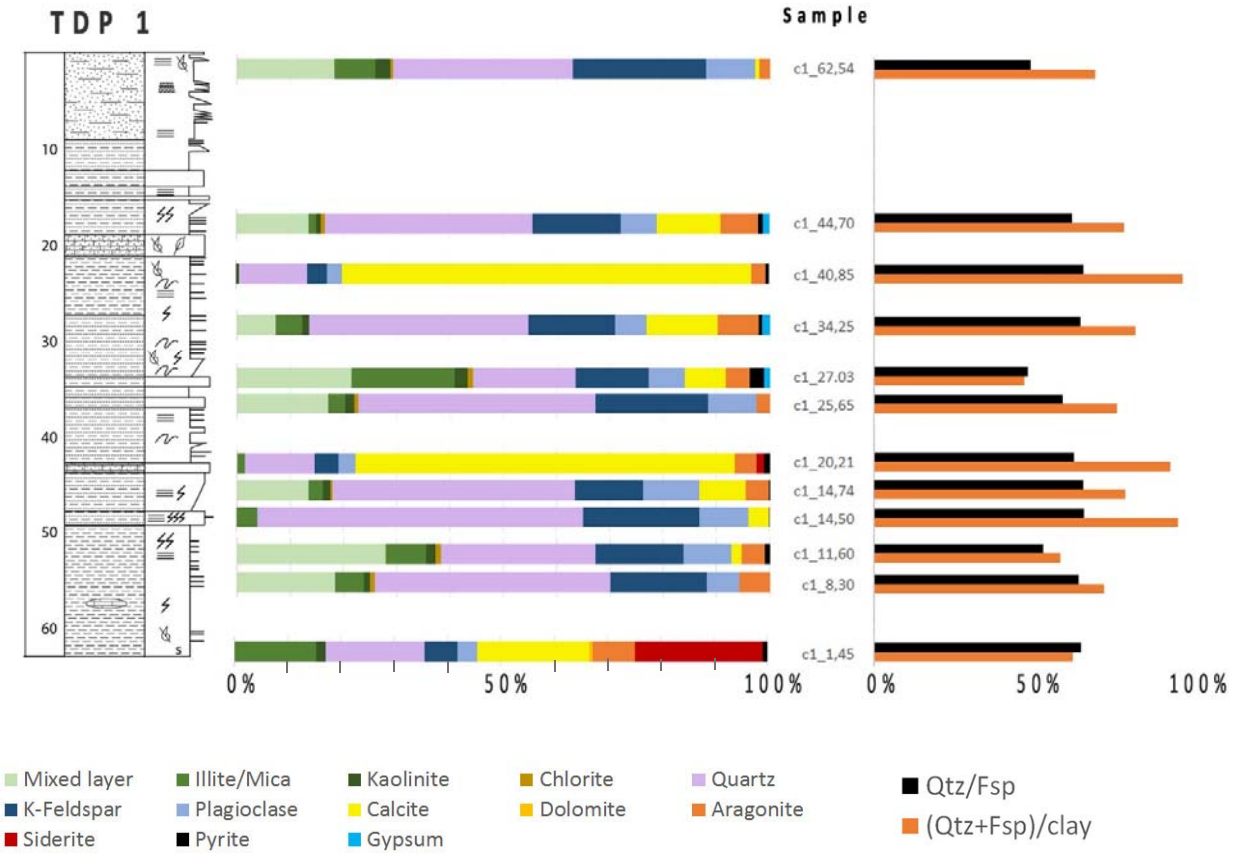

Figure 5.3.10 *– Quantified XRD-bulk results of the twelve Pande Formation samples. Q/(Q+F)*100 (black lines) and (Q+F)/((Q+F)+clay)*100 (orange lines) ratios are shown on the right.*

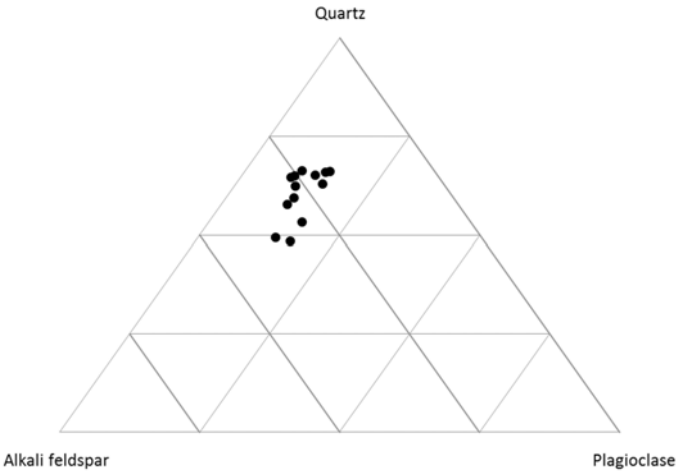

Figure 5.3.11– *QAF (quartz-alkali feldspar-potassium feldspar) plot that shows ratio between quartz, alkali feldspar and plagioclase in Pande Formation.*

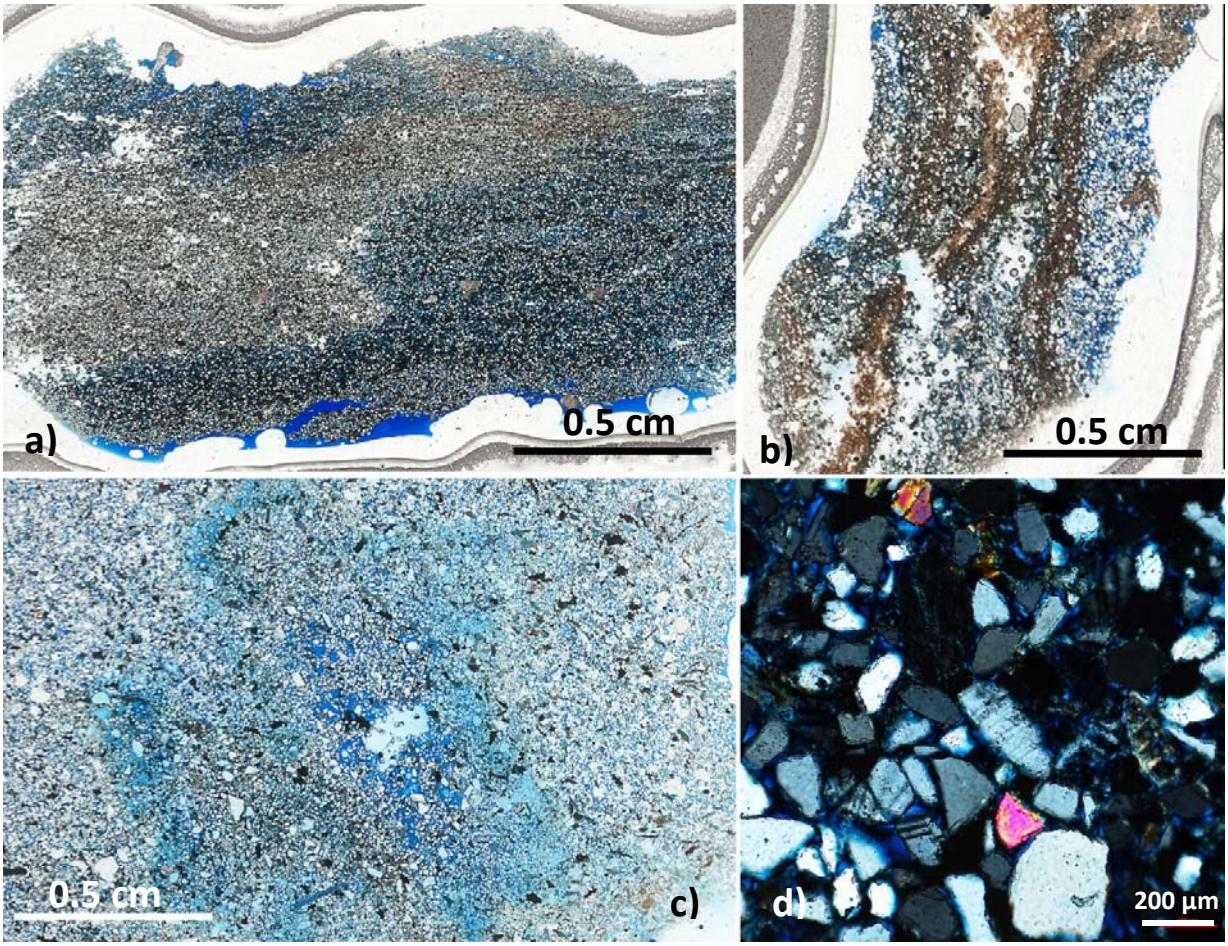

Figure 5.3.12– *Scanned thin sections of three samples belonging to the Pande Formation.* ***a)*** *Silt/clay in sample c1_8.3 at ~56 m depth (Fig. 5.1.2).* ***b)*** *Calcareous laminated silty clay from sample c1_34.25 at ~29 m (Fig.5.1.2).* ***c)*** *Sample c1_14.50 is a poorly sorted sandstone at ca. 49 m.* ***d)*** *Close up view of sample c1_14.50.*

Table 5.3.1 – *Summarized description of selected thin section samples from the Kilwa Group. The description of the weathering scale (1-5) of the feldspars is shown in Figure 4.4.1.*

Fm.	Sample	Litho.	Depo. environment.	Dominating framework	Avg. grain size	Grain shape	Sorting	Comments	Figure
Pande Fm.	c1_8.3	Silt/Clay	Marine	Matrix supported	73 µm	Subangular to subrounded	Moderate to good	Divided into two parts: **1.** Silt part with 10-15% porosity. Monocrystalline quartz dominant (Polycryst. <1%). Some mica. **2**. Shaly clay in the middle. < 1 % porosity. In both, feldspar show little weathering (1-2).	Fig. 5.3.12a
	c1_14.50	Sandstone	Marine	Grain supported	125 µm	Subrounded	Poorly	Contains fossils, up to 1.5 mm. Mono-crystalline quartz dominates. Mica present. K-fsp is very frequent compared to plagiclase, with little to no weathering (1-2 scale).	Fig. 5.3.12c and d
	c1_25.66	Silt/Clay	Marine	Matrix supported	78 µm	Subrounded	Well	Monocrystalline quartz dominates. Matrix is clay and calcite cement. Mica frequent. Feldspar show very little weathering (1-2). Some feldspar show higher degree of weathering (ca 3). Possible siderite present.	
	c1_34.25	Calcareous silt	Marine	Matrix supported	108 µm	Subrounded	Moderate	Feldspar show some weathering (2-3). Quartz is mostly monocrystalline, polycrystalline <1%. Clay and calcite cement in layers. Fossils and mica present. Possible siderite.	Fig. 5.3.12c
Masoko Fm.	c2_64.45	Calcareous sandstone	Marine	Matrix supported (clacite cement)	157 µm	Subrounded to rounded	Well	Highly cemented fine to medium calcarenite. Parallel bedding, with upwards fining sequences, going from darker to lighter color. 1-2 mm benthic forams present. Feldspar show generally little weathering (1-2). Quartz is monocrystalline. Some mica evident. Possilbe some dolomite.	Fig. 5.3.9
	c2_69.52	Silty clay	Marine	Matrix supported	72 µm	Subrounded	Well	Silty clay with monocrystalline quarts grains. Calcite cement present. Some of the feldspar show medium weathering (3-4), where it starts to dissolve.	
Kivinje Fm.	c7B_19.99	Calcareous silty clay	Marine	Matrix supported (clacite cement)	79 µm	Subrounded	Moderate to well	Sample with fibrous calcite "beef" layer. Cone in cone structures. Quartz is monocrystalline. Possilbe siderite present. Some feldspar weathering (1-3).	Fig. 5.3.6b
	c7B_124.03	Calcareous sandstone	Marine	Matrix supported (clacite cement)	345 µm	Subrounded	Poor	Highly cemented fine to medium calcarenite. 1-2 mm benthic forams present. Polycrystalline quartz ~2%. Majority of the feldspar is k-fsp, and is well preserved (1-2). Some feldspar grains (plagioclase mostly) show high weathering (3-4).	Fig. 5.3.6c
	c7B_152.50	Calcareous sandstone	Marine	Matrix supported (clay + clacite cement)	247 µm	Subangular to subrounded	Poor	Monocrystalline quartz, some polycrystalline qtz grains. Calcite cement overgrowth. Lots of benthic forams (1-5mm). Feldspar show some degree of weathering (2-3).	
NangurukuruFm.	c9_14-16	Cemented sandstone	Marine	Matrix/grain	88 µm	Subrounded	Moderate	Highly cemented monocrystalline quartz sandstone.Plagioclase has highest abundance of the feldspars. It show some degree of weathering (1-3.). Some mica present.	Fig. 5.3.3a
	c9_90-92	Cemented sandstone/ silt	Marine	Matrix supported	68 µm	Subrounded	Poor	Highly cemented monocrystalline quartz sandstone. Some polycrystalline quartz (2-3%). Very poory sorted.	Fig. 5.3.3b
	c9_31-32	Silty clay	Marine	Matrix supported	49 µm	Subangular	Poor	Silty clay with monocrystalline quartz. Some grain are polycrystalline in nature.	Fig. 5.3.3c

5.3.2. Clay-fraction Mineralogy and SEM Results

Twenty-three samples were selected from Kilwa Group for clay mineralogy analysis. Based on the diffractograms, the observed clay minerals "groups" in this study are smectite, illite, kaolinite and chlorite (Fig 5.3.13). Mixed-layer clay minerals were also identified (Table. 5.3.2).

Qualitative Clay-fraction Mineral Content

The XRD patterns for the clay-sized fraction (< 2 μm) contained peaks produced by expandable clay minerals between 5.9 – 7.5°2θ (15 – 12 Å *d* value), mica at 8.8°2θ (10.1 Å), kaolinite and chlorite at 12.3°2θ (7.2 Å), kaolinite 002 peak at 24.9°2θ (3.58 Å) and chlorite 004 reflection at ~25.1°2θ (3.54 Å). Peaks at 20.8 °2θ (4.26 Å) and 26.6 °2θ (3.34 Å) represent quartz. The other peaks between 27.4 – 27.9°2θ (3.2 – 3.1 Å) belongs to the feldspar group. Relative large amount of calcite at 29.4 °2θ (3.86 Å) is also present in the samples.

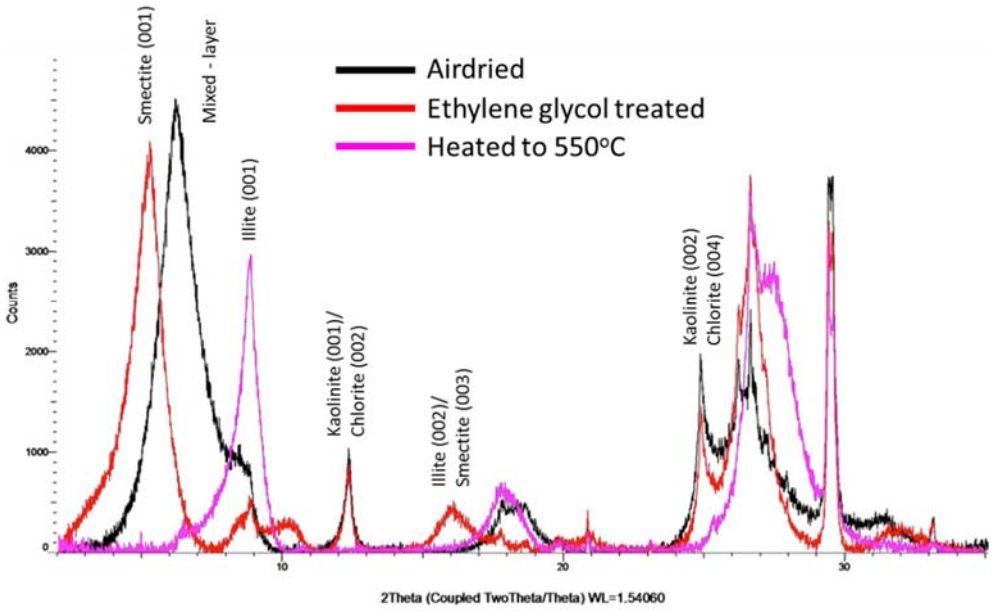

Figure 5.3.13– *This figure is an example of three diffractograms (airdried, ethylene glycol treated and heated) from Pande Formation.*

The presence of smectite was revealed by the air-dried peak at ~6.3°2θ (13.9 Å) shifting to ~5.3°2θ (16.8 Å) after EG and collapse to ~8.8°2θ (10.1 Å) after heating the sample. The increased intensity

at ~8.8°2θ (10.1 Å) after 550°C heat treatment is caused by the superposition of collapsed smectite layers. The presence of kaolinite was established by the 001 peak at 12.3°2θ (7.2 Å) in both air-dried and EG patterns. These peaks are destroyed with the 550°C heat treatment, but small amounts of chlorite was found at the ~25.1°2θ (3.54 Å) peak.

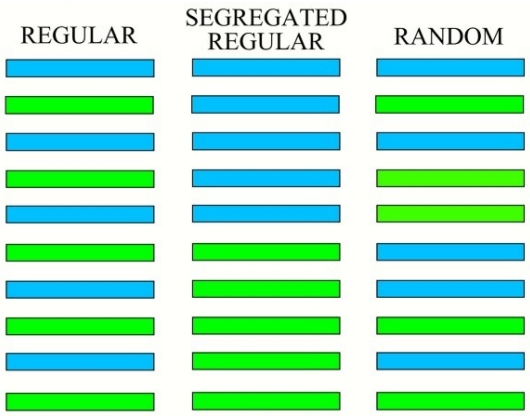

Based on Moore and Reynolds Jr (1989) the mixed clays in Kilwa Group show Reichweite(R) 0 ordering, i.e. random interstratification (Fig. 5.3.14). This was determined by the position of EG-solved smectite/illite peak position near 5° 2θ.

Figure 5.3.14*– The three types of ordering. R=1, R=3, and R=0, respectively. Modified from Macewan and Ruiz-Amil (1975).*

Vertical variation in NEWMOD predicted clay mineral abundance

The vertical variations in the proportions of the end members and mixed-layered clay minerals in Kilwa Group can be linked to climate and source rock (Fig. 5.3.15). For illustrative purposes the data is presented in a continuous trend although a possible unconformity may exist between Nagurukuru (Late Cretaceous) and Kivinje (Late Paleocene) formations (Nicholas et al., 2006). The default parameters used in NEWMODE are presented in Appendix 6.

Table 5.3.2 and Figure 5.3.15 shows the dominant constituent of all end member clay minerals and the different mixed-layered species. Fe-rich smectite (S) and kaolinite (K) are the two dominant end member clay minerals in upper three formations, 10-24 wt.% (of the clay-fraction) and 14-19.5 wt.% respectively. Kaolinite show highly variable ranging, i.e. high standard deviation, in Kivinje (6.7) and Masoko (6.0) formations. For example, in Kivinje Formation the kaolinite value range from 11.4 to 32.4 wt.%. Smectite content in Pande Formation show similar high standard deviation (6.2), ranging from 14.3 to 30.1 wt.%. The Nangurukuru Formation show very small concentrations of smectite, average 1.6 wt.%, which is also reflected in the small value in the smectite-vermiculite

mixed-layered clay. This formation on the other hand contains more chlorite (C) and illite (I) than in the rest of the formations.

The most abundant clay mineral is randomly ordered mixed-layered I-S, with 50% smectite and 50% illite layers (Fe-poor), up to 34 % of the total clay fraction. The I-rich I-C (random 80% illite layers) show second highest abundance in the samples, from 15 to 22 %. It gradually decreases upwards in the stratigraphy, but shows high content variation in the individual formations (Fig. 5.3.15). Fe-rich random S-V (vermiculite) with 50% smectite layers, increase gradually from 1.2 % in Nangurukuru Formation and up to wt.5.9 % in Pande Formation. Abundance of S-rich I-S (random with 70% S) is highest in Masoko Formation, with 11.4 %. Fe-rich S-K random ordered with 80% S layers, has highest abundance in Pande Formation (9.8 %).

Table 5.3.2 – *Summary of clay-sized fraction mean (% of the clay fraction) with standard deviation in the parentheses from Nangurukuru, Kivinje, Masoko, and Pande formations. The semi-quantitative values of the clay minerals are based on the NEWMOD models. The lower part of the table show the simulation Fe, K and hydroxide layer used in the models.*

Notes: ***n*** *= number of samples.* ***I*** *= Illite,* ***S*** *= Smectite,* ***K*** *= Kaolinite,* ***C*** *= Chlorite and* ***V*** *= Vermiculite.* ***Fe-poor I-S*** *(random with 50% S layers),* ***I-rich I-C*** *(random with 80% I layers),* ***Fe-rich S-V*** *(random with 50% S layers),* ***S-rich I-S*** *(random with 70% S layers) and* ***Fe-rich S-K*** *(random with 80% S layers).*

Formation	**Nangurukuru** *(n = 5)*	**Kivinje** *(n = 7)*	**Masoko** (*n = 5)*	**Pande** *(n = 6)*
Smectite (S)	1,59 (0,7)	10,18 (3,7)	8,39 (3,3)	23,74 (6,2)
Illite (I)	4,72 (0,8)	3,29 (0,7)	1,65 (0,2)	0,89 (0,1)
Kaolinite (K)	16,71 (1,2)	19,53 (6,7)	15,41 (6,0)	14,38 (2,4)
Chlorite (C)	6,63 (0,5)	2,34 (0,4)	2,58 (0,3)	0,99 (0,6)
Fe-rich S-V	1,23 (0,4)	4,20 (0,6)	3,34 (0,9)	5,95 (1,9)
Fe-poor I-S	34,02 (1,4)	26,91 (3,8)	25,05 (3,9)	19,66 (2,7)
S-rich I-S	7,03 (2,1)	9,94 (1,4)	11,40 (1,2)	9,48 (1,2)
Fe-rich S-K	6,07 (0,7)	6,48 (1,5)	5,83 (1,2)	9,79 (1,5)
I-rich I-C	21,95 (2,4)	17,10 (3,7)	26,34 (6,7)	15,13 (6,1)

I-rich I-C	**S-rich I-S**	**Fe-rich S-K**	**Fe-rich S-V**	**Fe-poor I-S**
Illite Fe = 1.5	Illite K = 1	Smect. Fe = 1.35	Smect. Fe = 1.4	Fe = 0
Illite K = 0.9	Illite Fe = 0			
Hydroxide layer = 0.9	Smect. Fe = 0			

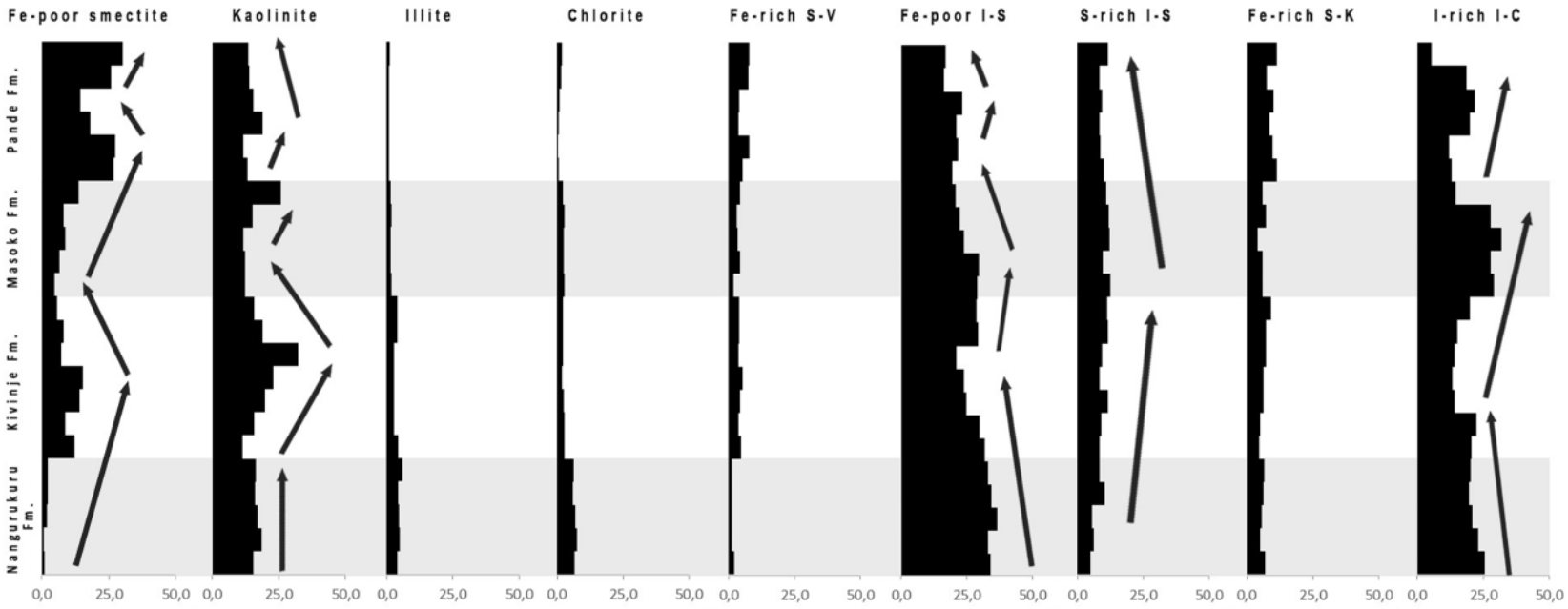

Figure 5.3.15– *Stratigraphy variation in the abundance (% of the clay-sized fraction) of the end members and mixed-layered clay minerals in Nangurukuru, Kivinje, Masoko and Pande Formation.* ***I*** *= Illite,* ***S*** *= Smectite,* ***K*** *= Kaolinite,* ***C*** *= Chlorite and* ***V*** *= Vermiculite.* ***Fe-poor I-S*** *(random with 50% S layers),* ***I-rich I-C*** *(random with 80% I layers),* ***Fe-rich S-V*** *(random with 50% S layers),* ***S-rich I-S*** *(random with 70% S layers) and* ***Fe-rich S-K*** *(random with 80% S layers).*

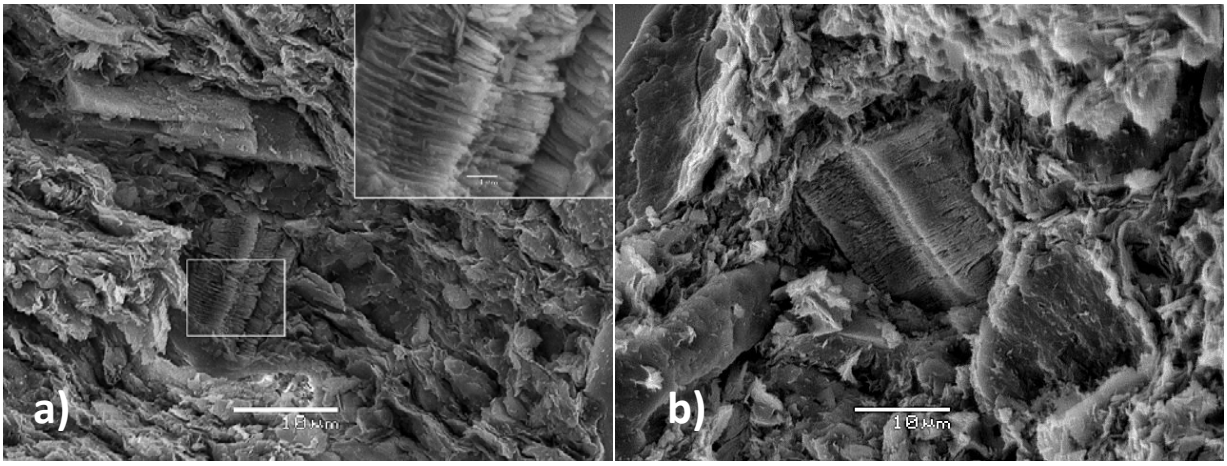

Figure 5.3.16– *The characteristic kaolinite booklets observed in SEM analysis.* ***a)*** *From Pande Formation at 24m.* ***b)*** *From Kivinje Formation at 29m.*

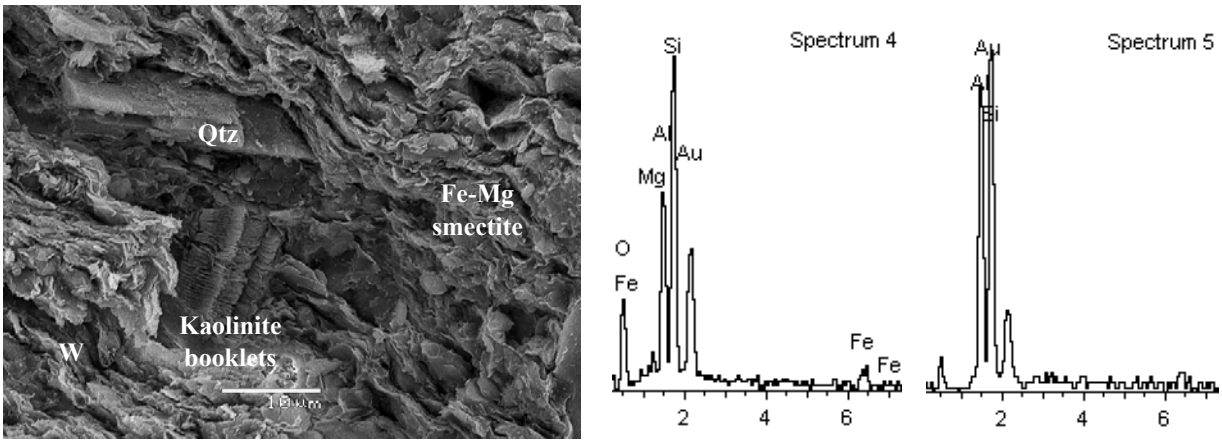

Figure 5.3.17 – *Fe-Mg smectite (spectrum 4) and kaolinite booklets (spectrum 5). Sample from Pande Formation. Region of wavy flakes (W).*

5.4 TRACE AND RARE-EARTH ELEMENT DATA

The average value of trace and rare earth elements (REE) from the Nangurukuru, Kivinje, Masoko and Pande formations, and the offshore Paleocene and Cenomanian Statoil samples are presented in Table 5.4.1. Average ratios of selected elements are listed in Table 5.4.2.

Large-Ion Lithophile (LIL) Elements (Rb, Cs, Ba and Sr)

The average concentration (ppm) of Rb, Cs, Ba and Sr in the Kilwa Group are similar to upper continental crust (UCC), North American shale composite (NASC) and post-Archean Australian shales (PAAS) (McLennan et al., 1980, Gromet et al., 1984, Condie, 1993) (Table 5.4.1). Proposed by Taylor and McLennan (1985), the PAAS represents the average composition of the upper continental crust.

The Pande Formation show relative lower average Sr content (225.83 ppm) than the lower three formations (449.60 – 621.33 ppm).

Rb and Sr values are somewhat higher, especially Sr in the offshore Paleocene samples, compared to Cenomanian samples (Table 5.4.1). Average Zr/Rb ratios are lower to (0.62) in Paleocene compare to average 1.20 in Cenomanian. The same is for (Zr + Rb)/Sr values, showing lower values in Paleocene 0.23 to 0.58 in Cenomanian.

Ferromagnesian Trace Elements (Cr, V, Ni, Sc and Co)

Average abundance of Cr (90.17 – 128.17 ppm), V (62.83 – 103.67 ppm), Ni (45.35 – 54.82 ppm), Sc (0.98 – 2.78) and Co (15.57 – 19.50 ppm) are somewhat variable throughout the Kilwa Group (Table 5.4.1). Compared to the other formations, Nangurukuru Formation show slightly higher Cr values (128 ppm), close to NASC (124.5 ppm). Same trend is observed for the Co, while abundance of Ni are more or less similar to those in UCC (Table 5.4.1). The higher abundance of Cr leaves the Nangurukuru Formation with somewhat higher Cr/V and lower V/Ni ratios compared to the other formations and offshore samples. Cr/V ratios gradually decreases upwards in the stratigraphy (Table 5.4.2). This is due to increased V concentrations from Nagurukuru and up to Pande formation.

Table 5.4.1 – *Average of selected trace elements and rare earth elements (REE) of the Kilwa Group clays and from Statoil offshore clays samples. NASC, PAAS, UCC values from Condie, (1993).*

	Kilwa Group - Onshore				Statoil Block 2 - Offshore				
Element	**Nangurukuru Fm.**	**Kivinje Fm.**	**Masoko Fm.**	**Pande Fm.**	**Paleocene**	**Cenomanian**	**NASC**	**PAAS**	**UCC**
	n = 6	n = 10	n = 6	n = 6	n = 2	n = 2			
Sc	13,62	13,24	13,33	14,50	12,25	17,80	15,00	16,00	13,40
V	62,83	88,80	84,67	103,67	52,00	105,50	130,00	150,00	86,00
Cr	128,17	116,30	90,17	90,67	81,50	97,50	125,00	110,00	112,00
Co	19,50	16,43	15,57	18,43	17,50	19,25	26,00	23,00	18,00
Ni	54,82	46,33	48,93	45,35	66,65	60,00	58,00	55,00	60,00
Cu	32,70	38,22	30,05	44,25	35,30	59,95	-	-	-
Zn	89,47	79,37	90,52	81,83	91,85	96,80	-	-	-
Rb	94,60	104,89	88,88	92,55	98,65	120,50	125,00	160,00	87,00
Sr	567,17	449,60	621,33	225,83	752,50	457,00	142,00	200,00	269,00
Y	15,07	17,77	12,93	22,28	19,65	28,15	35,00	27,00	25,00
Zr	72,67	61,00	64,50	95,17	60,00	142,00	200,00	210,00	162,40
Nb	0,97	5,10	3,72	6,75	0,20	10,95	13,00	19,00	10,30
Cs	3,55	3,68	3,32	2,89	3,73	5,18	5,16	-	-
Ba	330,83	395,30	410,67	330,33	373,50	399,00	636.00	650,00	626,00
Hf	2,00	1,77	1,93	2,75	1,35	3,30	6,30	5,00	4,40
Th	9,58	13,32	11,57	9,42	10,25	12,50	12,30	14,60	9,10
U	2,02	2,23	2,38	2,53	0,95	1,50	2,66	3,10	2,40
La	37,32	49,44	39,58	38,45	28,30	32,55	31,1	38,00	30,00
Ce	79,00	112,60	68,00	75,00	56,00	64,50	66,7	80,00	64,00
Pr	6,87	8,52	6,92	8,83	7,05	7,30	7,90	8,90	7,10
Nd	37,83	51,70	34,17	43,83	36,50	42,00	27,4	32,00	26,00
Sm	4,43	5,50	4,48	6,27	3,80	5,25	5,59	5,60	4,50
Eu	0,96	1,17	0,94	1,51	0,95	1,32	1,18	1,10	0,88
Gd	3,88	4,89	3,87	5,93	4,10	5,30	6,03	4,70	3,80
Tb	0,52	0,66	0,52	0,80	0,55	0,75	0,85	0,77	0,64
Dy	2,97	3,65	2,78	4,67	3,30	5,00	5,80	4,40	3,50
Ho	0,57	0,70	0,53	0,90	0,70	0,95	1,04	1,00	0,80
Er	1,63	1,99	1,50	2,48	1,80	2,75	3,40	2,90	2,30
Tm	0,25	0,29	0,20	0,33	0,25	0,40	0,50	0,40	0,33
Yb	1,92	2,68	1,60	2,13	1,65	2,60	3,06	2,80	2,20
Lu	0,29	0,45	0,25	0,42	0,30	0,66	0,456	0,43	0,32
Σ REE	178,39	244,23	165,33	191,57	145,24	171,33	174,20	183,00	146,40
LREE	165,45	227,76	153,15	172,38	131,65	151,60	152,84	165,60	132,50
HREE	11,98	15,31	11,24	17,76	12,65	18,41	20,40	17,40	13,90
LREE/HREE	13,72	15,30	13,86	9,85	10,28	8,29	7,50	9,50	9,54
Eu/Eu*	0,73	0,70	0,70	0,78	0,75	0,79	0,68	0,66	0,70
$(La/Yb)_n$	12,50	12,54	15,93	11,88	10,85	7,83	6,10	8,20	-
$(Gd/Yb)_n$	1,69	1,61	2,00	2,36	2,07	-	-	-	8,70
Zr/Rb	0,77	0,58	0,72	1,03	0,60	1,18	1,60	-	1,80
(Zr + Rb)/Sr	0,31	0,50	0,23	0,89	0,23	0,58	2,30	-	0,90

Notes: *1) n = number of samples; All elements in ppm; REE chondrite-normalising factors from (Taylor and McLennan, 1985). 2)* $\sum REE = \sum(La\text{-}Lu)$; $Eu/Eu^* = (Eu)n/((Sm)n*(Gd)n)^{1/2}$, $\sum LREE/\sum HREE = \sum(La\text{-}Sm)/\sum(Gd\text{-}Lu)$ *(McLennan, 1989).*

Table 5.4.2 – *Ratio range of selected elements from both the Kilwa Group and Statoil offshore clays. NASC, PAAS and UCC values from Condie, (1993).*

	Th/U	Th/Sc	La/Th	La/Sc	Cr/V	Cr/Ni	Zr/Cr	Eu/Eu*
Pande Fm.	2.3 – 4.7	0.5 – 0.8	3.4 – 4.6	2.3 – 2.8	0.6 – 1.4	0.9 – 3.4	0.7 – 1.3	0.74 – 0.80
Masoko Fm.	4.1 – 7.6	0.7 – 0.9	3.2 – 3.6	2.6 – 3.2	0.9 – 1.2	1.5 – 2.3	0.5 – 1.2	0.66 – 0.73
Kivinje Fm.	4.6 – 7.6	0.1 – 1.2	3.2 – 4.5	2.9 – 4.3	0.8 – 2.1	1.7 – 3.6	0.4 – 0.7	0.68 – 0.73
Nangurukuru Fm.	3.8 – 5.7	0.6 – 0.8	3.5 – 4.3	2.5 – 3.0	1.7 – 2.9	1.6 – 2.8	0.4 – 0.8	0.70 – 0.74
Offshore Paleocene	10.5 – 11.0	0.80	2.7 – 2.8	2.3	1.5 – 1.6	1.1 – 1.4	0.6 – 0.8	0.75
Offshore Cenomanian	7.9 – 8.9	0.6 – 0.7	2.5 – 2.7	1.7 – 1.9	0.8 – 1.1	1.4 – 1.9	1.4 – 1.5	0.74 – 0.83
NASC	4,60	0,82	2,52	2,00	0,96	2,15	1,60	0,68
PAAS	4,70	0,91	2,60	2,37	0,73	2,00	1,90	0,66
UCC	3,79	0,68	3,20	2,16	1,30	1,86	1,45	0,70

Other Trace Elements (Zr, Hf. Rb, Nb)

The average Zr content (61 – 95.17 ppm) in all four formations is considerably lower than for NASC (200 ppm) and UCC (162 pmm). Zr/Rb ratios shows an increase upwards in the stratigraphy, with highest ratios in Pande Formation (Fig. 5.3.3). The average Nb content is particularly low in Nangurukuru Formation (0.97 ppm), compared to a much higher abundance in UCC (10.30 ppm) (Table 5.4.1). The anomalously low Nb is also observed in the offshore Paleocene sample.

Rare Earth Elements (REEs, Th, U)

The concentrations and chondrite-normalized patterns of REEs in the Kilwa Group clays are shown in Table 5.4.1 and Figure 5.4.1. The pattern display enrichment of light REE (LREE) (high $(La/Yb)_n$, $(La/Sm)_n$, and ∑LREE/∑HREE) and flat heavy REE (HREE) ($(Gd/Yb)_n$ = 1.61 – 2.36). This pattern, with negative Eu-anomaly, is similar to that of UCC. The ∑LREE/∑HREE ratio is lowest in Pande Formation (9.85).

The average Th content in the Kilwa Group samples show small variation in the Kilwa Group (9.42 – 13.32 ppm), similar to typical NASC and UCC values (Table 5.4.1). Kivinje and Masoko Formation appear to have the highest concentration of Th, 13.32 ppm and 11.57 ppm respectively, compare to the other formations. The Th/U ratios are also highest in these two formations (Table 5.4.2).

Average Th/U ratios are higher in offshore samples (7.90 – 11.00) (Table 5.4.2) compared to those observed in the Kilwa Group (3.81 - 6.00). These higher Th/U ratios in the offshore samples is due to low uranium content. The highest observed Th/U ratio was in the offshore Paleocene samples, average 10.75 versus 8.37 in Cenomanian.

Chondrite-normalized REE pattern observed in Statoil offshore clays (Fig. 5.4.2) are very similar to that observed in the Kilwa Group clays (Fig 5.4.1), with LREE enrichment, negative Eu anomalies and relative flat HREE. NASC normalized Paleocene 3 sample show highest depletion in all REE compared to the rest of the offshore samples (Fig. 5.4.3b). La and Ce elements are slightly deplete in all of the offshore clay samples compared to the Kilwa Group (Fig. 5.4.3b).

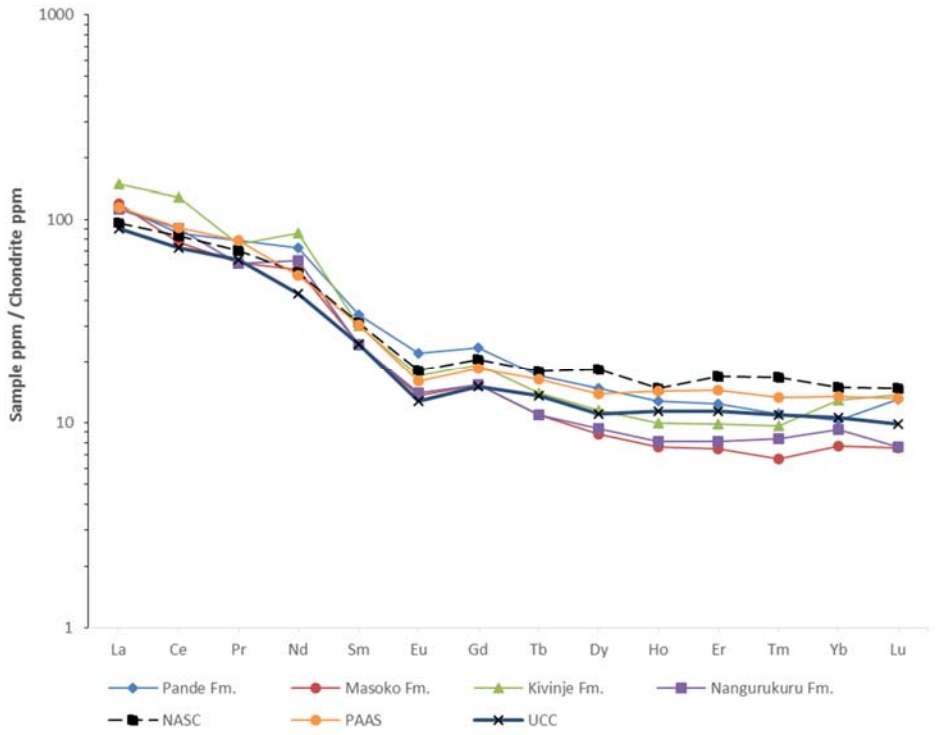

Figure 5.4.1 – Average c*hondrite-normalized REE values for the Kilwa Group clays. Chondrite values from McLennan et al. (1980).*

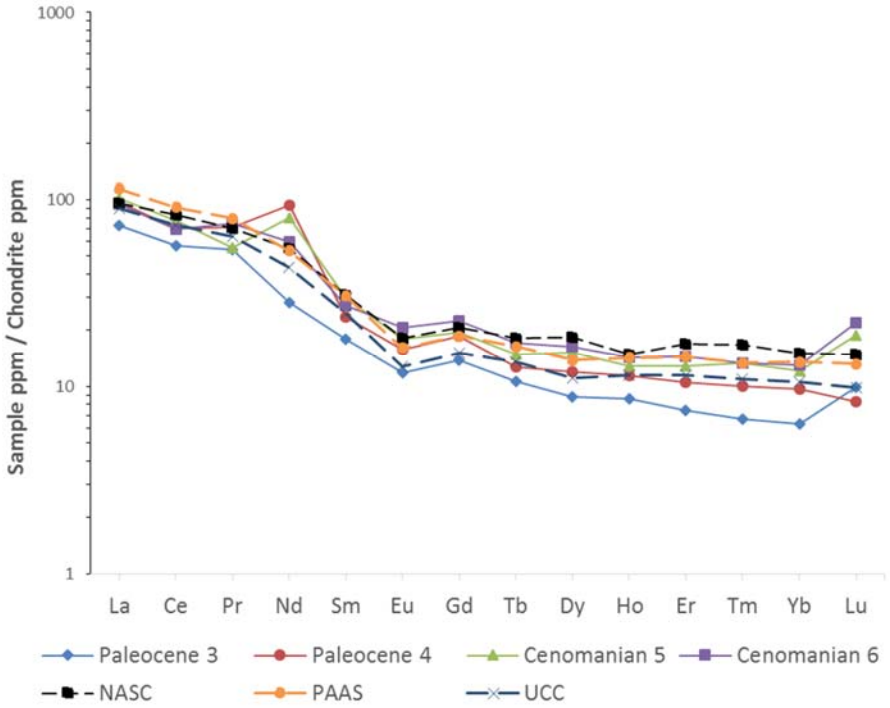

Figure 5.4.2 – *Average chondrite-normalized REE values for the Statoil clays. Statoil 3 and 4 sample are from Paleocene, while Statoil 5 and 6 are from Cenomanian.*

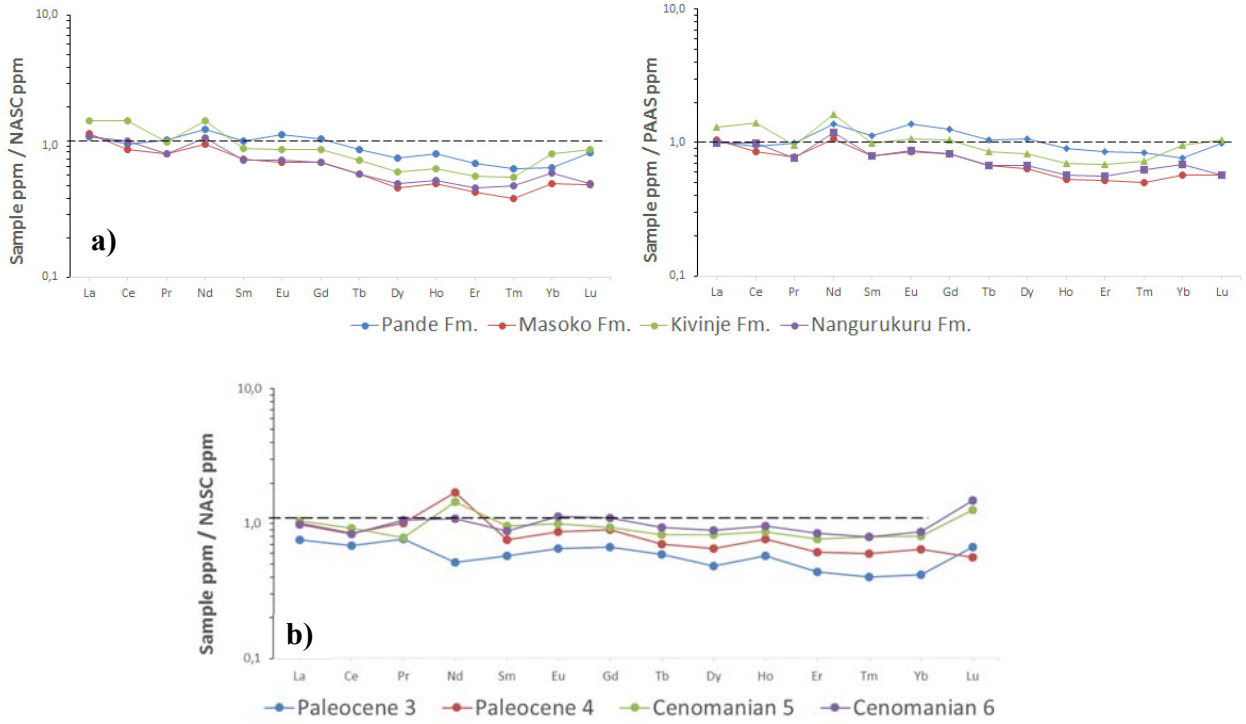

Figure 5.4.3 – *NASC and PAAS normalized average values of Kilwa Group (a) and NASC normalized Statoil clays (b). Average NASC and PAAS values from McLennan et al. (1980). Values greater than one indicate sediments are enriched with respect to the NASA or PAAS and those less than one indicate the elements are depleted.*

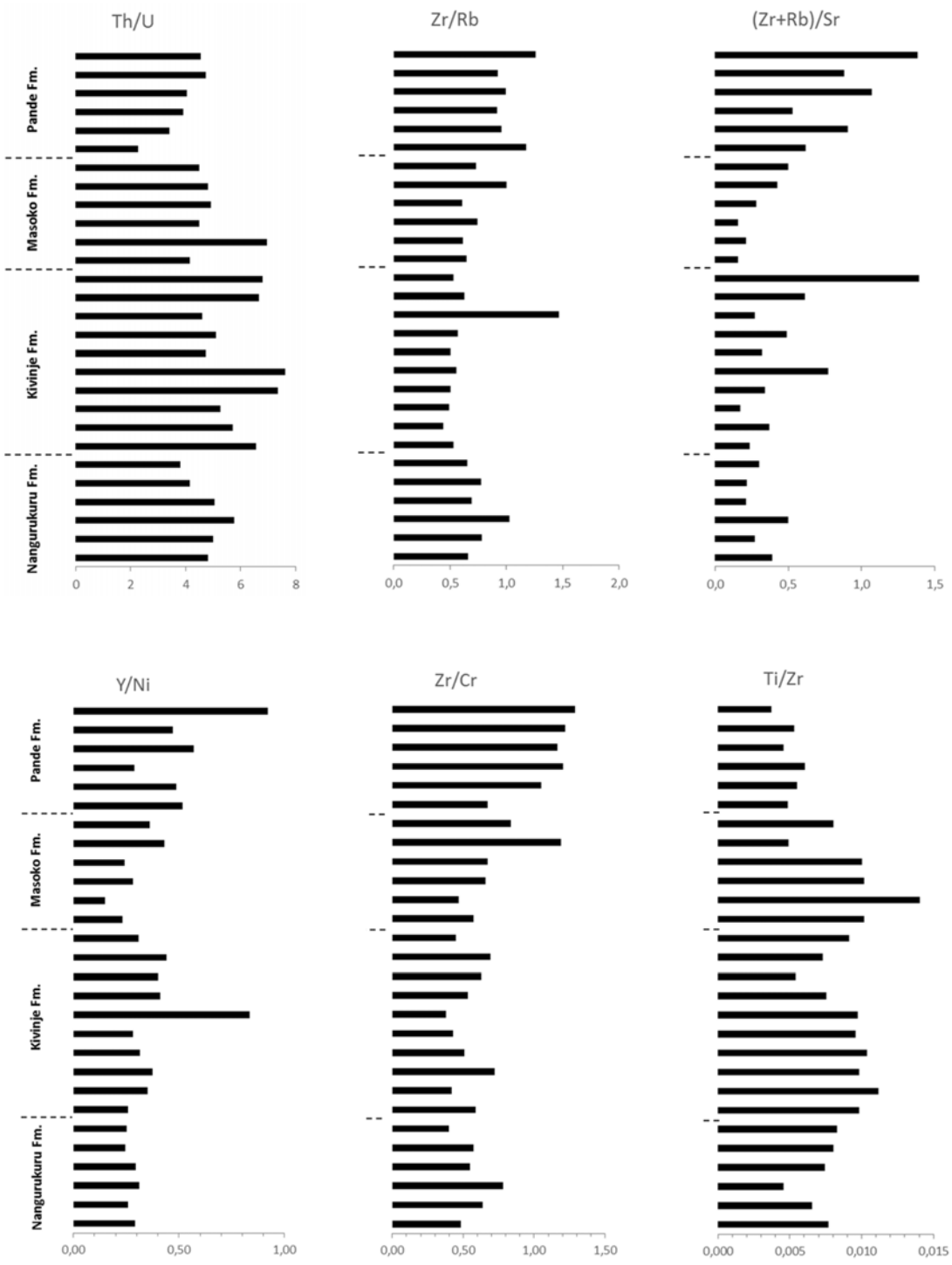

Figure 5.4.4 – *Stratigraphical variations in the Th/U, Zr/Rb, (Zr + Rb)/Sr, Y/Ni, Zr/Cr and Ti/Zr ratios in the Kilwa Group. For illustrative purposes the data is presented in a continuous trend although a possible unconformity may exist between Nagurukuru (Late Cretaceous) and Kivinje (Late Paleocene) formation.*

Average Th/U ratios of present day continental crust is around 4.25-4.30. For the upper and lower mantle the ratios are 2.6 and 3.8 respectively (Paul et al. 2003) (Fig. 5.4.5). Some of the samples from Pande Formation are characterized by low Th/U values, with similar values of lower and upper mantle. The rest of the samples have equal or greater Th/U values than 4. Kivinje Formation has the highest Th/U ratios, greater than 5.

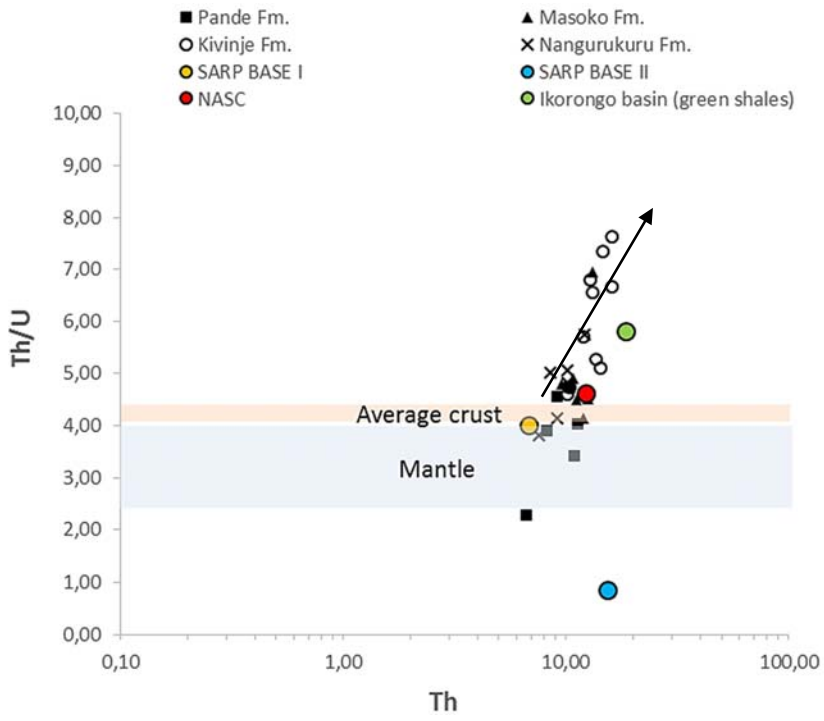

Figure 5.4.5 – *Plot of Th/U ratio versus Th abundance for the Kilwa Group clays. The arrow shows a general high weathering trend of sediments derived from UCC (McLennan et al 1993). SARP BASE I & II values are from basement samples of Tanzanian Craton (Archean) in Dodoma area. Data source from Fossum (2012). NASC values from McLennan et al. 1980.*

The La-Th-Sc triangular plot (Fig. 5.4.6) shows variation of the elements La, Th and Sc. The data for the studied samples show very low scattering, and fall within mixed source field close to UCC, felsic volcanic rocks and greywacke values.

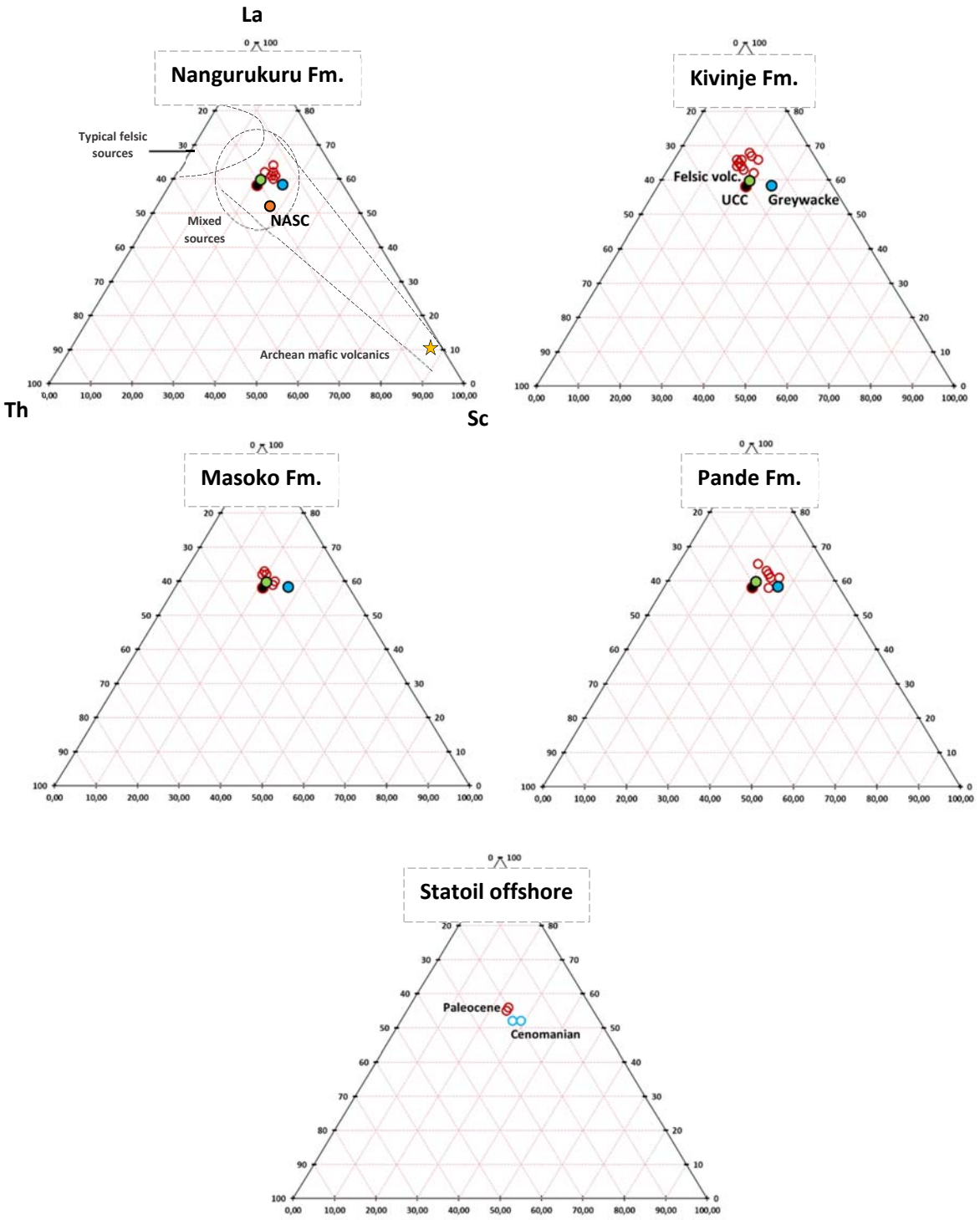

***Figure* 5.4.6 –** *Ternary plot showing the geochemical relationship between the compatible Sc and incompatible elements Th in Nangurukuru, Kivinje, Masoko and Pande formations. Offshore Statoil samples also shown in the lower plot. UCC (black circle), Paleozoic felsic volcanic rocks (green circle), greywacke (blue circle) and NASC (orange circle) values from Condie 1993. The restricted field for the mixed sources, mafic volcanic and felsic data from Taylor and McLennan 1985.*

6. DISCUSSION

6.1. FACIES ASSOCIATION INTERPRETATION

Previous geochemical, lithological and biostratigraphic studies in the Mandawa Basin (Pearson et al., 2004, Pearson et al., 2006, Nicholas et al., 2006; Jeménez Berrocoso et al., 2010 and Hudson, 2011) showed that the Kilwa Group was deposited in a mid to outer shelf environment across a passive margin. Due to excellent preservation of planktonic foraminifer shells (Fig. 6.1.1), significant results have been achieved by these authors on palaeontological and palaeoclimatological issues. Based on the planktonic versus benthic (P:B) foraminifers values, slight variations in water depths during deposition of the clays in the Kilwa Group can be envisioned. This change in water depth is especially noticeable in the upper Pande Formation, where significant shallowing may have been present in the Early Oligocene. Pearson et al. (2004) suggested that this shallowing was related to the growth of the Antarctic ice cap and the related eustatic sea level drop. The shallowing trend is reflected in a generally coarser lithology of the Pande Formation, compared to the underlying formations. A possible shelf-wide unconformity exists between the Lower Oligocene and Miocene. This change in facies, from Lower Oligocene clays to overlying Miocene clays, may be present in the upper ~10 m of Pande Formation (Fig. 5.1.2).

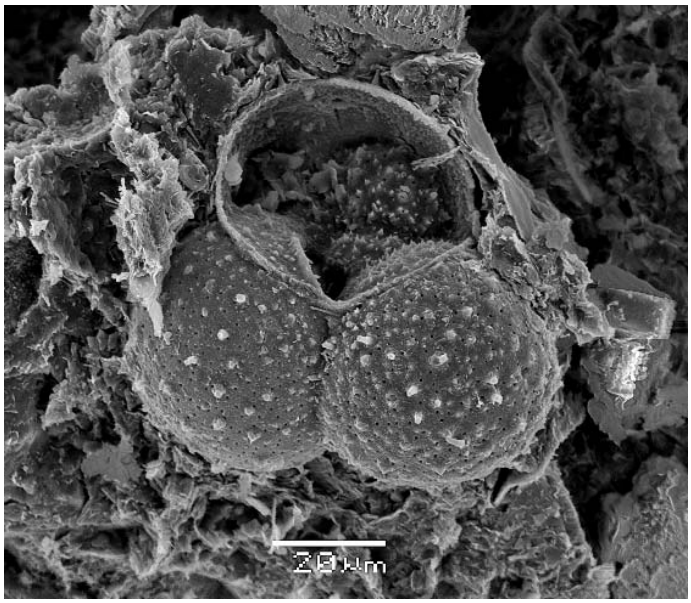

Figure 6.1.1 *– Planktonic foraminifer from Masoko Formation (TDP 2) from SEM. The sample is from ~ 77 m (Fig.51.2).*

FA-a: Marine claystone

The clay and claystones of the Kilwa Group often exhibit parallel lamination and small burrows. No sedimentary structures produced by wave and tidal processes are observed, which could indicate deposition below the storm wave base (Reading, 1996). The generally small grain size and

the presence of lamination indicate relative low-energy conditions. Similar characteristics can also be observed in shallow water, e.g. lagoonal deposits. The P:B values are generally high, which reflects more distal and deep marine setting (Pearson et al., 2004). Thin carbonate and siliciclastic units, which can can range in thickness from a few millimeters to ~10cm, often punctuate these claystones (Fig. 5.1.1 and Fig. 5.1.2). The coarser unites consists of allochthonous material, e.g. larger benthic foraminifers (Fig. 5.1.3d) and plant material, and is interpreted to be stirred up by storm events and induced by density currents. An open mid to outer shelf environments is therefore proposed, where majority of the fine-grained material settle from suspension fall-out and possible from low-density turbidity currents (Dalrymple and James, 2010).

FA-b: Nummulitic limestone and slump breccia beds

Facies association FA-b is observed in both in Masoko and Kivinje formations (Fig. 5.1.1 and 5.1.2). Typical lithology for FA-b is limestone (calcarenite) beds and matrix supported slump breccia packed with great numbers of large benthic *Nummulites,* up to 5 cm in diameter. Clay deposits with well-preserved lamination separate these limestone beds. The Nummulitic limestone beds, found in middle and upper Masoko Formation (Fig. 5.1.2), display a normal grading and cross-lamination sedimentary structures (Fig. 5.1.4a). Rip-up clay clasts are observed in both the breccia and limestone beds (Fig. 5.1.4b). These sedimentary features may suggest FA-b to be deposited on a carbonate slope (apron), probably on the lower part of the slope. Based on these assumptions, higher-energy environments in the shallow waters may have reworked the carbonate sediments by wave and storm action, which later could have redeposited n deeper water by the distinct turbiditic pulses (Dalrymple and James, 2010).

Studies by Pearson et al. (2004) and Pearson et al. (2006) showed high P:B values during the deposition of FA-b, which may indicate a rise of sea level during this period, especially during deposition of the Masoko Formation. In the same papers, it was proposed that a possible fault could have developed during deposition of the limestone horizons. A stratigraphic gap of the microfossil assemblages, and incline bedding was observed in Masoko Formation. This fault may have been one of the triggering mechanisms of the turbidites. Similar faults may also have been present during the deposition of the slump breccia at the base of the Kivinje Formation.

FA-c: 'Nereites sandstones'

The FA-c facies association is only observed in the Nagurukuru Formation (Fig. 5.1.1). The sandstone beds observed in this facies association are characterized by having a sharp bounding surface, often irregular (Fig. 5.1.5d). These sandstone beds also feature prominent sole marks on their basal sufrace, ripples at the top of the beds, vertical burrows and grazing trails (Fig. 5.1.5a,b). The latter can be assigned to the Nereites ichnofacies. These thin 'Nereites sandstone' units (cm scale) are divided by parallel laminated clays, which may have been deposited during more stable and quite conditions. The features in FA-c is consistent with deposits from turbiditic currents, possible from finer distal part of the turbidites, in relative deep waters (MacEachern et al., 2010).

FA-d: Sandstone and clay rich deposits

The relative coarser nature of the facies in Pande Formation compared to the underlying formations, may suggest deposition in a more shallow marine environment, possibly mid to inner shelf. Planktonic foraminifers are extremely rare or totally absent in this formation (Pearson et al., 2004). Terrestrial plant fragments were frequently observed, which might suggest a relative proximity to the shore compared to the units below. Fa-d starts with clays at the base, with presence of siderite bands (Fig. 6.1.2b) and large limestone concretions (Fig. 5.1.6d). From the bulk XRD analysis and core log analysis, the lowest sample of the Pande Formation contains large content of siderite (Fig. 5.3.10 – sample c1_1.45). The sporadically observed soft sediment deformation structures in this formation may indicate high sedimentation rates or movements on the delta slope. This, together with the limestone concretions (Fig. 5.1.6d), may indicate a prodelta or interdistributary bay deposit (Fig 6.1.2). The sandy coquina layers found in this formation may suggest delta shifting positions and more high-energy marine conditions took over (Fig. 5.1.6b).

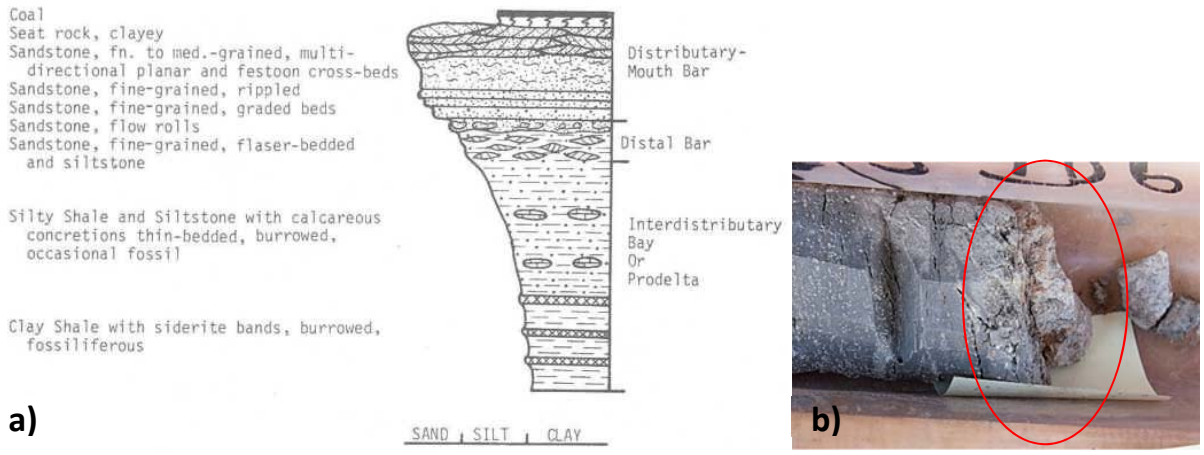

Figure 6.1.2 *– **a)** Coarsening upwards delta sequence, with siderite bands at the base and calcareous concretions further up. Figure from Horne et al. (1978). **b)** Siderite band at the base of Pande Formation ~ 1.45 m (Fig. 5.1.1).*

6.2. PETROGRAPHY

Sediment composition is an important source of information that may shed light on depositional conditions, basinal development and provenance. The final composition is often the result of a combination of different factors, e.g. weathering, reworking of the rocks and sediments, sedimentation, tectonics of the area and diagenesis.

The combined ~ 1 km thick, rather homogeneous appearance of the Kilwa Group, displays subtle variations both in the mineralogical and geochemical bulk composition. The excellent preserved microfossils and the very low thermal maturity (Pearson et al. (2004), and this study, see Appendix 7), suggest that the sediments in Kilwa Group were never deeply buried.

Carbonate minerals

Typical carbonate content in the clays within the Kilwa Group clays below 20%. In the coarser lithologies the carbonate content varies extensively. The calcite is usually present as carbonate grains, e.g. foraminifers and calcareous nannofossils transported from the shallow shelf, but could also be early diagenetic cements seen in the periodically thin sandstone and limestone layers. Sources of possible calcite cement in these sandstone units falls into two categories relative to the sandstone: internal and external (Bjørkum and Walderhaug, 1998).

Internal sources are those found within the sandstones, i.e. biogenic carbonate (Bjørkum and Walderhaug, 1990). The transportation of dissolved calcite (aragonite or high-Mg calcite) in the sandstone will usually be over a short distance by diffusion and reprecipitate as calcite cement. Bjørkum and Walderhaug (1990) estimated the distance to be around few mm to meter range. The presence of aragonite in the Kilwa Group samples assent to XRD-bulk analysis. During the core logging possible aragonite shell fragments were observed (Fig. 5.1.3e). Another possible source of the observed calcite cement is transportation of CO_2 into the sandstones from external source. If Ca^{2+} is present in the sediments, e.g. from dissolved plagioclase, it might react with the CO_2 and form calcite cement. Bjørkum and Walderhaug (1998) argued that the initial amount of available plagioclase in calcite cemented sandstones is very small or totally absent.

External sources of calcite are those outside the sandstone in which the calcite cement forms. Large volume of fluid is necessary to supply enough dissolved calcite. Generally the water flux and transportation distance for these sources of calcite are high. To precipitate one pore of calcite cement, there has to be at least 100,000-300,000 pore volume exchange (Bjørkum and Walderhaug, 1990). Therefore, some sort of meteoric water flushing is needed to supply the large amount of water. Since the meteoric water tend to be undersaturated with respect to calcite and all other minerals, it will remove calcite from the system instead of supplying it (Bjørlykke and Jahren, 2010). The amount of water available, height of the precipitation area over the sea level, and permeability are some of the limiting factors controlling the depth of the flow.

External sources are unlikely to have supplied the calcite to the sandstone units, since large amounts of water is needed to flush through the sandstones. The low permeability of the thick clay units and the relative long distance to the outer shelf, could represent some of the restricting factors for external source of calcite cement. It is possible to assume that the density currents could have been the main transport mechanisms of the organic material to the deeper waters.

A particular characteristic of the Kivinje Formation clays is a secondary recrystallization feature commonly known as fibrous calcite (‘beef’ and ‘cone-in-cone’ textures) (Fig. 6.2.1) (Marshall, 1982; Martinez, 1994). The fibrous calcite is not part of the original beds but is a postdepositional phenomenon (Kolokol'tsev, 2002). The overburden pressure build up, and the action of carbon dioxide in a nonuniform dissolution of calcite may result in formation of these conical shaped aggregates of fibrous calcite crystals (Tarr, 1922; Tarney and Schreiber, 1977). The growth of these

cone features forces the sediments away from the growing crystals (displacive growth), and is thought to have formed while the surrounding clay material still were plastic (Gilman and Metzger 1967; Franks, 1969). Another hypothesis suggest that the origin of fibrous calcite may had an initial aragonitic composition. The transformation of aragonite to calcite result in an increased volume ≥ 8%, which could lead to pressure growth, and cone shaped aggregates (Kolokol'tsev, 2002).

Figure 6.2.1 *– Fibrous calcite observed in thin section from Kivinje Formation (Fig. 5.1.1 ~ 54 m).*

Siliciclastic minerals

The sandstone units within the claystones are mostly arkosic, consisting of quartz, feldspar, occasionally clay minerals, and relative high content of calcite. No lithic fragments were observed in these sandstones during microscopic studies. Monocrystalline quartz is the dominant mineral in all samples (Table 5.3.1). Polycrystalline quartz is more frequently observed in the lower three formations in the Kilwa Group, which may suggest a metamorphic influx, with possible gneiss and schist sources (Blatt, 1967). These type of rocks are present in the Usagaran System in Tanzania from Proterozoic period (Fig. 2.1.3). The monocrystalline quartz is thought to derive from more plutonic sources. The common textural features observed by thin sections analysis of the sandstone units are:

- moderate to poorly sorting,
- mainly subrounded to subangular framework grains
- matrix supported.

Based on these observations, the textural maturity of the sandstone units can be classified as submature (Folk, 1954).

The K-feldspar/plagioclase ratios, and quartz/total feldspar ratios are generally higher in younger Pande Formation compared to the underlying formations. Plagioclase weathers more rapidly, and is destroyed easier than K-feldspar and quartz (Nesbitt and Markovics, 1997; Nestbitt et al., 1996; Culler, 2000). This may suggest more rewashing and sorting of the preexisting sediments or more intense weathering.

Clay minerals

Mudrocks and shales are in general volumetrically the most common of all sedimentary rocks in the sedimentary basins (Bjørlykke, 2010). Field observations or thin sections, the fine grained siliciclastic sediments rarely display clear sedimentary structures, that is commonly observed in coarser clastic successions. The application of geochemistry, various spectroscopy methods, X-ray diffraction, and scanning electron microscope techniques may provide valuable information on the provenance, basinal development, and diagenetic processes of the clays and claystones.

Raman spectroscopy was tried to differentiate the clay types. Due to high bioluminescence, i.e. high carbonate content in the samples, this method did not produce any useful results.

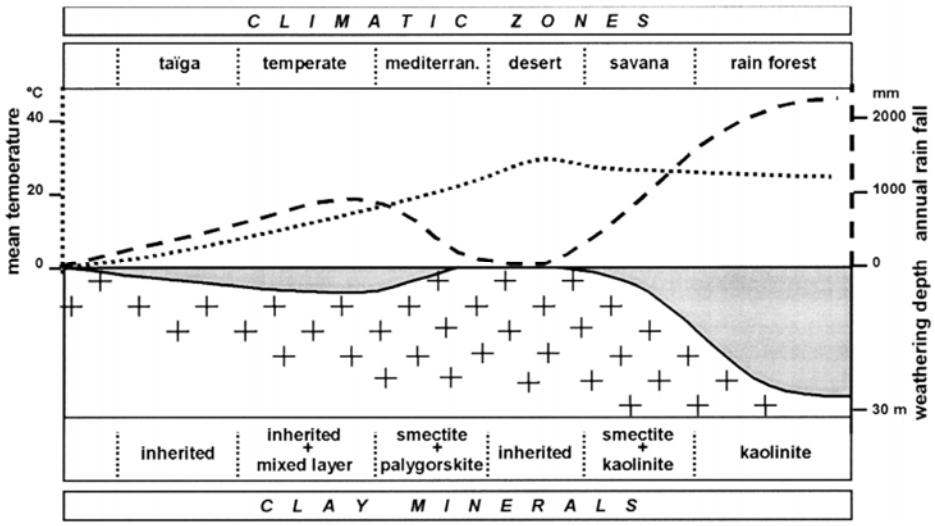

Figure 6.2.2 *- Diagram showing the distribution of the different clay minerals relative to the temp-erature, precipitation and climatic zones (from Thiry, 2000).*

The origin of clay minerals in sedimentary rocks are a product of weathering in the source area, physical sorting and chemical modification during transport and deposition, and diagenesis (Agha et al., 2013). Some clay material are also produced by hydrothermal processes (water-rock interaction at temperatures of 100-250^{o}C). Clay minerals in marine sediment can be useful indicators of paleclimatic conditions (Singer, 1984). The type and intensity of weathering, being physical or chemical, is the result of climate, lithology and morphological setting. Chemical weathering is considered to be the most important weathering mechanism of the clay minerals (Chamley, 1989; Potter et al., 2005). The distribution of clay minerals is often related to temperature, precipitation and climatic zones (Fig. 6.2.2) (Thiry, 2000). In areas with high temperatures and high precipitation, the weathering will be intense and fast. In more arid areas, e.g. deserts, the weathering will proceed at a much slower rate, since the chemical reactions are dependent on water.

Kaolinite is considered to form in soils in areas with high rainfall, steep relief, good drainage and warm climate (Potter et al., 1980, Chamley, 1989; Galán, 2006) (Fig. 6.2.2). However, it is important to note that kaolinite is not only present at the lower latitudes. It is also found e.g. in Artic sediments, as reworked products from adjacent landmasses (Chamley, 1989). Typically, kaolinite may form from almost all type of igneous, metamorphic, and sedimentary rocks under wet tropical climate (Chamley, 1989; Galán, 2006; Agha et al., 2013). Kaolinite may be the result of early diagenetic dissolution of feldspar:

$$\underset{\textit{Orthoclase}}{4K(Na)AlSi_3O_8} + \underset{\textit{Hydrogen ion}}{4H^+} + \underset{\textit{Water}}{2H_2O} \rightarrow \underset{\textit{Potassium ion}}{4K^+} + \underset{\textit{Kaolinite}}{Al_4Si_4O_{10}(OH)_8} + \underset{\textit{Quartz}}{8SiO_2}.$$

If the reaction products are not removed from the system by e.g. meteoric flushing, this reaction process will cease (Lanson, 2002). In porous sediments with sufficient meteoric flushing, authigenic kaolinite often grows in pore spaces in shape of small booklets (Pe-Piper et al., 2005).

In areas with seasonal climates, with pronounced dry seasons and poor drainage, smectite and irregular mixed-layer illite-smectite clays will usually form (presuming presence of K-bearing minerals such as K-feldspar and muscovite commonly found in granites), while the Fe-rich smectite forms easily from basaltic material (Gardner et al., 1980; Chamley, 1989; Galán, 2006). Illite can be an inherited directly due to mechanical erosion of K-rich minerals during weathering of acidic

or metamorphosed rocks in cool or arid regions (Galán, 2006; Agha et al. 2013), or form during diagenesis through transformation of smectite → mixed-layered illite-smectite → illite (Bergaya et al., 2006). Muscovite is the end product of the diagenesis of illite, but can also be found as detrital product in unaltered shales (Potter et al., 1980). In similar, cool or arid regions, chlorite may also be the dominant product of the clay mineral assemblage (Chamley, 1989). This is due to chlorite being very sensitive to weathering and therefore rare in humid regions. Chlorite is also considered a stable detrital product, where mechanical weathering prevails (Singer, 1984). Both K-feldspar and muscovite were observed during thin section and XRD-bulk analysis.

The random interlayered Fe-rich S-K is considered to be an intermediate stage in the progressive evolution from smectite to kaolinite (Srodon, 1999; Hong et al., 2012). This transformation of smectite to kaolinite generally indicate an increase in soil maturity (Vingiani et al., 2004). The formation of mixed-layer smectite-kaolinite is favored by subtropical and temperate climates, with distinct dry seasons (~3 months) (Delvaux and Heribillon, 1995; Srodon, 1999). Fe-rich S-K content is in good agreement with Fe-poor I-S content, showing similar trend upwards in the stratigraphy, which supports the formation of Fe-rich S-K in a semi-arid climate (Fig. 5.3.15). The presence of both Fe-rich (i.e. in the mixed-layer S-K and S-V) and Fe-poor smectite, dispite both developing under semi-arid climate and poor leaching, suggests different source rock. The relative abrupt increace in Fe-poor smectite content between the Nagurukuru and Kivnje formation (Fig. 5.3.15), may be probably related to the missing Lower Paleocene deposits in the Kilwa peninsula.

Kaolinite is present in all the clay-fraction samples from the Kilwa group, with a noticeable increase in the Kivinje Formation (Fig. 5.3.15). The kaolinite content increases up to 32 wt.% of the clay-sized fraction. The XRD-bulk estimations of the same sample (c7B_43.60) also revealed a slight increase in kaolinite content compared to the rest of the samples (Fig. 5.3.4). Pearson et al. (2006) suggested the possible Paleocene/Eocene thermal maximum (PETM) boundary close to this interval based on nannofossils. The climate conditions for kaolinite formation may have been suitable, with increased temperature and precipitation (Röhl et al., 2000, Sluijs et al., 2008). This onset of possible wet tropical climate is reflected by the decrease in Fe-poor smectite, Fe- and K-rich I-C and Fe-poor I-S content (Fig. 5.3.15). Subsequently, where the kaolinite content decreases and Fe- and K-rich I-C and Fe-poor I-S increases, may suggest return of semi-arid conditions. SEM analysis revealed possible authigenic kaolinite as small booklets (Fig. 5.3.15). Gundersveen (2014)

found these pore-filling kaolinite booklets in the pre-Kilwa Group porous sediments. Since the kaolinite booklets were found in low permeable Kilwa Group clays, the neoformation of kaolinite seem unlikely.

The relative abundance of clay minerals in sedimentary basins may be influenced by physical sorting during transportation by rivers and mixing of river and marine sources (Chamley, 1989; Galán, 2006). Due to size segregation of different clay minerals or differential flocculation (chemically induced aggregation), the relative abundance of clay minerals from coastline to open waters follow a typical lateral distribution: kaolinite, illite, and then mixed-layer I-S and smectite (Chamley, 1989; Agha, 2013). Nicholas et al. (2006) identified twelve minor sequence cycles of transgression and regression in the Kilwa Group. Based on this, the observed increase in the smectite content relative to kaolinite, I-S and I-C, could indicate marine transgression, i.e. landward input of clays (Fig. 5.3.15). For example, the opposite trend observed in the middle Pande formation, where the smectite is less abundant than Fe-poor I-S and Fe- and K-rich I-C, may be related to a regressive stage (Fig. 5.3.15). The presence of the coquina unit, and relative decrease in the clay content observed in this interval (Fig. 5.3.10 – sample c1_34.25 to c1_44.70), may accentuate to a seaward migration of the shoreline.

The relative low overburden, excellent preserved microfossils, uniform and continual subsidence across the margin (Pearson et al., 2004, 2006; Nicholas et al., 2006), very low thermal maturity and the friable (crumbly) nature of the Kilwa Group clays (e.g. Fig. 5.1.3c, d), indicate that deep burial seems highly improbable. Therefore the conversion of smectite to illite via burial is unlikely. This may be supported by the absence of ordered mixed-layered illite-smectite in the samples may support this (Lindgreen and Hansen, 1991).

Authigenic Fe-rich smectite-vermiculite may be formed as intermediates during the alteration of chlorite to kaolinite under non-oxidizing, moderately acid (pH 3.5 – 4.5), or possibly alkaline conditions (e.g. from altered basement rocks) (Craw, 1984; Craw et al., 1995).

6.3. TRACE ELEMENTS

The distribution of trace and rare earth element in the analyzed clays may give information on the possible provenance, depositional conditions, diagenetic history and weathering (McLennan et al.

1993). The discussion of trace element geochemistry and its origin in the Kilwa Group will constitute the main part of this discussion. Last, comparable aspects will be attempted in connection with the Statoil offshore clay samples.

Zr/Rb, (Zr + Rb) / Sr ratios

Trace elements may also be a good indicator of grain size variations and reflect compositional variations. Zr/Rb ratios can be used to interpret grain size, while (Zr + Rb)/Sr values reflect variations in ratio between siliciclastics and carbonates. Higher Zr/Rb ratios reflect more coarse grained units, while lower ratios in more clayey lithologies (Dypvik and Harris 2001). Sr is generally associated with (biogenic) carbonates. Low (Zr + Rb) / Sr values usually reflect carbonate rich units (Taylor and McLennan, 1985). In the Kilwa Group, the Zr/Rb ratios are relatively high in the Pande Formation compared to the underlying formations. This reflects the coarser lithology of the formation, which is observed both in the cores (Fig. 5.1.2) and in the XRD-bulk analysis (Fig. 5.3.10). The lower Zr/Rb and (Zr + Rb) /Sr values in Nangurukuru, Kivinje and Masoko formation, suggest a more fine-grained, carbonate-enriched sediments compared to Pande Formation. The somewhat elevated Zr/Rb and (Zr + Rb)/Sr values in the lower section of Nangurukuru Formation (Fig. 5.4.4), is probably related to episodic turbiditic currents bringing coarser and organic rich material from shallow shelf areas.

Source rock composition

Trace element analysis can contribute to the characterization of clay provenance. Using trace elements, the original source area of the clays may be categorized based on the relative abundance of different elements. The different geochemical "signals" may give clues to different source terrains, e.g. mafic or felsic rocks. For example, Zr, Th and La are more abundant in felsic sources, but scarce in ultramafic and mafic rocks. Many studies have noted (e.g. Taylor and McLennan, 1985; Condie, 1993; Garcia et al., 1994; Graver et al., 1996; Roser et al., 1996; Ishiga et al., 1999, Potter et al., 2005) that high concentrations of Cr, Ni, Co, V, and Sc in fine-grained sediments reflect a more mafic/ultramafic rock in the source region.

A decrease in the silica content in the samples corresponds to an increase in the abundance of most other elements (Taylor and McLennan, 1985). In order to reduce the diluting effect, e.g. from calcite and quartz, when comparing the composition of the different formations in the Kilwa Group, several trace element ratios can be applied (Table 5.4.2). Higher Zr/Cr, Y/Ni, and lower Ti/Zr ratios generally indicate contribution from a felsic source, and may be used to quantify the proportion of mafic or felsic material in the source area (Ishiga et al., 1999). The ratios can be altered due to weathering, transport and diagenesis.

From Figure 5.4.4, the geochemical indices show a gradual increase in Zr/Cr and Y/Ni, and decrease in Ti/Zr ratios from Nangurukuru to Pande formation. This may suggest an increase in felsic supply upsection due to relative enrichment of Ti, Ni, and Cr in mafic rocks. However, the variations in concentrations of these metals could be related to enhanced survival of abrasion-resistant minerals (e.g. zircon and apatite) rich in Zr and Y, compared to less stable mafic phases (e.g. pyroxene and amphiboles) rich in Ti, Cr, and Ni (Ishiga et al., 1999). Therefore, the higher Zr/Cr values observed in the youngest Pande Formation are most likely due to sediments in this formation containing more rewashed deposits. This is also reflected in higher abundance of quartz compared to feldspar (Fig. 5.3.10), which suggests more mature sediments. The increase and decrease of Ti/Zr ratios (Fig. 5.4.4) may be due to that Ti is generally more concentrated in the finer sediments (titanite and/or rutil) compared to Zr (Taylor and McLennan, 1985). Negative correlation ($r = -0.79$) can be observed be between Ti/Zr and Zr/Rb in the Kilwa Group, i.e. Ti/Zr is inversely related to Zr/Rb. For example, lower part of Nagurukuru Formation there is an increase in Zr/Cr and Zr/Rb, and decrease in Ti/Zr ratios (Fig. 5.4.4). This might corresponds to the facies association FA-c (Fig. 5.1.1), where the turbidites have transported coarser detritus from the shallow shelf areas to deeper waters.

Non of the samples, from Kilwa Group and offshore, show anomalous concentrations of Cr and Ni (Table 5.4.1). The samples indicate an irrelevant contribution of mafic and ultramafic sources. Garver et al. (1996) showed Cr/Ni values of about 1.4 in shale samples with ultramafic component, while ultramafic rocks have about 1.6.

In sandstones these ratios are typically higher than 3.0. Garver and Royce (1993) suggested that, Cr/Ni values higher than 1.6 could indicate a mafic origin (e.g. basalt and andesite). Although the average Cr/Ni ratio is 2.3 for the Kilwa Group, the values variate (Table 5.4.2). In the offshore samples, the Cr/Ni is somewhat lower, with average values of 1.25 (Paleocene) – 1.65 (Cenomanian). The Cr is moderately correlated with Ti in the Masoko Formation (correlation coefficient = 0.79). It is suspected that these sediments may reflect a small contribution of mafic volcanic rocks from the source area.

The Cr/Ni is highly correlated with Zr/Rb (correlation coefficient ≥ 0.8) in the upper three formation of the Kilwa Group (Fig. 6.3.1). This could be a result of fractionation in the sedimentary cycle, by which the Cr is preferentially concentrated in the coarser lithologies (Graver et al., 1996).

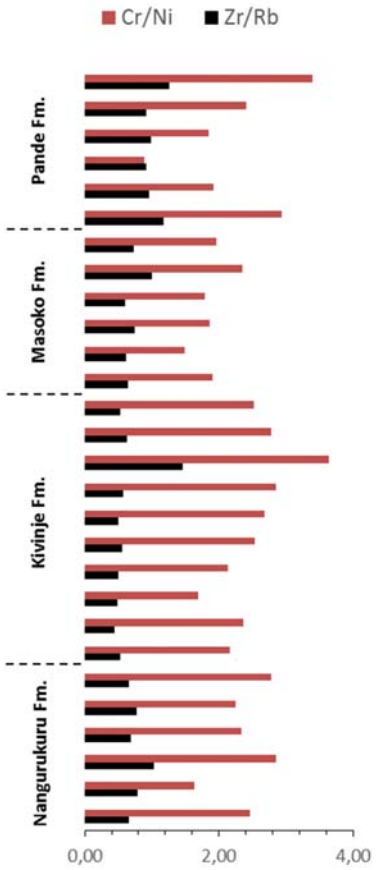

Figure 6.3.1 – *Cr/Ni and Zr/Rb ratios in the Kilwa Group clays.*

Rare Earth Elements

One of the most reliable indicators of sediment provenance is the REE patterns. They are highly resistant to fractionation during weathering and diagenesis and easily preserved in terrigenous sediments (Taylor and McLennan, 1985, McLennan, 1989, McLennan et al., 1995, Sethi et al., 1998; Potter et al., 2005). Due to nearly quantitative transfer of REE from source region to depositional site (largely as suspended rather than dissolved load), the terrigenous sediments should reflect the average composition of the source region (Condie, 1991; Graver and Scott, 1995).

Chondrite normalized REE patterns of the Kilwa Group clays show distinct enrichment in LREE, small negative Eu-anomalies, modest heavy-REE slop (Fig. 5.4.1), possibly reflect a granitic source region that derived from a garnet-rich lower crust (McLennan et al., 1993). Moreover, the relative enrichment of incompatible (e.g. LREE and Th) (i.e. elements which are not easily included in the crystal structure of rock-forming minerals, but are concentrated in the residual liquid), over

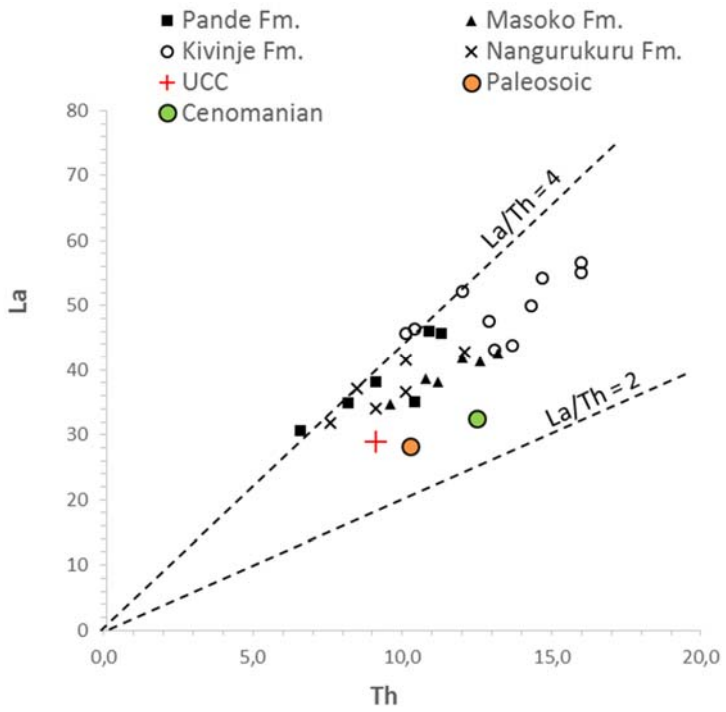

Figure 6.3.2 *– Plot of La vs Th in Kilwa Group and Statoil offshore clays (orange and green dots). UCC data from Condie (1993).*

compatible elements (e.g. HREE), indicate more felsic average provenance and a relatively severe weathering regime (Taylor and McLennan, 1985, McLennan et al., 1993). The relative felsic composition of the Kilwa Group clays are also reflected in the La/Th ratios (McLennan et al., 1980), which falls between La/Th = 2 and La/Th = 4 (Fig. 6.3.2). There is a clear correlation ($r > 0.85$) between La and Th, which is attributed to the coherent nature of these elements during, weathering, transport, diagenesis (McLennan et al., 1980).

Nerbråten (2014) showed high concentrations of garnet in samples from Nangurukuru (TDP 9) and Kivinje (TDP 7B) formations, with smaller concentrations in the two statigraphically overlying units. She also showed significant garnet enrichment in core samples from Mid-Cretaceous (TDP 24 and 21) (Fig. 4.1.2 – map for TDP locations). Microprobe analysis of garnets from the Kilwa Group (Nerbråten, 2014) and garnet analysis from the Mozambique Belt (Prochaska and Pohl, 1983), i.e. Usagaran System (Fig. 2.1.3), are very similar in composition (Fig. 6.3.3). This could reflect a garnet rich source.

In the heavy mineral assemblages of selected Kilwa Group samples (Nerbråten, 2014), zircon was observed in all Kilwa Group samples with varying concentrations. Large concentration of zircon was also observed in the Masasi basement sample (BA-1-13) (Nerbråten, 2014). The strong

correlation of Zr and Hf (≥ 0.9) and Zr/Hf ratios of 35 to 36 in the Kilwa Group clays (Table 6.3.1), close to that of zircon with Zr/Hf ratio of 39 (Murali et al., 1983), suggest that these elements are housed chiefly in zircons (Condie, 1991).

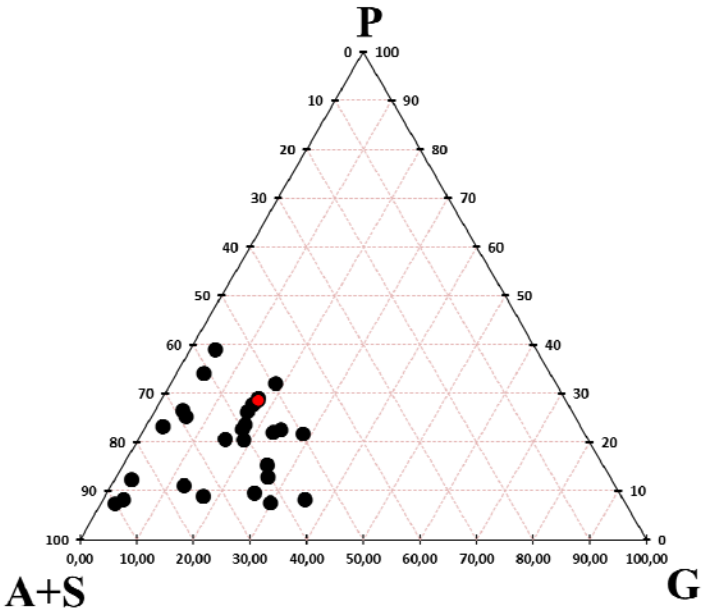

Figure 6.3.3 *– Example of garnet composition showing the Mozambique Belt garnet sample (red dot), having the similar composition as samples from Pande Foramtion. Pyrope (**P**), Grossular (**G**), Almandine (**A**) and Spessartine (**S**). Ternary plot and data of Pande Formation from Nerbråten 2014. Data of Mozambique Belt from Prochaska and Pohl (1983).*

The Zr-La correlation is nonexistent in the Kivinje and Nangurukuru formations, and poor to moderate in the Masoko and Pande formations. This indicate that zircon may have some control on the distribution of La (LREE) in the two uppermost units. The distribution of LREE in the underlying units is most likely by a combination of minerals. However, the Nagurukuru Formation show relative moderate to high correlation between Zr-Yb (HREE) and Zr-Hf (Table 6.3.1). Studies have shown that significant portion of HREE are concentrated in zircons (Cullers et al., 1979; Gromet et al., 1984; Taylor and McLennan, 1985; Milodowski and Zalasiewicz 1991). Hence, it would appear that zircon probably constitutes a more important control on the HREE distribution in the Nagurukuru Formation compared to the other formations.

Table 6.3.1 – *Linear correlation coefficients of Kilwa Group clays.*

	Zr-Hf	Zr-La	Zr-Yb
Pande Fm	0,90	0,68	-0,18
Masoko Fm	0,99	0,72	0,67
Kivinje Fm	0,97	-0,27	0,53
Nangurukuru Fm	0,99	0,49	0,78

Redox conditions

The Th/U ratios can provide information of redox conditions in the waters (Taylor and McLennan, 1985, Jones and Manning, 1994, Dypvik and Harris, 2001). High uranium (U) values, U > 6 ppm, may indicate reducing conditions, i.e. anoxic sediments. This is due to reducing of soluble U^{6+} to much less soluble U^{4+} and precipitate as U compound (Taylor and McLennan, 1985, Anderson et al., 1989). Th/U values below 1 could be related to enrichment of U during deposition under reducing conditions (Dypvik and Harris, 2001). The relative low U content (< 3 ppm) and high Th/U values (Table 5.4.2) in the Kilwa Group and offshore clays, does not show any anomalously U enrichment relative to its crustal abundance (Table 5.4.1). Therefore, it is more likely that these values reflect the chemical composition of the source rock, since erosion and transportation of sediments typically occur under fairly oxidizing conditions at relative constant pressure and temperature (Taylor and McLennan, 1985).

The enrichment of Co, Cr, Ni, and V in the host sediments relative to their crustal abundance may be related to anoxic conditions (Calvert and Pedersen, 1993; Dypvik and Zakharov, 2012). The absence of significant metal enrichment of these elements in the Kilwa Group and the offshore samples, suggest that bottom waters were not anoxic during the deposition. However, the somewhat lower U, Cr, and V values in the offshore samples compared to the Kilwa Group samples (Table 5.4.1), may indicate slightly more oxidizing conditions during sediment deposition, where possible ocean currents are ventilating the water masses.

Study by Milodowski and Zalasiewicz (1991) showed that NASC normalized REE compositions in mixed turbidite-anoxic hemipelagites were highly enriched in LREE. Relative to NASC, Kilwa Group and offshore REEs display no pronounced enrichment in LREE (Fig. 5.4.3). This may be related to the oxic conditions observed by the elements previously mentioned.

Statoil offshore clays

In the Nagurukuru Formation (Late Cretaceous) the highest Zr/Rb and (Zr + Rb)/Sr ratios are 1.03 and 0.5 respectively, and found in facies association FA-c, rich in turbidites. At a time with much sediment transport from shallow shelf to deep waters. The Zr/Rb and (Zr + Rb)/Sr ratios (Table 5.4.1) of the Statoil Cenomanian clay samples are close to that of Nagurukuru Formation, which may indicate similar origin and depositional environment. In the offshore Paleocene samples the (Zr + Rb)/Sr and Zr/Rb ratios are somewhat lower compared to the Cenomanian ones (Table 5.4.1). The XRD-bulk quantification on one of the offshore Paleocene samples, done by PhD student Katrine Fossum (UiO), revealed this higher proportion of calcite and lower proportion of siliciclastic (Fig.6.3.4). Kilwa Group clay samples from similar period bears a close resemblance in mineralogical composition compared to the offshore samples (Fig. 5.3.4 - Late Paleocene and 5.3.1 - Late Cretaceous).

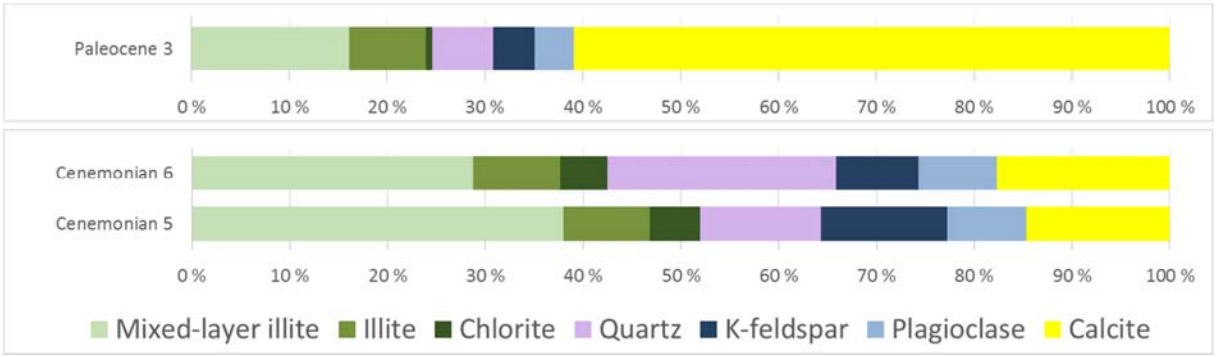

Figure 6.3.4 – *Quantitative representation of the XRD-bulk analysis of the Statoil offshore samples.*

Previous pre-Santonian extensional tectonics in the area (see Nicholas et al. (2007)), could have played an important role, when it comes to sediment transportation and the depositional conditions. The Th/Sc ratios also show resemblance between the onshore Kilwa Group and offshore Statoil samples (Table 5.4.2). McLennan and Taylor (1991) suggest that the Th/Sc ratio best reflects the overall bulk composition of the source area, i.e. provenance. This could mean that the sediment sources for both the onshore Nagurukuru and Kivinje Formation, and the offshore Statoil samples may have been comparable during deposition of these clays. More offshore samples are needed for

further analysis in order to get a better representation of the trace element distribution through time, and to get a better correlation with the onshore Kilwa Group.

Based on the data presented, and the somewhat lower U concentration in the offshore Cenomanian samples, a possible depositional model is suggested in Figure 6.3.5. Comparable scenario may be applicable during deposition of the Kivinje Formation and the offshore Paleocene.

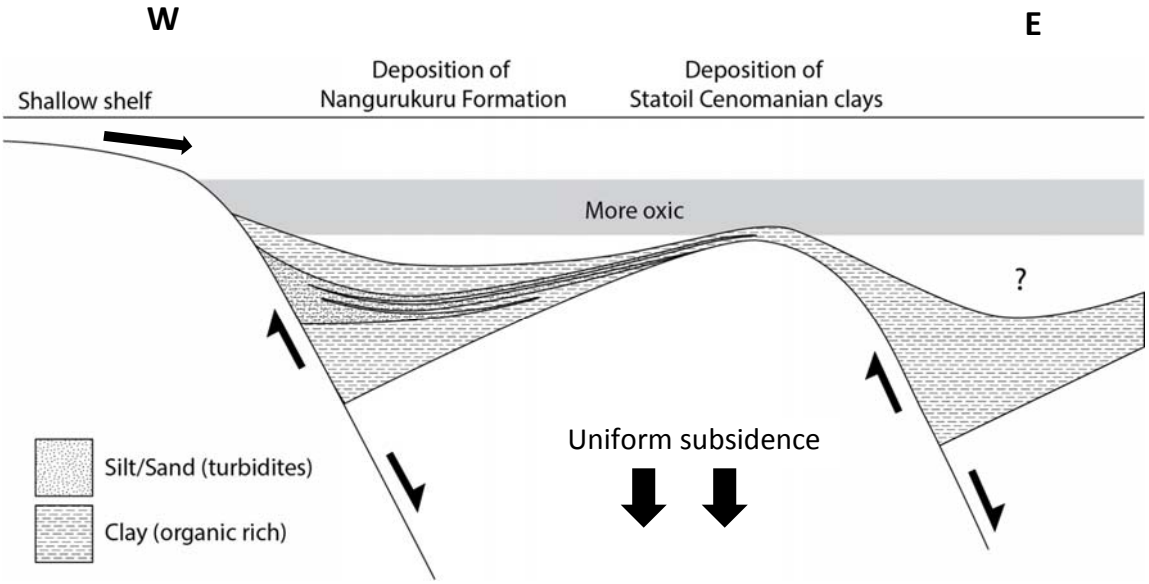

Figure 6.3.5– *Depositional model of the Nangurukuru Formation and Statoil Cenomanian samples.*

6.4. PROVENANCE

Late Cretaceous to Early Oligocene clay assemblages deposited across a passive margin show ubiquitous occurrences of several clay species in all of the Kilwa Group samples. These different clay species typically develop from various parent rocks, climate and weathering conditions. This suggest that Kilwa Group clay minerals could primarily be detrital alteration products of feldspars and muscovite. The basic lattice of the clay minerals is reasonably stable in most marine depositional environments (Weaver, 1958), reflecting primarily the nature of the source materials. Slight modifications (e.g., diagenesis) might occur in the different depositional environments. The potential source area of the Kilwa Group clays were probably located within the adjacent Tanzanian landscape, e.g. Archean Tanzanian Craton, younger crystalline rocks (e.g. Proterozoic Usagaran

System) and pre-Kilwa Group Mesozoic continental and marine sediments (Fig. 2.1.3). Nicholas et al., (2006) suggested that large palaeofluvial system might have been present between todays Rufiji to the north and Ruvuma to the south of the Mandawa Basin. The clay minerals These rivers could have been the transport mechanism of the weathered Kilwa Group clay minerals from the adjacent land.

The relative increase in the Fe-poor smectite in the Pande Formation (Fig. 5.3.15), may be attributed to weathering of exposed felsic volcanic rocks (e.g. rhyolites) in a poorly drained, low-lying landscape. This shift towards more felsic volcanic rock contribution in the Pande Formation may also be observed in the Th/Sc vs. Cr/Th plot (Fig. 6.4.1).

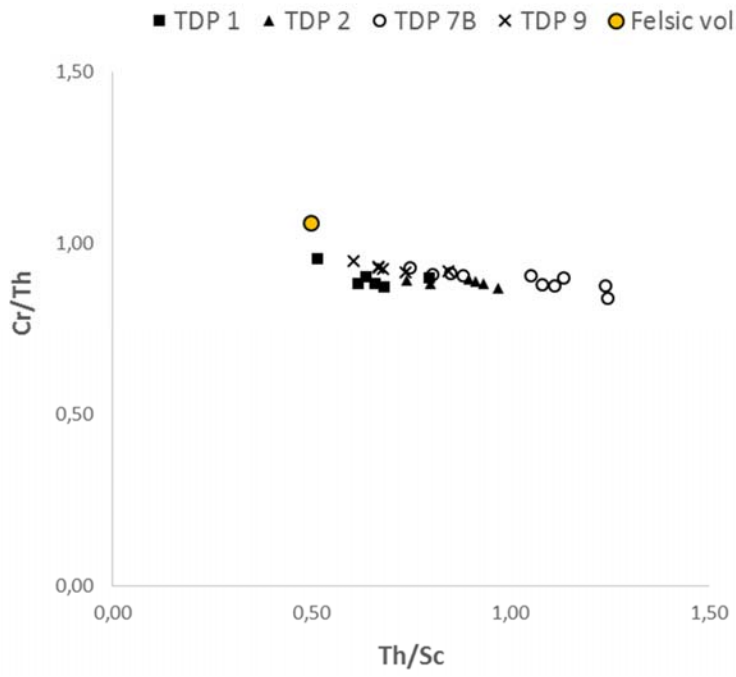

***Figure 6.4.1**– Th/Sc vs. Cr/Th plot (ppm) for the Kilwa Group clays. The average felsic volcanic rock values from Condie (1993).*

The exposed Proterozoic Usagaran System (Masasi basement spur) to the west of the Mandawa Basin (Hudson, 2011) (Fig. 6.4.2), is mainly of felsic composition, but also contains volcanic rocks, crystalline limestone, mica, schist, granulite and highly metamorphosed gneisses. This could be a potential source for the Fe-poor smectite and kaolinite, while the surrounding Mesozoic shales could be the sources of randomly interstratified illite-smectite minerals. Nicholas et al., (2006)

suggested that Masasi basement spur might also have been the source of the Kilwa Group clays during the ~55 Ma.

The observed Fe-rich smectite in the mixed-layer smectite-vermiculite and smectite-kaolinite reflect weathering of a basic rock. The basic source possibly came into existence because of uplift in the source area and exposed the basic sources. The presence of illite-chlorite mixed-layer clay may support this, since they are generally associated with altered low-to medium grade metabasalt, gneiss or granite (Srodon, 1999).

Both chlorite and illite collectively constitute ~11 % of the clay-fraction in the Nangurukuru Formation, and reduced down to ~ 2 % in the Pande Formation (Fig. 5.3.15). They are probably of detrital origin, e.g. from the Mesozoic fine siliciclastic sediments. However, the illite can also derive from residual mica, e.g. from the Masasi basement rocks west of the Mandawa Basin. No authigenic illite were observed during SEM analysis of the Kilwa Group clays. Authigenic illite can be recognized as elongated fibrous crystals (Lanson et al., 2002).

The weathering trend of UCC is shown in the Th/U ratio versus Th plot in Figure 5.4.4 for the Kilwa Group clays. Clastic sedimentary rocks related to the upper crust have Th/U values characterized to be equal or higher ratios than 4, whilst lower values are related to a mantle contribution (Paul et al., 2003). The Th/U versus Th values (Fig. 5.4.4) show similar values as NASC, Tanzania Craton (SARP BASE I) and green shales from Ikorongo basin in northern Tanzania. The Tanzanian Craton is unlikely to be a direct source of the Kilwa Group clays, due to the great distance between the source and deposition site (> 500 km). However, the continental and marine siliciclastic sedimentary rocks from the Mesozoic (Fig. 2.1.3) may contain weathered sediments from the Tanzanian Craton. These reworked Mesozoic sediments could potentially be one of the sources of the Kilwa Group clays. The mixed sources are reflected in both the clay minerals assemblages and trace elements (e.g. Fig. 5.4.6).

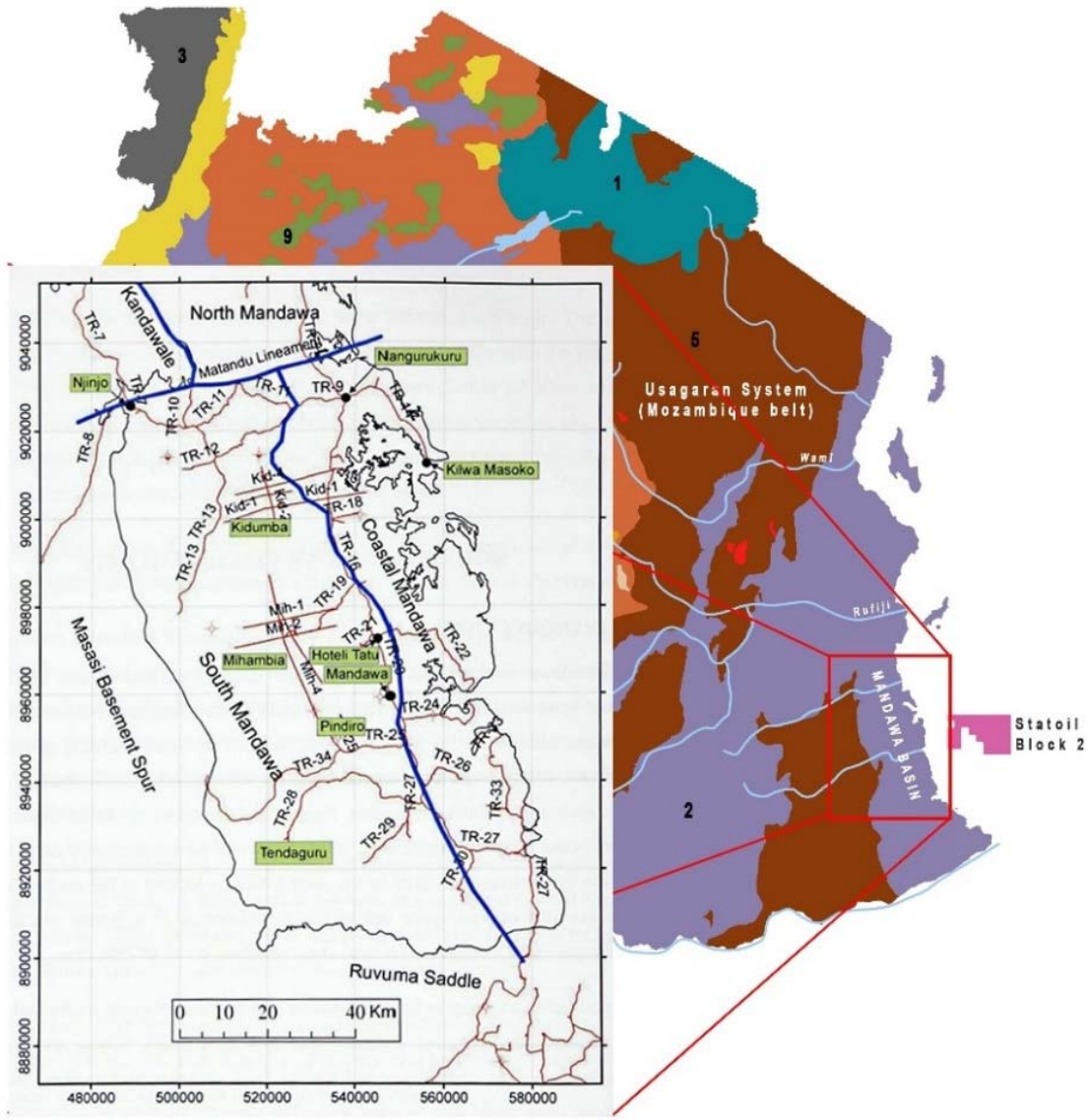

Figure 6.4.2 *– Close up geological map of the Mandawa Basin and Masasi basement spur to the west. From Hudson, 2012.*

7. CONCLUSIONS

The Kilwa Group represents a clay dominated succession that could have accumulated on the mid (possible inner) to outer shelf with periodically influx of shallow shelf detritus transported by density currents. The Kilwa Group facies suggests a quite shelf environment, below the storm wave base. Two main lithologies were observed in the Kilwa Group: dominated calcareous rich marine-clays, and limestones (e.g. Fig. 5.1.2 – TDP 2). Thin beds (cm scale) of carbonate cemented fine-grained sandstones and siltstones occur within the clays, often containing terrestrial plant material.

The bulk mineralogical composition and abundance of trace elements in the clays and claystones show evidence of subtle changes during deposition; changes reflecting sea level fluctuations, and climate changes. However, the presence of relative shallow marine facies in the uppermost Pande Formation compared to the deep-water facies in the units below, may have been caused by substantial regional uplift or eustatic sea level drop during Early Oligocene.

Detail analysis of the clay minerals revealed the possible origin of the Kilwa Group clays. The abundance variations of clay-fraction minerals in the Kilwa Group clay and claystones, show the importance of weathering as a major process contribution to variations in the clay assemblages. The clay minerals were developed from varied source rocks in different climate conditions. Abundant kaolinite reflects soil composition under humid tropical conditions, with intense weathering of igneous, metamorphic, or sedimentary rocks of the adjacent landscape. The Fe-poor smectite, illite-smectite mixed mineral and illite were derived from weathering of felsic sources, (e.g. Masasi basement crystalline rocks or the surrounding Mesozoic shales), favored by well marked dry season climate conditions. The decrease of chlorite upwards in the stratigraphy and increase in smectite indicates a change from colder to more humid, semi-arid climate.

The application of selected trace elements and REE analyses provides valuable information on provenance and basinal depositional conditions. The Kilwa Group clays display comparable composition with deposition of well-mixed material in oxygenated water masses. There are some minor variations within the formations, which generally reflect the geochemical differences in the source area, together with grain –size differences in the formations (e.g. Zr/Rb ratios). The chondrite normalized REE patterns further strengthen the predominance of felsic sources, which was observed in the clay mineral assemblages. However, the various source signals may have been

smoothed by transitional storage before the final deposition. Figure 7.1.1 propose a possible depositional environment of the Kilwa Group sediments.

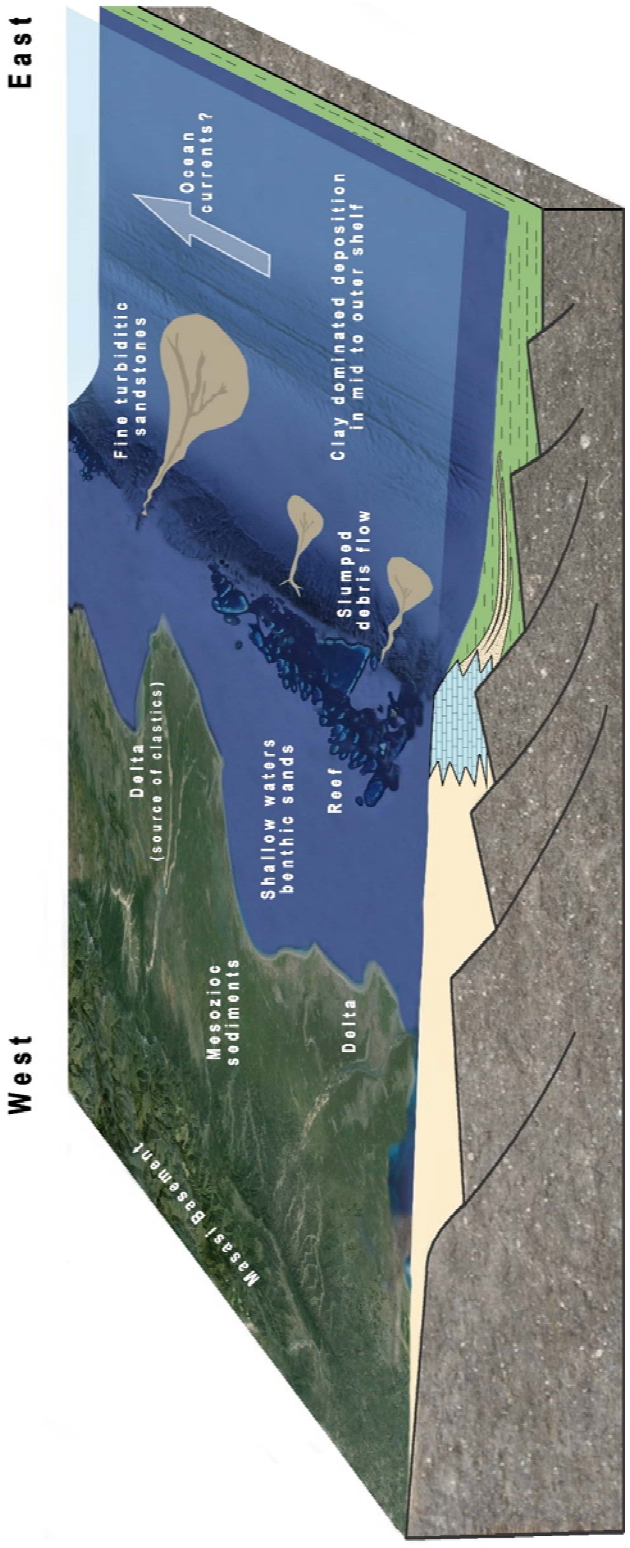

***Figure 7.1.1**– Shelf depositional model for the Kilwa Group clays. The deposition of the Kilwa Group clays took place across a passive margin, mid (possible inner) to outer shelf. Periodically influx of coarser, carbonate rich, detritus was transported from the shallow shelf area to deeper waters by turbiditic currents and debris flows. The weathered product of the adjacent Masasi basement and the surrounding Mesozoic sediments were most likely transported by major rivers during the deposition of the Kilwa Group.*

REFERANCES

AGHA, M. A., FERRELL, R. E., HART, G. F., EL GHAR, M. S. A., & ABDEL-MOTELIB, A. 2013. Mineralogy of Egyptian Bentonitic Clays II: Geologic Origin. *Clays and Clay Minerals*, *61*(6), 551-565.

ALLIED PETROLEUM CORP 2012. *Africa Geology*. Available at: http://alliedpetroleumcorp.com/africa-geology.html. (Accessed on Mai, 2014).

ANDERSON, R. F., FLEISHER, M. Q. & LEHURAY, A. P. 1989. Concentration, oxidation state, and particulate flux of uranium in the Black Sea. *Geochimica et Cosmochimica Acta,* 53**,** 2215-2224.

BERGAYA, F., THENG, B.K.G., AND LAGALY, G. 2006. Handbook of clay science: Amsterdam, Elsevier, XXI, 1224 s. p.

BISCAYE, P. E. 1965. Mineralogy and sedimentation of recent deep-sea clay in the Atlantic Ocean and adjacent seas and oceans. *Geological Society of America Bulletin*, *76*(7), 803-832.

BJØRLYKKE, K. (2010). *Petroleum geoscience: From sedimentary environments to rock physics*. Springer, 1st ed., 508.

BJØRLYKKE, K. & JAHREN, J. 2010. Sandstones and Sandstone Reservoirs. *In:* BJØRLYKKE, K. (ed.) *Petroleum Geoscience: From Sedimentary Environments to Rock Physics.* Springer 1st ed., 113-140.

BJØRKUM, P. A. & WALDERHAUG, O. 1990. Geometrical arrangement of calcite cementation within shallow marine sandstones. *Earth-Science Reviews,* 29, 145-161.

BJØRKUM, P. A. & WALDERHAUG, O. 1998. Calcite cement in shallow marine sanstones: growth mechanisms and geometry. *In:* MORAD, S. (ed.) *Carbonate cementation in sandstones distribution patterns and geochemical evolution.* Blackwell Science.

BLATT, H. 1967. Original characteristics of clastic quartz grains. *Journal of Sedimentary Research,* 37 (2).

BOGGS, S. JR. 2006. Principles of Sedimentology and Stratigraphy: Pearson Prentice Hall. *Upper Saddle River*.

CALVERT, S. E., & PEDERSEN, T. F. 1993. Geochemistry of recent oxic and anoxic marine sediments: implications for the geological record. *Marine geology*, *113*(1), 67-88.

CHAMLEY, H. 1989. Clay sedimentology, Springer-Verlag.

CONDIE, K. C. 1991. Another look at rare earth elements in shales. *Geochimica et Cosmochimica Acta,* 55**,** 2527-2531.

CONDIE, K. C. 1993. Chemical composition and evolution of the upper continental crust: contrasting results from surface samples and shales. *Chemical Geology,* 104**,** 1-37.

CULLERS, R. L. 2000. The geochemistry of shales, siltstones and sandstones of Pennsylvanian–Permian age, Colorado, USA: implications for provenance and metamorphic studies. *Lithos*, *51*(3), 181-203.

CULLERS, R., CHAUDHURI, S., KILBANE, N., & KOCH, R. 1979. Rare-earths in size fractions and sedimentary rocks of Pennsylvanian-Permian age from the mid-continent of the USA. *Geochimica et Cosmochimica Acta*, *43*(8), 1285-1301.

CRAW, D., SMITH, D. W., & YOUNGSON, J. H. 1995. Formation of authigenic Fe2+-bearing smectite-vermiculite during terrestrial diagenesis, southern New Zealand. *New Zealand journal of geology and geophysics*, *38*(2), 151-158.

CRAW, D. 1984. Ferrous-iron-bearing vermiculite-smectite series formed during alteration of chlorite to kaolinite, Otago Schist, New Zealand. *Clay Miner,* 19**,** 509-520.

DALRYMPLE, R. W. AND JAMES, N. P. 2010. *Facies models 4.* St. John's, Nfld.: Geological Association of Canada. 586p.

DELVAUX, B., & HERBILLON, A. 1995. Pathways of mixed-layer kaolin-smectite formation in soils.

DYPVIK, H. & ZAKHAROV, V. 2012. Late Jurassic-Early Cretaceous fine-grained epicontinental Arctic sedimentation – mineralogy and geochemistry of shales from the Late Jurassic-Early Cretaceous transition. *Norwegian Journal of Geology*, 92, 65-87.

DYPVIK, H. & HARRIS, N. B. 2001. Geochemical facies analysis of fine-grained siliciclastics using Th/U, Zr/Rb and (Zr+ Rb)/Sr ratios. *Chemical Geology,* 181**,** 131-146.

ESRI. 2014. Basemaps, Reference Maps, and Speciality Maps.

FOSSUM, K. 2012. Sedimentology, petrology and geochemistry of the Kilimatinde Cement, central Tanzania. Masters, University of Oslo.

FRANKS, P. C. 1969. Nature, origin, and significance of cone-in-cone structures in the Kiowa Formation (Early Cretaceous), north-central Kansas. *Journal of Sedimentary Research*, *39*(4).

GALÁN, E. 2006. Genesis of clay minerals. Pp. 1129_1162 in: Handbook of Clay Science (F. Bergaya, B.K.G. Theng, and G. Lagaly, editors). Elsevier, Oxford, UK.

GARCIA, D., FONTEILLERS, M., MOUTTE, J. 1994. Sedimentary fractionations between Al, Ti, and Zr and genesis of strongly peraluminous granites. Jour. Geol 102, 411±422.

GARDNER, J., DEAN, W. & VALLIER, T. 1980. Sedimentology and geochemistry of surface sediments, outer continental shelf, southern Bering Sea. *Marine Geology,* 35**,** 299-329.

GARVER, J., ROYCE, P. & SMICK, T. 1996. Chromium and nickel in shale of the Taconic foreland: a case study for the provenance of fine-grained sediments with an ultramafic source. *Journal of Sedimentary Research,* 66.

GARVER, J. I. & SCOTT, T. J. 1995. Trace elements in shale as indicators of crustal provenance and terrane accretion in the southern Canadian Cordillera. *Geological Society of America Bulletin,* 107**,** 440-453.

GARVER, J. I., AND ROYCE, P. R. 1993. Chromium and nickel in shale of the foreland deposits of the Ordovician Taconic Orogeny: Using shale as a provenance indicator for ultramafic rocks: Geological Society of America Abstracts with Programs, v. 25, p. 17.

GILMAN, R. A., & METZGER, W. J. 1967. Cone-in-cone concretions from western New York. *Journal of Sedimentary Research*, *37*(1).

GROMET, L. P., HASKIN, L. A., KOROTEV, R. L. & DYMEK, R. F. 1984. The "North American shale composite": its compilation, major and trace element characteristics. *Geochimica et Cosmochimica Acta,* 48**,** 2469-2482.

GUNDERSVEEN, E. 2014. Sedimentology, Petrology and Diagenesis of Mesozoic Sandstones in the Mandawa Basin, Coastal Tanzania.

HUDSON, W. 2011. The Geological Evolution of the Petroleum Prospective Mandawa Basin Southern Coastal Tanzania, Trinity College.

HONG, H., CHURCHMAN, G. J., GU, Y., YIN, K., & WANG, C. 2012. Kaolinite–smectite mixed-layer clays in the Jiujiang red soils and their climate significance. *Geoderma*, *173*, 75-83.

HORNE, J., FERM, J., CARUCCIO, F. & BAGANZ, B. 1978. Depositional models in coal exploration and mine planning in Appalachian region. *AAPG bulletin,* 62**,** 2379-2411.

ISHIGA, H., DOZEN, K. & SAMPEI, Y. 1999. Geochemical constraints on marine invasion and provenance change related to the opening of the Japan Sea: an example from the Lower

Miocene shales in the Hoda section, Shimane Peninsula, SW Japan. *Journal of Asian Earth Sciences,* 17**,** 443-457.

JIMÉNEZ BERROCOSO, Á., MACLEOD, K. G., HUBER, B. T., LEES, J. A., WENDLER, I., BOWN, P. R., MWENEINDA, A. K., ISAZA LONDOÑO, C. & SINGANO, J. M. 2010. Lithostratigraphy, biostratigraphy and chemostratigraphy of Upper Cretaceous sediments from southern Tanzania: Tanzania drilling project sites 21–26. *Journal of African Earth Sciences,* 57**,** 47-69.

JONES, B. & MANNING, D. A. 1994. Comparison of geochemical indices used for the interpretation of palaeoredox conditions in ancient mudstones. *Chemical Geology,* 111**,** 111-129.

KILIMAJARO MINING COMPANY. 2008. *Geology of Tanzania.* Available at: http://www.**kilimanjarominingcompany**.com/africanminingoperations/uranium/documents/Uranium%20InTanzania06.08.pdf (Accessed on Mai, 2014).

KOLOKOL'TSEV, V. G. 2002. The cone-in-cone structure and its origin. *Lithology and Mineral Resources*, *37*(6), 523-535.

LANSON, B., BEAUFORT, D., BERGER, G., BAUER, A., CASSAGNABERE, A., AND MEUNIER, A. 2002. Authigenic kaolin and illitic minerals during burial diagenesis of sandstones: a review: Clay Minerals, v. 37, p. 1-22.

LINDGREEN, H. AND HANSEN, P.L. 1991. Ordering of illite/smectite in Upper Jurassic claystones from the North Sea. Clay Minerals, 26, 105-125.

MACEACHERN, J. A., PEMBERTON, S. G., MURRAY, K. G. & BANN, K. L. 2010. Ichnology and facies models. *In:* NOEL, P. J. & DALRYMPLE, R. W. (eds.) *Facies Models 4.* The Geological Association of Canada.

MACEWAN, D. M. C., & RUIZ-AMIL, A. 1975. Interstratified clay minerals. In *Soil components*. Springer Berlin Heidelberg, 265-334.

MARSHALL, J. D. 1982. Isotopic composition of displacive fibrous calcite veins: reversals in pore-water composition trends during burial diagenesis. *Journal of Sedimentary Research,* 52.

MARTINEZ, S. J. 1994. New insights in the origin of cone-in-cone structures. *Carbonates and evaporites*, *9* (2), 172-186.

MBEDE, E. I. 1991. The sedimentary basins of Tanzania – reviewed. *Journal of African Earth Sciences,* 13, 291-297.

MCLENNAN, S. 1989. Rare earth elements in sedimentary rocks; influence of provenance and sedimentary processes. *Reviews in Mineralogy and Geochemistry,* 21**,** 169-200.

MCLENNAN, S., HEMMING, S., MCDANIEL, D. & HANSON, G. 1993. Geochemical approaches to sedimentation, provenance, and tectonics. *Special Papers-Geological Society of America***,** 21-21.

MCLENNAN, S., HEMMING, S., TAYLOR, S. & ERIKSSON, K. 1995. Early Proterozoic crustal evolution: Geochemical and Nd Pb isotopic evidence from metasedimentary rocks, southwestern North America. *Geochimica et Cosmochimica Acta,* 59**,** 1153-1177.

MCLENNAN, S. M. & TAYLOR, S. 1980. Th and U in sedimentary rocks: crustal evolution and sedimentary recycling. *Nature,* 285**,** 621-624.

MILODOWSKI, A. E., & ZALASIEWICZ, J. A. 1991. Redistribution of rare earth elements during diagenesis of turbidite/hemipelagite mudrock sequences of Llandovery age from central Wales. *Geological Society, London, Special Publications*, *57*(1), 101-124.

MOORE, D. M. & REYNOLDS JR, R. C. 1989. X-ray Diffraction and the Identification and Analysis of Clay Minerals, Oxford University Press (OUP).

MPANDA, S. 1997. Geological development of the East African coastal basin of Tanzania.

MUKHERJEE, S. 2013. Clays: Industrial Applications and Their Determinants. *The Science of Clays.* Springer Netherlands, 335 p.

MURALI, A. V., PARTHASARATHY, R., MAHADEVAN, T. M., & DAS, M. S. 1983. Trace element characteristics, REE patterns and partition coefficients of zircons from different geological environments—a case study on Indian zircons. *Geochimica et Cosmochimica Acta*, *47*(11), 2047-2052.

NESBITT, W. H. & MARKOVICS, G. 1997. Weathering of granodioritic crust, long-term storage of elements in weathering profiles, and petrogenesis of siliciclastic sediments. *Geochimica et Cosmochimica Acta,* 61**,** 1653-1670.

NESBITT, H., YOUNG, G., MCLENNAN, S. AND KEAYS, R. 1996. Effects of chemical weathering and sorting on the petrogenesis of siliciclastic sediments, with implications for provenance studies. *The Journal of Geology* 104, 525-542.

NERBRÅTEN, K., 2014. Petrology and Sedimentary Provenance of Mesozoic and Cenozoic Sequences in the Mandawa Basin.

NICHOLAS, C. J., PEARSON, P. N., MCMILLAN, I. K., DITCHFIELD, P. W. & SINGANO, J. M. 2007. Structural evolution of southern coastal Tanzania since the Jurassic. *Journal of African Earth Sciences,* 48**,** 273-297.

NICHOLAS, C. J., PEARSON, P. N., BOWN, P. R., DUNKLEY JONES, T., HUBER, B. T., KAREGA, A., LEES, J. A., MCMILLAN, I. K., O'HALLORAN, A., SINGANO, J. M. & WADE, B. S. 2006. Stratigraphy and sedimentology of the Upper Cretaceous to Paleogene Kilwa Group, southern coastal Tanzania. *Journal of African Earth Sciences,* 45**,** 431-466.

PAUL, D., WHITE, W. & TURCOTTE, D. 2003. Constraints on the 232Th/238U ratio (κ) of the continental crust. *Geochemistry, Geophysics, Geosystems,* 4.

PEARSON, P. N., NICHOLAS, C. J., SINGANO, J. M., BOWN, P. R., COXALL, H. K., VAN DONGEN, B. E., HUBER, B. T., KAREGA, A., LEES, J. A., MACLEOD, K., MCMILLAN, I. K., PANCOST, R. D., PEARSON, M. & MSAKY, E. 2006. Further Paleogene and Cretaceous sediment cores from the Kilwa area of coastal Tanzania: Tanzania drilling project sites 6–10. *Journal o f African Earth Sciences,* 45**,** 279-317.

PEARSON, P. N., NICHOLAS, C. J., SINGANO, J. M., BOWN, P. R., COXALL, H. K., VAN DONGEN, B. E., HUBER, B. T., KAREGA, A., LEES, J. A., MSAKY, E., PANCOST, R. D., PEARSON, M. & ROBERTS, A. P. 2004. Paleogene and Cretaceous sediment cores from the Kilwa and Lindi areas of coastal Tanzania: Tanzania Drilling Project Sites 1–5. *Journal of African Earth Sciences,* 39**,** 25-62.

PE-PIPER, G., DOLANSKY, L., AND PIPER, D.J.W. 2005. Sedimentary environment and diagenesis of the Lower Cretaceous Chaswood Formation, southeastern Canada: The origin of kaolin-rich mudstones: Sedimentary Geology, v. 178, p. 75-97.

POTTER, P. E., MAYNARD, J. B. & DEPETRIS, P. J. 2005. Mud and mudstones: Introduction and overview Springer.

POTTER, P. E., MAYNARD, J. B. & PRYOR, W. A. 1980. Sedimentology of shale: study guide and reference source, Springer-Verlag Berlin.

PROCHASKA, W. & POHL, W. 1983. Petrochemistry of some mafic and ultramafic rocks from the Mozambique Belt, northern Tanzania. *Journal of African Earth Sciences (1983),* 1**,** 183-191.

READING, H.G. 1996. Sedimentary environments: processes, facies and stratigraphy: Wiley-Blackwell.

RÖHL, U., BRALOWER, T., NORRIS, R. & WEFER, G. 2000. New chronology for the late Paleocene thermal maximum and its environmental implications. *Geology,* 28**,** 927-930.

ROSER, B.P., COOPER, R.A., TULLOCH, A.J. 1996. Reconnaissancesandstone geochemistry, provenance, and tectonic setting of the lower Paleozoic terranes of West Coast and Nelson, New Zealand. New Zealand Jour. Geol. Geophy 39, 1±16.

SALMAN, G. & ABDULA, I. 1995. Development of the Mozambique and Ruvuma sedimentary basins, offshore Mozambique. *Sedimentary Geology,* 96**,** 7-41.

SCHLÜTER, T. & HAMPTON, C. 1997. Geology of East Africa, Borntraeger Berlin.

SETHI, P., HANNIGAN, R. & LEITHOLD, E. 1998. Rare-earth element chemistry of Cenomanian-Turonian Shales of the north American Greenhorn Sea, Utah.

SINGER, A. 1984. The paleoclimatic interpretation of clay minerals in sediments—a review. *Earth-Science Reviews*, *21*(4), 251-293.

SLUIJS, A., RÖHL, U., SCHOUTEN, S., BRUMSACK, H. J., SANGIORGI, F., SINNINGHE DAMSTÉ, J. S. & BRINKHUIS, H. 2008. Arctic late Paleocene–early Eocene paleoenvironments with special emphasis on the Paleocene-Eocene thermal maximum (Lomonosov Ridge, Integrated Ocean Drilling Program Expedition 302). *Paleoceanography,* 23.

STATOIL. 2014. *Vellykket produksjonstest av Zafarani-reservoaret i Tanzania*. Available at: http://www.statoil.com/no/NewsAndMedia/News/2014/Pages/03Mar_Tazania.aspx (Accessed on Mai, 2014).

SRODON, J. 1999. Nature of mixed-layer clays and mechanisms of their formation and alteration. *Annual Review of Earth and Planetary Sciences,* 27**,** 19-53.

TARNEY, J. & SCHREIBER, B. C. 1977. Cone-in-cone and beef-in-shale textures from DSDP Site 330, Falkland Plateau, South Atlantic. 36**,** 865-870.

TARR, W.A., 1922. Cone-in-Cone, *Am. J. Sci.*, vol. 4, no. 21, pp. 199–21.

TAYLOR, S. R. & MCLENNAN, S. M. 1985. The continental crust: its composition and evolution.

THIRY, M. 2000. Palaeoclimatic interpretation of clay minerals in marine deposits: an outlook from the continental origin. *Earth-Science Reviews,* 49**,** 201-221.

VINGIANI, S., RIGHI, D., PETIT, S., & TERRIBILE, F. 2004. Mixed-layer kaolinite-smectite minerals in a red-black soil sequence from basalt in Sardinia (Italy). *Clays and clay minerals*, *52*(4), 473-483.

WEAVER, C., E. 1958. A discussion on the origin of clay minerals insedimentary rocks. *Clays and clay minerals*. Nat Acad Sci-Nat Res Council 566:159–173

WENTWORTH, C.K. 1922. A scale of grade and class terms for clastiv sediments. In *Journal of geology* 27, 377-392.

ZAKARIASSEN, E. 2014. Pers. com.

APPENDICES

Appendix 1: Logging sheet

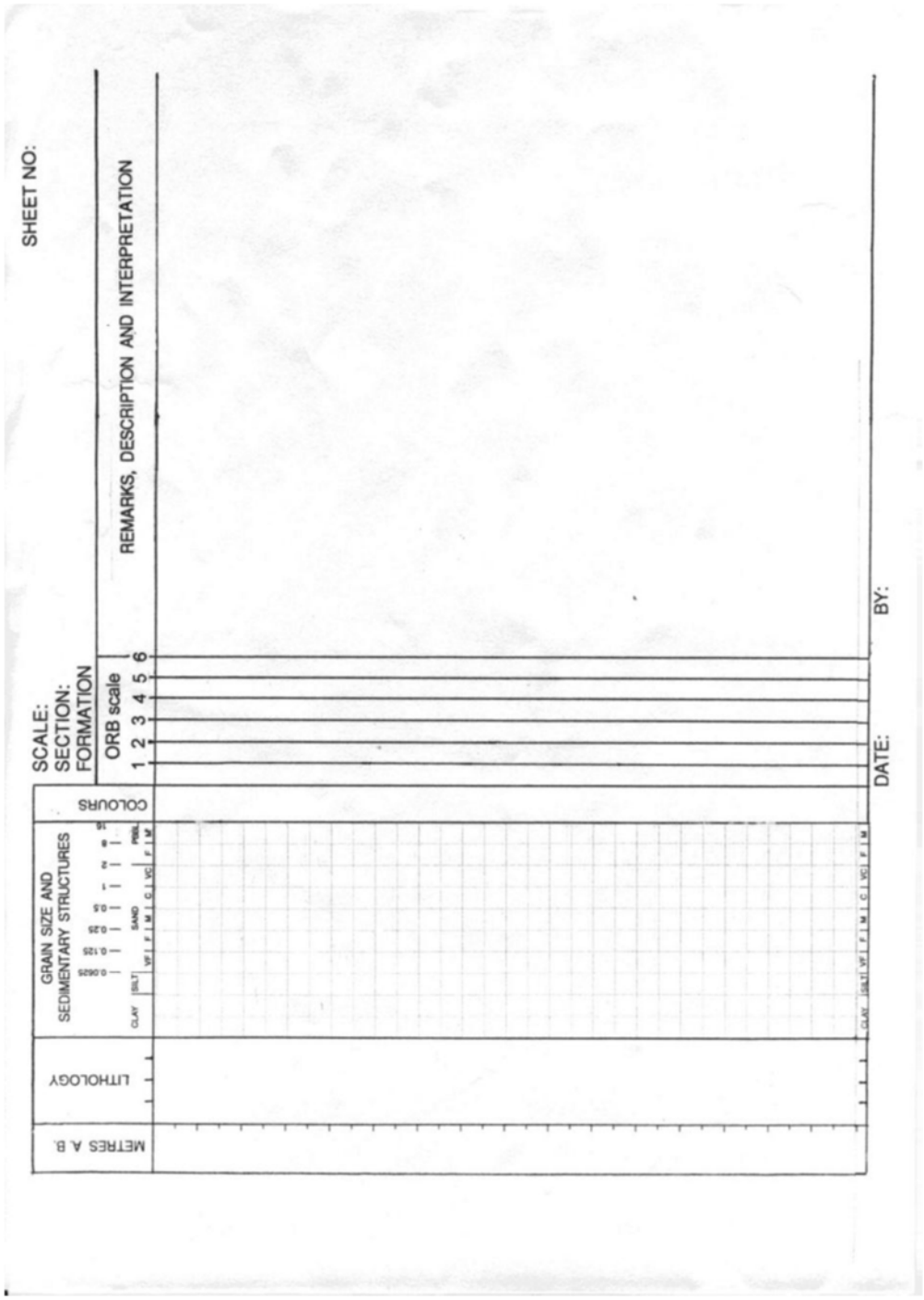

Appendix 2 – Trace elements results (Kilwa Group)

Analyte Symbol	Au	Ag	Cu	Cd	Mo	Pb	Ni	Zn	S	Al	As	Ba	Be
Unit Symbol	ppb	ppm	ppm	ppm	ppm	ppm	ppm	ppm	%	%	ppm	ppm	ppm
Detection limit	2	0,05	0,2	0,1	1	0,5	0,5	0,5	0,01	0,01	0,5	1	0,1
Analysis Method	NAA	P/TD-MS	D-ICP-MS	D-ICP-MS	TD-ICP	D-ICP-MS	P/TD-MS	P/TD-MS	TD-ICP	TD-ICP	INAA	TD-ICP-MS	D-ICP-MS
C1-8.5	< 2	0,4	46,3	0,1	1	17,2	47,1	78,8	1,12	8,43	4	279	2,1
C1-24.31	< 2	0,27	58,1	0,1	< 1	21,8	53,2	111	0,82	9,79	< 0.5	362	3,1
C1-44.70	< 2	0,37	51,6	0,1	< 1	16,6	71	91,8	3,37	6,13	4,6	34	2
C1-49.79	< 2	0,52	61,3	< 0.1	< 1	14,1	45,9	87,5	0,9	9,42	< 0.5	267	2,8
C1-57.70	< 2	0,09	24,4	< 0.1	< 1	14,2	30,4	70	0,14	8,54	< 0.5	425	2
C1-62.54	< 2	0,09	23,8	< 0.1	4	12,6	24,5	51,9	0,02	7,6	< 0.5	615	1,5
C2-3.57	< 2	0,31	33,1	< 0.1	< 1	13,1	54	92,6	0,41	5,94	< 0.5	343	1,8
C2-16.43	< 2	0,14	45,2	< 0.1	< 1	15,7	67,2	100	0,21	6,16	< 0.5	247	1,9
C2-35.40	< 2	0,39	27,4	< 0.1	< 1	11,4	45,7	113	0,59	4,91	5,4	305	1,6
C2-52.20	< 2	0,14	29,7	< 0.1	< 1	13,6	49,8	92,9	0,25	6,92	< 0.5	337	1,9
C2-69.52	< 2	0,1	18,8	< 0.1	< 1	15	33,6	64,3	0,35	6,9	< 0.5	800	1,7
C2-76.55	< 2	0,11	26,1	0,2	< 1	17,2	43,3	80,3	0,31	7,06	5,3	432	1,7
C7B-3.02	< 2	0,38	34,4	0,2	< 1	15,7	44	63,4	0,52	6,98	< 0.5	460	2,2
C7B-15.30	< 2	0,12	44,8	< 0.1	< 1	19,6	52,5	78	0,19	8,32	< 0.5	445	2,7
C7B-29.70	< 2	0,28	31,1	0,2	< 1	16,4	42,5	89,3	0,45	7,37	< 0.5	472	2,1
C7B-37.60	< 2	0,23	47,6	0,2	< 1	20,4	48,8	96,5	0,35	7,4	< 0.5	385	2,3
C7B-43.60	< 2	0,15	48,9	< 0.1	< 1	20	62,3	113	0,05	9,04	< 0.5	446	2
C7B-54.21	< 2	0,35	21,4	< 0.1	< 1	12,1	37,3	54,8	0,15	5,78	< 0.5	254	2,4
C7B-68.53	< 2	0,09	36,4	0,1	< 1	13,5	45,7	81,4	0,27	8	< 0.5	458	2,3
C7B-92.73	< 2	0,45	33,6	0,2	< 1	12,2	37,1	75,6	0,31	5,2	7,7	321	2,2
C7B-113.50	< 2	0,46	35,9	0,1	< 1	16,4	40,7	78,7	0,37	7,89	< 0.5	437	2,5
C7B-156.08	< 2	0,34	48,1	< 0.1	< 1	14,2	52,4	63	0,25	9,06	< 0.5	275	2,5
C9-68-69	< 2	0,21	36,1	0,1	< 1	10,9	69,4	84,2	0,19	6,23	< 0.5	309	1,7
C9-25-27	< 2	0,34	34,7	< 0.1	< 1	15,5	58	103	0,15	7,61	< 0.5	371	2,1
C9-34-35	< 2	0,25	32,7	0,1	< 1	13,2	52,2	85	0,28	6,35	8,8	280	1,8
C9-40-42	< 2	0,31	29,5	0,4	< 1	14,7	52,3	93,5	0,22	6,34	2,9	306	1,7
C9-23-24	< 2	0,29	37,2	< 0.1	< 1	13,1	48,5	88,3	0,2	6,58	< 0.5	282	1,8
C9-31-32	< 2	0,31	26	< 0.1	< 1	12,1	48,5	82,8	0,12	7,34	6,8	437	2

Kilwa Group cont.

Analyte Sy	Bi	Br	Ca	Co	Cr	Cs	Fe	Hf	Hf	Ga	Ge	Hg
Unit Symb	ppm	ppm	%	ppm	ppm	ppm	%	ppm	ppm	ppm	ppm	ppb
Detection	0,1	0,5	0,01	0,1	1	0,05	0,01	0,1	1	0,1	0,1	10
Analysis M	D-ICP-MS	INAA	TD-ICP	D-ICP-MS	D-ICP-MS	D-ICP-MS	INAA	TD-MS	INAA	TD-MS	TD-MS	TD-MS
C1-8.5	0,1	< 0.5	2,85	18,9	138	2,52		2,5	2	19,3	0,1	< 10
C1-24.31	0,2	< 0.5	0,93	17,5	102	3,96	4,96	2,9	4	24,8	0,5	< 10
C1-44.70	0,1	< 0.5	2,43	36	63	2,36	6,01	2,3	5	14,6	0,1	40
C1-49.79	0,2	< 0.5	1,34	16,9	85	3,24	4,68	3	4	22,4	0,2	10
C1-57.70	0,1	< 0.5	0,82	12,9	73	3,14	3,61	2,7	6	19,5	0,1	80
C1-62.54	0,1	< 0.5	0,74	8,4	83	2,13	3,34	3,1	13	15,9	0,1	< 10
C2-3.57	0,2	8,4	7,02	12,2	103	3,51	3,79	1,8	4	17,3	0,3	< 10
C2-16.43	0,2	8,3	3,48	22	100	3,73	4,75	1,5	< 1	20,9	0,2	30
C2-35.40	0,2	10,4	7,39	11,2	85	3,17	3,71	1,7	2	16,3	0,4	< 10
C2-52.20	0,2	10	5,97	17,1	89	3,89	4,11	1,8	< 1	19,3	0,2	30
C2-69.52	0,1	10,7	5,87	12,7	79	2,56	2,85	2,8	8	15,4	0,2	30
C2-76.55	0,2	16	4,58	18,2	85	3,04	3,35	2	5	17,6	0,2	30
C7B-3.02	0,2	< 0.5	4,4	15,4	95	3,79	3,83	1,6	4	18,5	0,2	40
C7B-15.30	0,2	< 0.5	2,14	17,4	124	4,14	4,88	1,5	4	20,8	0,1	70
C7B-29.70	0,2	< 0.5	6,76	14,7	72	3,83	4,21	1,6	3	18,9	0,2	60
C7B-37.60	0,3	< 0.5	2,75	11,8	104	3,86	4,24	1,7	4	19,6	0,2	< 10
C7B-43.60	0,3	< 0.5	0,63	22,9	158	4,16	5,48	2	3	23,2	0,2	40
C7B-54.21	0,2	< 0.5	4,48	11,6	100	2,62	13	1	2	13,9	0,1	< 10
C7B-68.53	0,3	< 0.5	2,56	16,7	130	3,7	4,56	2	4	20,2	0,2	10
C7B-92.73	0,2	< 0.5	8,28	14,6	135	2,82	4,25	2,3	2	17,1	0,8	10
C7B-113.50	0,2	< 0.5	1,63	18,3	113	3,91	4,24	2,2	5	19,8	0,6	10
C7B-156.0	0,3	< 0.5	0,53	20,9	132	3,99	4,59	1,8	3	22,6	0,3	10
C9-68-69	0,2	< 0.5	9,4	17,3	113	3,26	4,92	2	4	15,9	0,2	80
C9-25-27	0,2	< 0.5	5,27	22,3	143	3,88	4,97	1,9	5	19,4	0,3	50
C9-34-35	0,2	< 0.5	7,86	17,9	117	3,81	4,44	2	2	17,1	0,1	50
C9-40-42	0,2	5,7	8,31	18,8	145	3,47	4,02	1,6	3	16,1	0,1	60
C9-23-24	0,2	< 0.5	8,92	25	113	3,51	4,76	1,7	5	16,8	0,2	70
C9-31-32	0,2	< 0.5	3,69	15,7	138	3,35	4,73	2,8	8	18,3	0,3	60

Kilwa Group cont.

Analyte Sy	In	Ir	K	Li	Mg	Mn	Nb	P	Rb	Re	Sb	Sc	Se	Sn
Unit Symb	ppm	ppb	%	ppm	%	ppm	ppm	%	ppm	ppm	ppm	ppm	ppm	ppm
Detection	0,1	5	0,01	0,5	0,01	1	0,1	0,001	0,2	0,001	0,1	0,1	0,1	1
Analysis M	TD-MS	INAA	TD-ICP	TD-MS	TD-ICP	TD-ICP	TD-MS	TD-ICP	D-ICP-MS	TD-MS	INAA	INAA	D-ICP-MS	TD-MS
C1-8.5	< 0.1	< 5	1,64	31,7	1,53	377	11	0,035	79,2	0,007	< 0.1	12,8	1	2
C1-24.31	< 0.1	< 5	1,88	50	1,51	331	6,7	0,038	112	0,003	< 0.1	17,1	0,7	3
C1-44.70	< 0.1	< 5	2,01	28,7	1,1	335	8,9	0,036	82,8	< 0.001	< 0.1	12,4	< 0.1	2
C1-49.79	< 0.1	< 5	1,96	40,5	1,6	283	13	0,061	99,7	0,001	< 0.1	18,3	< 0.1	4
C1-57.70	< 0.1	< 5	2,26	23,6	1,28	218	0,7	0,02	96,7	0,003	< 0.1	15,2	< 0.1	< 1
C1-62.54	< 0.1	< 5	2,31	17,5	0,93	200	0,2	0,013	84,9	< 0.001	0,3	11,4	0,3	< 1
C2-3.57	< 0.1	< 5	2,14	38,1	1,66	307	7,9	0,042	91,1	< 0.001	< 0.1	13,4	0,4	2
C2-16.43	< 0.1	< 5	2,26	46,4	1,84	328	2,2	0,036	76,3	< 0.001	< 0.1	16,5	0,3	1
C2-35.40	< 0.1	< 5	2,08	32,7	1,7	283	9,4	0,049	75,5	< 0.001	< 0.1	12	1,3	2
C2-52.20	< 0.1	< 5	2,12	53,4	1,56	240	1,8	0,033	98,9	0,014	0,6	14,6	0,9	1
C2-69.52	< 0.1	< 5	2,32	32,9	1,25	240	0,6	0,034	94	< 0.001	< 0.1	10,5	0,4	1
C2-76.55	< 0.1	< 5	2,18	48	1,39	271	0,4	0,033	97,5	0,008	< 0.1	13	0,2	1
C7B-3.02	< 0.1	< 5	2,23	34,1	1,41	199	7,9	0,022	106	0,006	< 0.1	12,1	1	2
C7B-15.30	< 0.1	< 5	2,57	40,1	1,53	263	0,3	0,031	118	0,003	< 0.1	14,1	0,4	< 1
C7B-29.7(	< 0.1	< 5	1,93	37,8	1,26	239	2,8	0,022	106	0,004	< 0.1	11	0,7	2
C7B-37.6(	< 0.1	< 5	2,03	52	1,31	192	3	0,022	105	0,006	< 0.1	13,2	1,4	2
C7B-43.6(	< 0.1	< 5	2,03	72,4	1,47	228	0,4	0,03	122	0,005	< 0.1	15,2	0,4	< 1
C7B-54.2	< 0.1	< 5	1,2	36	2,95	2050	7,6	0,106	75,9	0,001	< 0.1	11,8	0,2	1
C7B-68.5	< 0.1	< 5	2,09	42,1	1,46	369	0,4	0,029	122	0,001	< 0.1	12,6	0,7	1
C7B-92.7	< 0.1	< 5	1,81	35,3	1,23	435	9,8	0,029	58	0,001	< 0.1	13,5	1,6	2
C7B-113.5	< 0.1	< 5	2,09	41,2	1,46	241	10,5	0,026	125	0,004	< 0.1	12,9	1	2
C7B-156.0	< 0.1	< 5	1,8	65	1,65	305	8,3	0,024	111	0,007	< 0.1	16	0,2	2
C9-68-69	< 0.1	< 5	2,03	34,1	1,18	358	0,4	0,033	92,1	0,004	< 0.1	12,7	0,5	< 1
C9-25-27	< 0.1	< 5	2,38	38	1,35	303	1,4	0,034	105	0,003	< 0.1	15,1	0,3	< 1
C9-34-35	< 0.1	< 5	1,92	42,4	1,2	259	0,4	0,02	86,6	0,007	< 0.1	13,4	0,5	< 1
C9-40-42	< 0.1	< 5	1,99	39,5	1,12	297	0,2	0,019	89	0,008	0,5	12,5	1,1	< 1
C9-23-24	< 0.1	< 5	1,89	38,5	1,18	316	1,1	0,021	89,9	0,007	< 0.1	13,7	0,5	< 1
C9-31-32	< 0.1	< 5	2,52	37,3	1,22	227	2,3	0,028	105	0,001	0,8	14,3	0,4	< 1

Kilwa Group cont.

Analyte Sy	Sr	Ta	Te	Ti	Th	Tl	U	V	W	Y	Zr	La	La	Ce
Unit Symb	ppm	ppm	ppm	%	ppm	ppm	ppm	ppm	ppm	ppm	ppm	ppm	ppm	ppm
Detection	0,2	0,1	0,1	0,01	0,1	0,05	0,1	2	1	0,1	1	0,1	0,5	0,1
Analysis M	TD-MS	D-ICP-MS	TD-MS	TD-ICP	D-ICP-MS	TD-MS	D-ICP-MS	TD-ICP	INAA	TD-MS	TD-MS	TD-MS	INAA	TD-MS
C1-8.5	278	0,7	0,2	0,43	6,6	0,45	2,9	113	< 1	24,3	93	31,2	30,7	63,1
C1-24.31	242	< 0.1	< 0.1	0,55	10,9	0,59	3,2	129	< 1	26	107	44,6	46,1	89
C1-44.70	299	0,6	< 0.1	0,4	8,2	0,46	2,1	89	< 1	20,4	76	28,9	34,9	62,5
C1-49.79	186	1,6	< 0.1	0,61	11,3	0,45	2,8	145	< 1	26,1	99	40,7	45,7	83,9
C1-57.70	211	< 0.1	< 0.1	0,35	10,4	0,47	2,2	89	< 1	14,3	89	31,8	35,1	58,2
C1-62.54	139	< 0.1	< 0.1	0,26	9,1	0,4	2	57	< 1	22,6	107	32,4	38,2	76,2
C2-3.57	957	0,4	< 0.1	0,41	12	0,6	2,9	93	< 1	12,5	59	25,9	42	52,4
C2-16.43	579	< 0.1	< 0.1	0,37	13,2	0,66	1,9	93	< 1	10	47	19	42,6	40,1
C2-35.40	844	0,7	< 0.1	0,37	11,2	0,57	2,5	95	< 1	12,9	56	25,6	38,2	53,9
C2-52.20	567	< 0.1	< 0.1	0,36	10,8	0,6	2,2	89	< 1	12	60	29,4	38,6	57,9
C2-69.52	445	< 0.1	< 0.1	0,31	9,6	0,46	2	69	< 1	14,5	94	31,6	34,7	66,9
C2-76.55	336	< 0.1	< 0.1	0,24	12,6	0,57	2,8	69	< 1	15,7	71	35,7	41,4	74,8
C7B-3.02	686	0,2	< 0.1	0,41	13,1	0,55	2	97	< 1	11,4	56	26,7	43,2	52,2
C7B-15.30	460	< 0.1	< 0.1	0,19	12	0,58	2,1	67	< 1	18,5	52	35,7	52,1	72,8
C7B-29.7(	910	< 0.1	< 0.1	0,33	13,7	0,51	2,6	88	< 1	15,9	52	38,9	43,8	79,2
C7B-37.6(	467	< 0.1	< 0.1	0,38	14,7	0,55	2	106	< 1	15,4	53	31,5	54,2	66,4
C7B-43.6(	246	< 0.1	< 0.1	0,28	16	0,65	2,1	74	< 1	17,6	68	45,3	56,6	89,3
C7B-54.2	355	0,5	< 0.1	0,33	10,4	0,37	2,2	73	< 1	31,1	38	40,9	46,4	93,1
C7B-68.5	392	< 0.1	< 0.1	0,32	14,3	0,52	2,8	79	< 1	18,8	69	38,9	49,9	76,8
C7B-92.7	527	0,8	< 0.1	0,36	10,1	0,46	2,2	86	< 1	14,9	85	21,7	45,6	47,4
C7B-113.5(	331	0,5	< 0.1	0,48	16	0,57	2,4	112	< 1	17,9	78	40,2	55,1	82,5
C7B-156.0	122	0,2	< 0.1	0,52	12,9	0,54	1,9	106	< 1	16,2	59	38,7	47,5	77,9
C9-68-69	610	< 0.1	< 0.1	0,21	8,5	0,47	1,7	61	< 1	18	72	31,2	37,1	62,2
C9-25-27	444	< 0.1	< 0.1	0,28	10,1	0,53	2,1	79	< 1	17	69	31	41,5	63,6
C9-34-35	713	< 0.1	< 0.1	0,16	9,1	0,54	2,2	63	< 1	12,8	67	25,7	34,1	53,8
C9-40-42	486	< 0.1	< 0.1	0,13	7,6	0,48	2	49	< 1	13,2	58	27,9	31,8	57,3
C9-23-24	723	< 0.1	< 0.1	0,16	10,1	0,46	2	47	< 1	14,3	62	28,9	36,6	58,1
C9-31-32	427	0,2	< 0.1	0,32	12,1	0,49	2,1	78	< 1	15,1	108	31	42,8	61

Kilwa Group cont.

Analyte Sy	Ce	Pr	Nd	Nd	Sm	Eu	Gd	Dy	Tb	Ho	Er	Tm	Yb	Yb	Lu	Lu	Mass
Unit Symb	ppm	ppm	ppm	ppm	ppm	ppm	ppm	ppm	ppm	ppm	ppm	ppm	ppm	ppm	ppm	ppm	g
Detection	3	0,1	0,1	5	0,1	0,05	0,1	0,1	0,1	0,1	0,1	0,1	0,1	0,2	0,1	0,05	
Analysis M	INAA	TD-MS	TD-MS	INAA	TD-MS	TD-MS	TD-MS	TD-MS	TD-MS	TD-MS	TD-MS	TD-MS	TD-MS	INAA	TD-MS	INAA	INAA
C1-8.5	62	7,8	28,5	38	5,5	1,44	5,7	5	0,8	1	2,8	0,4	2,2	3,1	0,4	0,49	0,375
C1-24.31	83	10,9	38,6	57	7,3	1,74	6,9	5,3	0,9	1	2,8	0,4	2,2	1,9	0,3	0,35	0,788
C1-44.70	77	7,4	27,9	34	5,3	1,26	4,9	4,2	0,7	0,8	2,3	0,3	1,9	1,8	0,3	0,42	1,13
C1-49.79	80	10,3	38,8	60	7,2	1,71	6,7	5,4	0,9	1	2,9	0,4	2,4	2,5	0,4	0,53	0,918
C1-57.70	62	6,9	25,6	21	4,4	1	4,1	2,9	0,5	0,6	1,6	0,2	1,5	1,5	0,2	0,36	1,14
C1-62.54	86	9,7	38,8	53	7,9	1,93	7,3	5,2	1	1	2,5	0,3	2	2	0,3	0,39	1,02
C2-3.57	74	6,6	24,6	39	4,5	0,92	3,9	2,7	0,5	0,5	1,4	0,2	1,2	1,6	0,2	0,24	0,954
C2-16.43	76	5,1	19	36	3,5	0,69	3	2,2	0,4	0,4	1,2	0,2	1	1,3	0,2	0,21	1,04
C2-35.40	68	6,7	24,7	20	4,4	0,94	3,9	2,9	0,5	0,6	1,5	0,2	1,3	1,5	0,2	0,27	1,01
C2-52.20	60	7,2	26,2	36	4,4	0,92	3,7	2,7	0,5	0,5	1,4	0,2	1,2	1,3	0,2	0,1	1,08
C2-69.52	60	7,6	27,8	22	4,8	1,05	4,2	2,9	0,6	0,6	1,7	0,2	1,4	2	0,2	0,38	1,1
C2-76.55	70	8,3	29,7	52	5,3	1,1	4,5	3,3	0,6	0,6	1,8	0,2	1,4	1,9	0,2	0,27	1,05
C7B-3.02	99	6,5	23	60	4	0,82	3,3	2,4	0,5	0,5	1,4	0,2	1,3	2,3	0,2	0,35	1,13
C7B-15.30	128	8,5	31	45	5,5	1,21	5,1	3,8	0,7	0,7	2,2	0,3	1,8	2,4	0,3	0,5	1,04
C7B-29.70	101	9,2	32,5	41	5,6	1,12	4,6	3,4	0,6	0,6	1,8	0,3	1,5	1,7	0,2	0,41	1,14
C7B-37.60	117	7,6	27,7	96	5	1,04	4,5	3,4	0,6	0,6	1,9	0,3	1,6	2,6	0,3	0,31	1,07
C7B-43.60	121	10,4	37,1	67	6,3	1,27	5,4	3,7	0,7	0,7	2	0,3	1,7	2,8	0,3	0,44	1,07
C7B-54.21	105	9,8	36,9	50	7,2	1,66	7,1	5,4	1	1,1	2,9	0,4	2,3	3,8	0,4	0,46	1,14
C7B-68.53	117	8,9	32	38	5,7	1,19	5,1	3,9	0,7	0,7	2,1	0,3	1,8	3,6	0,3	0,52	1,26
C7B-92.73	114	6	22,9	32	4,5	0,94	4	3,4	0,6	0,7	1,9	0,3	1,6	2,3	0,3	0,46	1,09
C7B-113.5	116	9,4	33,1	52	5,7	1,24	5,1	3,7	0,6	0,7	1,9	0,3	1,8	3,9	0,3	0,47	1,03
C7B-156.0	108	8,9	31,7	36	5,5	1,17	4,7	3,4	0,6	0,7	1,8	0,2	1,7	1,4	0,3	0,55	1,1
C9-68-69	102	7,2	26,3	59	4,7	1,06	4,3	3,4	0,6	0,6	1,9	0,3	1,6	2,5	0,3	0,47	0,913
C9-25-27	83	7,4	26,6	25	4,9	1,03	4,3	3,4	0,6	0,7	1,8	0,3	1,6	1,9	0,2	0,19	0,85
C9-34-35	60	6,1	22,2	32	4	0,85	3,3	2,6	0,4	0,5	1,5	0,2	1,3	1,5	0,2	< 0.05	0,705
C9-40-42	72	6,5	23,4	21	4,1	0,9	3,6	2,6	0,4	0,5	1,4	0,2	1,3	2,1	0,2	0,14	0,329
C9-23-24	65	6,7	23,9	23	4,2	0,91	3,6	2,7	0,5	0,5	1,5	0,2	1,3	1,5	0,2	0,41	0,891
C9-31-32	92	7,3	26,3	67	4,7	1,01	4,2	3,1	0,6	0,6	1,7	0,3	1,5	2	0,2	0,22	1,08

Trace-elements Statoil offshore

Analyte Symbol	Au	Ag	Cu	Cd	Mo	Pb	Ni	Zn	S	Al	As	Ba	Be	Bi	Br	Ca	Co	Cr
Unit Symbol	ppb	ppm	ppm	ppm	ppm	ppm	ppm	ppm	%	%	ppm	ppm	ppm	ppm	ppm	%	ppm	ppm
Detection Limit	2	0,05	0,2	0,1	1	0,5	0,5	0,5	0,01	0,01	0,5	1	0,1	0,1	0,5	0,01	0,1	1
Analysis Method	INAA	MULT INA	MULT TD	MULT TD-ICP/T	TD-ICP	MULT TD	MULT INA	MULT INA	TD-ICP	TD-ICP	INAA	MULT INA	MULT TD	MULT TD	INAA	TD-ICP	MULT INA	MULT INA
2/3-14 - Paleocene	< 2	2,02	32	< 0.1	< 1	6,3	55	78,7	0,02	4,94	< 0.5	281	1,4	0,1	< 0.5	18,7	9,4	75
2/4-14 - Paleocene	< 2	0,13	38,6	< 0.1	< 1	13,3	78,3	105	0,08	8,06	3,6	466	2,3	0,2	< 0.5	7,11	25,6	88
2/5-14 - Cenomanian	< 2	0,5	63,6	< 0.1	< 1	13,7	55,5	98,3	0,09	6,94	2,9	387	3,1	0,2	< 0.5	2,92	16,1	104
2/6-14 - Cenomanian	< 2	0,1	56,3	< 0.1	< 1	15,1	64,5	95,3	0,21	8,35	13	411	3,1	2,6	10,7	4,13	22,4	91

Analyte Sy	Cs	Eu	Fe	Hf	Hf	Ga	Ge	Hg	In	Ir	K	Li	Mg	Mn	Nb	Na	P	Rb	Re
Unit Symb	ppm	ppm	%	ppm	ppm	ppm	ppm	ppb	ppm	ppb	%	ppm	%	ppm	ppm	%	%	ppm	ppm
Detection	0,05	0,2	0,01	0,1	1	0,1	0,1	10	0,1	5	0,01	0,5	0,01	1	0,1	0,01	0,001	0,2	0,001
Analysis M	MULT INA	INAA	INAA	TD-MS	INAA	TD-MS	TD-MS	TD-MS	TD-MS	INAA	TD-ICP	TD-MS	TD-ICP	TD-ICP	TD-MS	INAA	TD-ICP	MULT INA	TD-MS
2/3-14 - P	3,03	1,1	3	1,1	2	12,8	0,2	< 10	< 0.1	< 5	1,11	21,8	0,94	512	0,3	0,64	0,032	75,3	0,005
2/4-14 - Pa	4,43	1,4	4,33	1,6	3	21	0,3	< 10	< 0.1	< 5	1,79	45,6	1,28	306	0,1	1,06	0,029	122	< 0.001
2/5-14 - Ce	5,08	2,2	4,12	3,7	4	28	1,3	50	< 0.1	< 5	2,72	68,8	1,86	337	19,8	0,8	0,046	109	< 0.001
2/6-14 - Ce	5,27	2,4	3,76	2,9	4	29	0,3	60	< 0.1	< 5	2,65	63,1	1,75	352	2,1	0,84	0,039	132	0,002

Analyte Sy	Sb	Sc	Se	Sn	Sr	Ta	Te	Tb	Ti	Th	Tl	V	U	W	Y	Zr	La	La	Ce
Unit Symb	ppm	ppm	ppm	ppm	ppm	ppm	ppm	ppm	%	ppm	ppm	ppm	ppm	ppm	ppm	ppm	ppm	ppm	ppm
Detection	0,1	0,1	0,1	1	0,2	0,1	0,1	0,5	0,01	0,1	0,05	2	0,1	1	0,1	1	0,1	0,5	0,1
Analysis M	INAA	INAA	MULT INA	TD-MS	TD-MS	MULT INA	TD-MS	INAA	TD-ICP	MULT INA	TD-MS	TD-ICP	MULT INA	INAA	TD-MS	TD-MS	TD-MS	INAA	TD-MS
2/3-14 - P	< 0.1	10,3	0,3	< 1	906	< 0.1	< 0.1	< 0.5	0,25	8,4	0,33	49	0,8	< 1	16,8	49	26,2	24,2	51,4
2/4-14 - Pa	0,2	14,2	0,6	< 1	599	< 0.1	< 0.1	< 0.5	0,25	12,1	0,52	55	1,1	< 1	22,5	71	34,3	32,4	67,8
2/5-14 - Ce	0,2	19,1	0,5	3	432	1	< 0.1	1,6	0,69	12,4	0,64	124	1,4	< 1	25,6	157	22,1	33,7	47,6
2/6-14 - Ce	0,3	16,5	0,4	< 1	482	< 0.1	< 0.1	< 0.5	0,38	12,6	0,61	87	1,6	< 1	30,7	127	34,1	31,4	66,3

Analyte Sy	Ce	Pr	Nd	Nd	Sm	Sm	Eu	Gd	Tb	Dy	Ho	Er	Tm	Yb	Yb	Lu	Lu	Mass	Ce
Unit Symb	ppm	ppm	ppm	ppm	ppm	ppm	ppm	ppm	ppm	ppm	ppm	ppm	ppm	ppm	ppm	ppm	ppm	g	ppm
Detection	3	0,1	0,1	5	0,1	0,1	0,05	0,1	0,1	0,1	0,1	0,1	0,1	0,1	0,2	0,1	0,05		0,1
Analysis M	INAA	TD-MS	TD-MS	INAA	TD-MS	INAA	TD-MS	TD-MS	TD-MS	TD-MS	TD-MS	TD-MS	TD-MS	TD-MS	INAA	TD-MS	INAA	INAA	TD-MS
2/3-14 - P	50	6,1	22	17	4,2	3,3	0,81	3,5	0,5	2,8	0,6	1,5	0,2	1,3	1,3	0,2	0,32	1,17	51,4
2/4-14 - Pa	62	8	28,6	56	5,3	4,3	1,08	4,7	0,6	3,8	0,8	2,1	0,3	1,9	2	0,3	0,27	1,58	67,8
2/5-14 - Ce	68	6,2	23,7	48	5,2	5,5	1,23	4,9	0,7	4,8	0,9	2,6	0,4	2,3	2,5	0,4	0,61	1,59	47,6
2/6-14 - Ce	61	8,4	31	36	6,3	5	1,41	5,7	0,8	5,2	1	2,9	0,4	2,5	2,7	0,4	0,71	1,43	66,3

Appendix 3 – Selected element correlations for the Kilwa Group

(Close up view on the next two pages)

	Cu	Pb	Ni	Zn	Ba	Be	Co	Cr	Cs	Hf	Hf	Ga	Ge	Mn	Nb	Rb	Sc	Se	Th
Cu	100																		
Pb	0,56	100																	
Ni	0,55	0,22	100																
Zn	0,43	0,35	0,62	100															
Ba	-0,47	0,09	-0,59	-0,33	100														
Be	0,64	0,50	0,03	0,03	-0,15	100													
Co	0,51	0,26	0,70	0,34	-0,58	0,07	100												
Cr	0,17	0,07	0,27	0,18	-0,07	0,13	0,15	100											
Cs	0,34	0,39	0,38	0,47	-0,02	0,39	0,12	0,38	100										
Hf	0,12	0,02	-0,31	-0,12	0,31	0,07	-0,09	-0,16	-0,40	100									
Hf	-0,30	-0,09	-0,44	-0,42	0,58	-0,23	-0,22	-0,22	-0,42	0,62	100								
Ga	0,67	0,59	0,19	0,36	0,03	0,66	0,11	0,29	0,67	0,18	-0,22	100							
Ge	0,08	-0,03	-0,11	0,19	0,01	0,29	-0,11	0,20	0,15	0,15	-0,13	0,21	100						
Mn	-0,22	-0,24	-0,14	-0,33	-0,25	0,18	-0,15	0,00	-0,30	-0,39	-0,24	-0,35	-0,10	100					
Nb	0,39	-0,04	-0,04	-0,03	-0,42	0,45	0,05	-0,11	-0,20	0,11	-0,28	0,10	0,44	0,20	100				
Rb	0,27	0,50	0,09	0,13	0,36	0,46	0,08	0,21	0,67	0,04	0,15	0,62	-0,04	-0,32	-0,22	100			
Sc	0,65	0,25	0,34	0,38	-0,34	0,53	0,26	0,21	0,44	0,21	-0,25	0,77	0,15	-0,15	0,15	0,23	100		
Se	-0,04	0,05	-0,15	0,22	0,02	0,00	-0,28	0,23	0,13	-0,18	-0,34	-0,05	0,50	-0,15	0,23	-0,15	-0,29	100	
Th	0,17	0,35	0,00	0,18	0,25	0,33	-0,10	0,08	0,62	-0,24	-0,10	0,52	0,27	-0,14	-0,01	0,64	0,18	0,07	100
Tl	0,30	0,46	0,46	0,61	-0,01	0,10	0,16	0,17	0,74	-0,29	-0,40	0,58	0,20	-0,43	-0,13	0,42	0,38	0,12	0,60
U	0,24	0,25	-0,16	0,25	-0,03	0,37	-0,15	-0,13	0,00	0,26	-0,15	0,33	0,21	0,00	0,40	0,13	0,17	0,07	0,09
V	0,61	0,33	0,02	0,20	-0,22	0,66	-0,03	-0,18	0,16	0,29	-0,26	0,60	0,35	-0,09	0,75	0,18	0,52	0,13	0,27
Y	0,30	0,15	-0,15	-0,22	-0,13	0,52	-0,02	-0,03	-0,36	0,27	0,14	0,08	-0,09	0,57	0,35	0,03	0,10	-0,27	-0,20
Zr	0,09	0,00	-0,30	-0,13	0,30	0,09	-0,08	-0,04	-0,40	0,98	0,61	0,15	0,21	-0,33	0,11	0,02	0,19	-0,13	-0,28
La	0,29	0,43	-0,12	-0,03	0,21	0,58	-0,01	0,08	0,22	0,17	0,13	0,48	-0,03	0,21	0,05	0,67	0,19	-0,29	0,39
Ce	0,23	0,37	-0,19	-0,12	0,21	0,53	-0,06	0,02	0,07	0,15	0,19	0,34	-0,05	0,34	0,09	0,54	0,09	-0,30	0,32
Pr	0,32	0,39	-0,20	-0,08	0,22	0,56	-0,09	-0,01	0,05	0,28	0,24	0,43	0,01	0,21	0,15	0,53	0,17	-0,27	0,31
Nd	0,28	0,32	-0,26	-0,14	0,22	0,51	-0,14	-0,07	-0,07	0,33	0,31	0,35	-0,03	0,25	0,17	0,43	0,14	-0,30	0,23
Sm	0,27	0,25	-0,29	-0,20	0,15	0,47	-0,16	-0,09	-0,23	0,37	0,35	0,24	-0,02	0,33	0,22	0,25	0,11	-0,28	0,08
Eu	0,27	0,20	-0,29	-0,25	0,08	0,43	-0,14	-0,13	-0,36	0,46	0,38	0,17	-0,08	0,32	0,28	0,12	0,10	-0,28	-0,11
Gd	0,27	0,23	-0,28	-0,23	0,08	0,48	-0,17	-0,08	-0,31	0,39	0,32	0,19	-0,05	0,40	0,28	0,15	0,11	-0,26	-0,03
Dy	0,36	0,21	-0,19	-0,19	-0,08	0,51	-0,06	-0,05	-0,37	0,39	0,22	0,16	-0,03	0,41	0,39	0,04	0,13	-0,20	-0,16
Tb	0,24	0,17	-0,27	-0,29	0,09	0,45	-0,15	-0,09	-0,40	0,38	0,34	0,11	-0,06	0,44	0,28	0,06	0,05	-0,26	-0,09
Ho	0,29	0,15	-0,26	-0,26	-0,07	0,49	-0,08	-0,03	-0,44	0,39	0,21	0,11	0,00	0,47	0,44	-0,04	0,10	-0,19	-0,22
Er	0,40	0,25	-0,16	-0,19	-0,10	0,56	-0,02	-0,03	-0,37	0,37	0,16	0,16	-0,05	0,42	0,39	0,04	0,13	-0,19	-0,16
Tm	0,44	0,27	-0,01	0,00	-0,14	0,61	-0,01	0,15	-0,18	0,29	0,03	0,23	0,10	0,39	0,39	0,09	0,17	-0,02	-0,06
Yb	0,42	0,23	-0,17	-0,23	-0,11	0,62	0,00	0,03	-0,30	0,38	0,17	0,21	-0,01	0,39	0,44	0,13	0,17	-0,19	-0,13
Lu	0,50	0,15	-0,03	-0,23	-0,25	0,55	0,02	0,15	-0,27	0,17	-0,07	0,18	0,01	0,44	0,50	0,00	0,16	-0,03	-0,07

	Tl	U	V	Y	Zr	La	Ce	Pr	Nd	Sm	Eu	Gd	Dy	Tb	Ho	Er	Tm	Yb	Lu
Tl	100																		
U	0,13	100																	
V	0,21	0,53	100																
Y	-0,51	0,36	0,29	100															
Zr	-0,33	0,27	0,24	0,32	100														
La	-0,03	0,36	0,27	0,85	0,15	100													
Ce	-0,14	0,32	0,22	0,74	0,15	0,97	100												
Pr	-0,10	0,40	0,32	0,75	0,28	0,95	0,97	100											
Nd	-0,19	0,37	0,30	0,80	0,32	0,89	0,94	0,99	100										
Sm	-0,31	0,37	0,28	0,87	0,38	0,77	0,87	0,92	0,97	100									
Eu	-0,42	0,37	0,30	0,91	0,47	0,68	0,78	0,85	0,91	0,97	100								
Gd	-0,39	0,38	0,31	0,93	0,40	0,72	0,82	0,87	0,92	0,98	0,99	100							
Dy	-0,45	0,42	0,37	0,97	0,42	0,63	0,73	0,78	0,84	0,92	0,96	0,97	100						
Tb	-0,46	0,32	0,27	0,93	0,40	0,63	0,74	0,80	0,86	0,94	0,96	0,97	0,96	100					
Ho	-0,51	0,37	0,36	0,96	0,43	0,58	0,68	0,73	0,79	0,88	0,94	0,95	0,98	0,95	100				
Er	-0,46	0,41	0,37	0,97	0,40	0,62	0,70	0,74	0,79	0,87	0,92	0,93	0,99	0,94	0,97	100			
Tm	-0,35	0,38	0,42	0,88	0,35	0,56	0,61	0,65	0,67	0,74	0,77	0,80	0,88	0,83	0,85	0,90	100		
Yb	-0,47	0,36	0,42	0,96	0,41	0,66	0,73	0,77	0,81	0,86	0,91	0,92	0,97	0,92	0,96	0,98	0,89	100	
Lu	-0,38	0,21	0,41	0,85	0,19	0,50	0,58	0,60	0,64	0,70	0,75	0,78	0,85	0,79	0,84	0,88	0,82	0,90	100

	Cu	Pb	Ni	Zn	Ba	Be	Co	Cr	Cs	Hf	Hf	Ga	Ge	Mn	Nb	Rb	Sc	Se	Th
Cu	1,00																		
Pb	0,56	1,00																	
Ni	0,55	0,22	1,00																
Zn	0,43	0,35	0,62	1,00															
Ba	-0,47	0,09	-0,59	-0,33	1,00														
Be	0,64	0,50	0,03	0,03	-0,15	1,00													
Co	0,51	0,26	0,70	0,34	-0,58	0,07	1,00												
Cr	0,17	0,07	0,27	0,18	-0,07	0,13	0,15	1,00											
Cs	0,34	0,39	0,38	0,47	-0,02	0,39	0,12	0,38	1,00										
Hf	0,12	0,02	-0,31	-0,12	0,31	0,07	-0,09	-0,16	-0,40	1,00									
Hf	-0,30	-0,09	-0,44	-0,42	0,58	-0,23	-0,22	-0,22	-0,42	0,62	1,00								
Ga	0,67	0,59	0,19	0,36	0,03	0,66	0,11	0,29	0,67	0,18	-0,22	1,00							
Ge	0,08	-0,03	-0,11	0,19	0,01	0,29	-0,11	0,20	0,15	0,15	-0,13	0,21	1,00						
Mn	-0,22	-0,24	-0,14	-0,33	-0,25	0,18	-0,15	0,00	-0,30	-0,39	-0,24	-0,35	-0,10	1,00					
Nb	0,39	-0,04	-0,04	-0,03	-0,42	0,45	0,05	-0,11	-0,20	0,11	-0,28	0,10	0,44	0,20	1,00				
Rb	0,27	0,50	0,09	0,13	0,36	0,46	0,08	0,21	0,67	0,04	0,15	0,62	-0,04	-0,32	-0,22	1,00			
Sc	0,65	0,25	0,34	0,38	-0,34	0,53	0,26	0,21	0,44	0,21	-0,25	0,77	0,16	-0,16	0,16	0,23	1,00		
Se	-0,04	0,05	-0,15	0,22	0,02	0,00	-0,28	0,23	0,13	-0,18	-0,34	-0,05	0,50	-0,16	0,23	-0,16	-0,29	1,00	
Th	0,17	0,35	0,00	0,18	0,25	0,33	-0,10	0,08	0,62	-0,24	-0,10	0,52	0,27	-0,14	-0,01	0,64	0,18	0,07	1,00
Tl	0,30	0,46	0,46	0,61	-0,01	0,10	0,16	0,17	0,74	-0,29	-0,40	0,58	0,20	-0,43	-0,13	0,42	0,38	0,12	0,60
U	0,24	0,25	-0,16	0,25	-0,03	0,37	-0,15	-0,13	0,00	0,26	-0,15	0,33	0,21	0,00	0,40	0,13	0,17	0,07	0,09
V	0,61	0,33	0,02	0,20	-0,22	0,66	-0,03	-0,18	0,16	0,29	-0,26	0,60	0,35	-0,09	0,75	0,18	0,52	0,13	0,27
Y	0,30	0,16	-0,15	-0,22	-0,13	0,52	-0,02	-0,03	-0,36	0,27	0,14	0,08	-0,09	0,57	0,35	0,03	0,10	-0,27	-0,20
Zr	0,09	0,00	-0,30	-0,13	0,30	0,09	-0,08	-0,04	-0,40	0,98	0,61	0,15	0,21	-0,33	0,11	0,02	0,19	-0,13	-0,28
La	0,29	0,43	-0,12	-0,03	0,21	0,58	-0,01	0,08	0,22	0,17	0,13	0,48	-0,03	0,21	0,05	0,67	0,19	-0,29	0,39
Ce	0,23	0,37	-0,19	-0,12	0,21	0,53	-0,06	0,02	0,07	0,15	0,19	0,34	-0,05	0,34	0,09	0,54	0,09	-0,30	0,32
Pr	0,32	0,39	-0,20	-0,08	0,22	0,56	-0,09	-0,01	0,05	0,28	0,24	0,43	0,01	0,21	0,15	0,53	0,17	-0,27	0,31
Nd	0,28	0,32	-0,26	-0,14	0,22	0,51	-0,14	-0,07	-0,07	0,33	0,31	0,35	-0,03	0,25	0,17	0,43	0,14	-0,30	0,23
Sm	0,27	0,25	-0,29	-0,20	0,15	0,47	-0,16	-0,09	-0,23	0,37	0,35	0,24	-0,02	0,33	0,22	0,25	0,11	-0,28	0,08
Eu	0,27	0,20	-0,29	-0,25	0,08	0,43	-0,14	-0,13	-0,36	0,46	0,38	0,17	-0,08	0,32	0,28	0,12	0,10	-0,28	-0,11
Gd	0,27	0,23	-0,28	-0,23	0,08	0,48	-0,17	-0,08	-0,31	0,39	0,32	0,19	-0,05	0,40	0,28	0,15	0,11	-0,26	-0,03
Dy	0,36	0,21	-0,19	-0,19	-0,08	0,51	-0,06	-0,05	-0,37	0,39	0,22	0,16	-0,03	0,41	0,39	0,04	0,13	-0,20	-0,16
Tb	0,24	0,17	-0,27	-0,29	0,09	0,45	-0,15	-0,09	-0,40	0,38	0,34	0,11	-0,06	0,44	0,28	0,06	0,05	-0,26	-0,09
Ho	0,29	0,15	-0,26	-0,26	-0,07	0,49	-0,08	-0,03	-0,44	0,39	0,21	0,11	0,00	0,47	0,44	-0,04	0,10	-0,19	-0,22
Er	0,40	0,25	-0,16	-0,19	-0,10	0,56	-0,02	-0,03	-0,37	0,37	0,16	0,16	-0,05	0,42	0,39	0,04	0,13	-0,19	-0,18
Tm	0,44	0,27	-0,01	0,00	-0,14	0,61	-0,01	0,15	-0,18	0,29	0,03	0,23	0,10	0,39	0,39	0,09	0,17	-0,02	-0,06
Yb	0,42	0,23	-0,17	-0,23	-0,11	0,62	0,00	0,03	-0,30	0,38	0,17	0,21	-0,01	0,39	0,44	0,13	0,17	-0,19	-0,13
Lu	0,50	0,16	-0,03	-0,23	-0,25	0,55	0,02	0,15	-0,27	0,17	-0,07	0,18	0,01	0,44	0,50	0,00	0,16	-0,03	-0,07

	Tl	U	V	Y	Zr	La	Ce	Pr	Nd	Sm	Eu	Gd	Dy	Tb	Ho	Er	Tm	Yb	Lu
Cu																			
Pb																			
Ni																			
Zn																			
Ba																			
Be																			
Co																			
Cr																			
Cs																			
Hf																			
Hf																			
Ga																			
Ge																			
Mn																			
Nb																			
Rb																			
Sc																			
Se																			
Th																			
Tl	1,00																		
U	0,13	1,00																	
V	0,21	0,53	1,00																
Y	-0,51	0,36	0,29	1,00															
Zr	-0,33	0,27	0,24	0,32	1,00														
La	-0,03	0,36	0,27	0,65	0,18	1,00													
Ce	-0,14	0,32	0,22	0,74	0,16	0,97	1,00												
Pr	-0,10	0,40	0,32	0,75	0,28	0,95	0,97	1,00											
Nd	-0,19	0,37	0,30	0,80	0,32	0,89	0,94	0,99	1,00										
Sm	-0,31	0,37	0,28	0,87	0,38	0,77	0,87	0,92	0,97	1,00									
Eu	-0,42	0,37	0,30	0,91	0,47	0,68	0,78	0,85	0,91	0,97	1,00								
Gd	-0,39	0,38	0,31	0,93	0,40	0,72	0,82	0,87	0,92	0,98	0,99	1,00							
Dy	-0,45	0,42	0,37	0,97	0,42	0,63	0,73	0,78	0,84	0,92	0,96	0,97	1,00						
Tb	-0,46	0,32	0,27	0,93	0,40	0,63	0,74	0,80	0,86	0,94	0,96	0,97	0,96	1,00					
Ho	-0,51	0,37	0,36	0,96	0,43	0,58	0,68	0,73	0,79	0,88	0,94	0,95	0,98	0,95	1,00				
Er	-0,46	0,41	0,37	0,97	0,40	0,62	0,70	0,74	0,79	0,87	0,92	0,93	0,99	0,94	0,97	1,00			
Tm	-0,35	0,38	0,42	0,88	0,35	0,56	0,61	0,65	0,67	0,74	0,77	0,80	0,88	0,83	0,85	0,90	1,00		
Yb	-0,47	0,36	0,42	0,96	0,41	0,66	0,73	0,77	0,81	0,86	0,91	0,92	0,97	0,92	0,96	0,98	0,89	1,00	
Lu	-0,38	0,21	0,41	0,85	0,19	0,50	0,58	0,60	0,64	0,70	0,75	0,78	0,85	0,79	0,84	0,88	0,82	0,90	1,00

Appendix 4 – Quantitative results from XRD-bulk (Siroquant)

TDP 1 – Pande Formation

Sample name	Mixed layer	Illite/Mica	Kaolinite	Chlorite	Quartz	K-Feldspar	Plagioclase	Calcite	Dolomite	Aragonite	Siderite	Pyrite	Gypsum	Chi Squared	R-Factor
c1_1,45	0	15,3	1,7	0	18,6	6,2	3,7	21,1	0,6	8	23,9	0,9	0	2,67	0,080
c1_8,30	18,3	5,4	1,2	0,9	44,2	18,1	6,1	0	0	5,8	0	0	0	3,96	0,114
c1_11,60	27,8	7,5	1,8	1	29	16,4	9	1,9	0	4,4	0	1	0	4,26	0,119
c1_14,50	0	3,8	0	0	61,1	21,8	9,2	3,9	0	0	0	0,1	0	4,43	0,123
c1_14,74	13,3	2,7	1,4	0,3	45,4	12,8	10,4	8,7	0	4,3	0	0,3	0	3,76	0,107
c1_19,75	12,3	2,5	1,2	0,5	27,1	14,3	5,5	29,3	0	4	0	1,4	1,9	3,05	0,091
c1_20,21	0	1,4	0	0	13,1	4,5	3,2	71,1	0	4,1	1,3	1,2	0	3,53	0,121
c1_25,65	17	3,2	1,7	0,8	44,4	21,2	9	0	0	2,6	0	0	0	4,00	0,114
c1_27.03	21,4	19,2	2,5	1	19,2	13,7	6,7	7,7	0	4,5	0	2,7	1,1	3,11	0,093
c1_34,25	7,2	5	1,2	0	41,2	16,2	5,9	13,3	0	7,7	0	0,7	1,5	3,45	0,103
c1_40,85	0	0	0,5	0	12,8	3,8	2,8	76,7	0	2,7	0	0,6	0	3,45	0,118
c1_44,70	13,5	1,4	0,9	0,8	38,9	16,6	6,7	12	0	7	0	0,9	1,3	3,41	0,102
c1_62,54	18,2	7,7	2,8	0,6	33,6	25	9,3	0,7	0	2,1	0	0	0	4,68	0,133
Average	11,46	5,78	1,30	0,45	32,97	14,66	6,73	18,95	0,05	4,40	1,94	0,75	0,45		

TDP 2 – Masoko Formation

c2_3,57	17,6	25,4	3,4	1,4	7,8	7,8	10,1	12	0	12,1	0	1,3	1	3,36	0,098
c2_11,30	17,8	25,5	3,7	3,3	9,2	10,2	11,2	9,5	0	7,1	0	1,5	1,1	4,01	0,116
c2_16,43	22,3	33,1	3,8	2,7	6,2	9,1	9,5	6,1	0	5,1	0	1,4	0,7	4,21	0,114
c2_35,40	13,6	34,4	2,3	1,2	8,1	6,1	10,9	14,9	0	7,4	0	0,9	0,3	3,44	0,095
c2_50,20	14,8	32,7	2	1,1	10,4	7,7	10,1	13,1	0	5,8	0	1	1,4	3,22	0,093
c2_52,20	21,6	28,1	2,5	0,6	9,4	8,1	13,1	10,2	0	5,3	0	0,7	0,3	3,57	0,102
c2_53,45	0	0	0	0	0,8	0	0	98,4	0	0	0	0,9	0	4,92	0,175
c2_59,33	0	0	0	0	2	0	4	93,9	0	0	0	0	0	4,51	0,155
c2_64,45	0	3,8	0	0	29	10,1	15,5	36,4	0	4,5	0	0	0	4,07	0,129
c2_69_52	16,9	12,2	2,8	1,2	21,7	14,9	11,2	12,3	0	4,6	0	1	1,2	3,23	0,096
c2_76,55	21,2	9,1	4,7	2,6	16,6	14,2	12,7	13,2	0	4,3	0	1,1	0,4	3,78	0,106
c2_98,05	0	0	0	0	1,4	0	0,4	98,2	0	0	0	0	0	4,37	0,156
Average	12,15	17,03	2,10	1,18	10,22	7,35	9,06	34,85	0,00	4,68	0,00	0,82	0,53		

Quantitative results from XRD-bulk cont.

TDP 7B – Kivinje Formation

Sample name	Mixed layer	Illite/Mica	Kaolinite	Chlorite	Quartz	K-Feldspar	Plagioclase	Calcite	Dolomite	Aragonite	Siderite	Pyrite	Gypsum	Chi Squared	R-Factor
c7B_0,48	0,0	0,0	0,0	0,0	3,0	0,0	2,8	90,6	3,5	0,0	0,0	0,0	0,0	4,38	0,150
c7B_5,30	2,4	0,9	1,0	0,0	6,7	1,5	2,7	70,9	13,4	0,0	0,0	0,5	0,0	3,64	0,119
c7B_6,13	0,0	0,0	0,2	0,0	2,1	0,0	0,9	89,6	6,6	0,0	0,0	0,7	0,0	4,56	0,155
c7B_14,55	8,9	8,9	2,5	1,6	11,2	6,0	9,9	32,7	0,0	17,6	0,0	0,7	0,0	3,08	0,095
c7B_15,30	18,3	36,1	5,5	4,7	11,8	6,8	9,3	3,3	0,0	3,2	0,0	0,9	0,0	3,37	0,096
c7B_19,99	10,5	18,2	2,8	2,1	13,0	6,5	10,4	28,1	0,0	7,1	0,5	0,7	0,2	3,25	0,095
c7B_25,14	0,0	2,2	0,9	0,0	3,8	1,4	2,9	87,5	0,0	0,8	0,0	0,5	0,0	4,11	0,135
c7B_26,45	0,0	0,9	0,0	0,0	9,5	1,8	3,2	65,8	0,0	12,0	0,0	4,0	2,9	3,46	0,116
c7B_29,70	23,8	14,9	6,3	0,4	10,5	10,6	9,4	11,7	0,0	10,8	0,3	0,7	0,8	3,10	0,089
c7B_30,21	0,0	3,8	0,9	0,0	2,7	1,4	2,4	84,8	0,0	3,4	0,0	0,5	0,0	3,63	0,122
c7B_37,60	13,2	35,5	5,6	2,6	9,9	8,9	12,0	3,1	0,0	5,8	0,0	1,2	2,2	4,80	0,127
c7B_43,60	25,3	18,6	7,9	4,1	14,9	11,6	13,4	0,4	0,0	3,1	0,0	0,5	4,1	4,76	0,130
c7B_54,14	0,0	1,7	0,9	0,0	2,0	10,7	2,7	80,0	0,0	0,3	0,0	0,6	0,0	3,95	0,130
c7B_56,45	19,4	3,2	2,4	0,0	21,8	6,9	8,7	29,1	0,0	5,5	0,0	1,1	1,9	2,85	0,085
c7B_68,53	23,5	35,6	4,7	2,8	7,8	8,8	9,9	1,2	0,0	4,1	0,0	0,9	0,8	4,28	0,114
c7B_80,10	20,3	8,5	3,0	0,0	6,4	2,6	5,6	47,1	0,0	3,5	0,0	1,4	1,7	3,07	0,093
c7B_113,50	22,5	20,1	4,1	2,9	15,9	11,7	14,3	1,7	0,0	4,4	0,0	0,9	1,5	4,69	0,127
c7B_124,03	3,3	4,4	1,1	0,0	18,4	5,0	7,7	54,0	0,0	2,4	0,0	2,6	1,1	3,25	0,102
c7B_152,50	7,6	4,4	1,7	0,0	11,1	4,8	6,4	58,2	0,0	2,9	0,0	1,5	1,4	3,13	0,099
Average	10,47	11,47	2,71	1,12	9,61	5,63	7,08	44,20	1,24	4,57	0,04	1,05	0,98		

TDP 9 – Nagurukuru Formation

c9_40-42	20,2	11,7	2,9	4,4	15,3	7,8	9,7	25	0	2,2	0	0	1	3,23	0,097
c9_90-92	7	6,3	5,2	4,5	21,2	10	14,2	29,4	0	1,2	0	0,7	0,4	3,56	0,108
c9_34-35	17,5	19,6	5,5	1,3	12,6	5,3	7,8	28,4	0	0,7	0	0,7	0,8	3,18	0,096
c9_23-24	15,8	17,9	4,3	2,3	13	7,6	9,7	27,7	0	0,9	0	0,8	0	3,36	0,102
c9_31-32	20	14,3	4,9	3,8	19,9	10,8	13,6	11,1	0	0,6	0	0,7	0,3	3,31	0,102
c9_68-69	19,2	18,8	4,1	1,2	10,3	5,8	8,6	30,3	0	0,3	0	0,6	0,8	3,35	0,094
c9_14-16	0	3	0	0	28,5	8,3	20,5	35,4	0	4,1	0	0,2	0	4,34	0,134
c9_25-27	19,1	26	2,1	2,8	12,3	9,4	12	14,1	0	1,6	0	0,5	0	3,60	0,108
Average	14,85	14,70	3,63	2,54	16,64	8,13	12,01	25,18	0,00	1,45	0,00	0,53	0,41		

Appendix 5 – Quantitative Kilwa Group clay-sized fraction (wt.%) from NEWMOD

Sample	Smectite (S)	Illite (I)	Kaolinite (K)	Chlorite (C)	Fe-rich S-V	Fe-poor I-S	S-rich I-S	Fe-rich S-K	I-rich I-C
c9_25-27cm	0,99	3,86	15,49	6,62	1,93	33,85	4,85	6,78	25,63
c9_68-69cm	0,71	4,96	18,64	7,44	1,06	32,96	6,24	4,96	23,03
c9_23-24cm	1,94	4,53	17,02	6,80	0,97	36,31	5,70	5,70	21,04
c9_34-35cm	2,13	4,26	16,00	6,08	1,09	34,12	10,16	6,39	19,77
c9_40-42cm	2,19	6,00	16,44	6,25	1,13	32,88	8,25	6,56	20,31
Average TDP 9	1,59	4,72	16,72	6,64	1,24	34,02	7,04	6,08	21,96
c7B_3.02	12,19	4,16	11,41	2,65	4,55	31,57	8,37	4,55	20,56
c7B_15.30	8,67	2,87	15,69	2,87	3,72	29,78	9,10	4,95	22,34
c7B_29.70	14,15	2,63	19,88	2,63	4,18	24,60	11,52	6,27	14,15
c7B_37.60	15,35	2,67	23,00	1,84	5,38	23,79	8,44	6,12	13,42
c7B_43.60	7,29	2,81	32,40	2,03	3,65	21,04	9,32	7,29	14,17
c7B_68.53	8,04	4,02	18,74	2,24	4,02	29,02	11,61	7,13	15,17
c7B_92.73	5,62	3,90	15,59	2,17	3,90	28,56	11,25	9,08	19,93
Average TDP 7B	10,19	3,30	19,53	2,35	4,20	26,91	9,94	6,48	17,11
c2_3.57	4,80	1,85	12,16	2,95	1,85	28,79	12,54	5,89	29,17
c2_16.43	6,56	1,43	12,24	2,34	4,28	29,60	9,67	5,97	27,91
c2_35.40	8,83	1,64	11,77	2,61	3,28	23,84	12,10	3,91	32,03
c2_52.20	8,03	1,75	14,98	2,78	3,14	22,29	11,84	7,31	27,89
c2_76.55	13,73	1,60	25,89	2,22	4,15	20,76	10,85	6,08	14,71
Average TDP 2	8,39	1,65	15,41	2,58	3,34	25,05	11,40	5,83	26,34
c1_8.30	26,71	0,94	13,21	0,47	5,24	19,27	9,92	11,30	12,93
c1_8.50	27,45	0,82	11,56	0,41	7,71	21,44	8,67	9,88	12,05
c1_24.31	18,00	0,81	18,70	0,67	3,78	21,08	8,53	8,53	19,89
c1_49.79	14,29	0,89	15,36	1,04	3,91	23,15	9,37	10,14	21,85
c1_57.70	25,85	0,80	13,88	1,42	7,29	16,21	8,47	7,53	18,56
c1_62.54	30,16	1,11	13,60	1,96	7,80	16,85	11,68	11,35	5,51
Average TDP 1	23,74	0,90	14,38	1,00	5,96	19,67	9,44	9,79	15,13

Note: Marked with yellow indicate end-member clays, and green for the mixed-layered clays.

Appendix 6 – Default parameters used in NEWMODE simulations

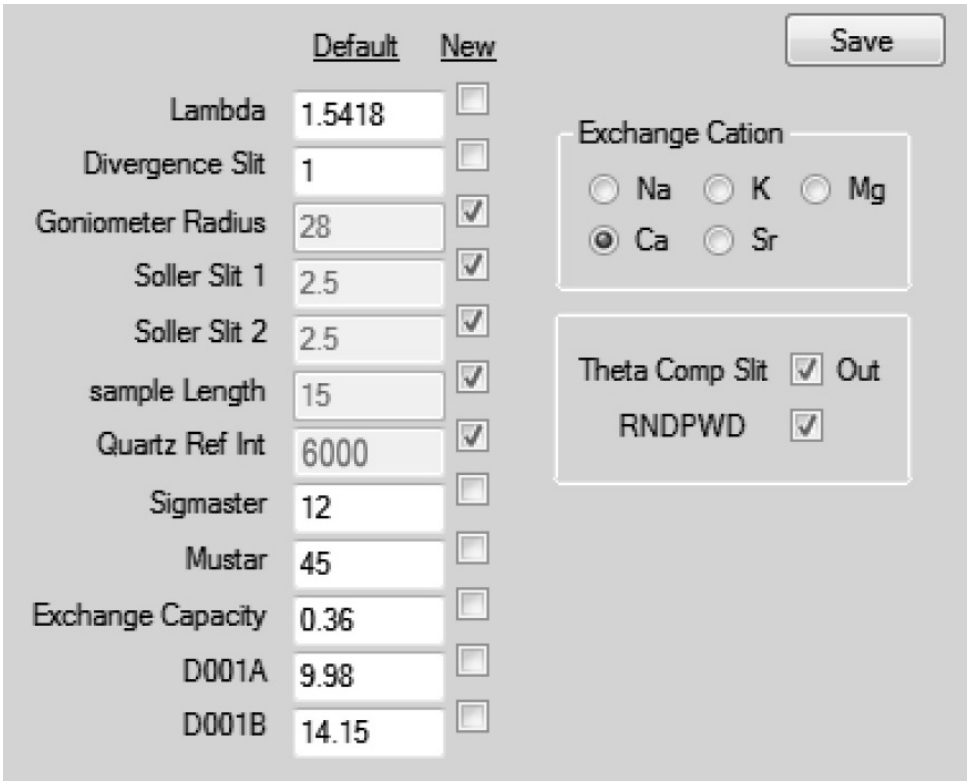

Appendix 7 – Rock Eval analysis

GENERAL DATA	CHEMICAL DATA								
	TOC	PYROLYSIS							
Client ID	Wt % rock	S1 mg/g	S2 mg/g	S3 mg/g	T max deg C	HI	OI	PI	S2/S3
TDP 1/20/1	0,66	0,50	0,43	1,91	381	65	289	0,54	0,23
TDP 1/3/2	0,08	0,31	0,13	0,48	296	163	600	0,70	0,27
TDP 7B/48/3	0,25	0,45	0,24	0,54	290	96	216	0,65	0,44
TDP 7B/44/1	0,45	0,22	0,18	1,36	411	40	302	0,55	0,13
TDP 7B/41/2	0,50	0,48	0,40	0,71	334	80	142	0,55	0,56
TDP 21/14/2	0,77	0,22	0,28	0,68	301	36	88	0,44	0,41
TDP 21/13/2	0,88					0	0	#####	#DIV/0!
TDP 21/15/2	0,46	0,14	0,36	0,37	425	78	80	0,28	0,97

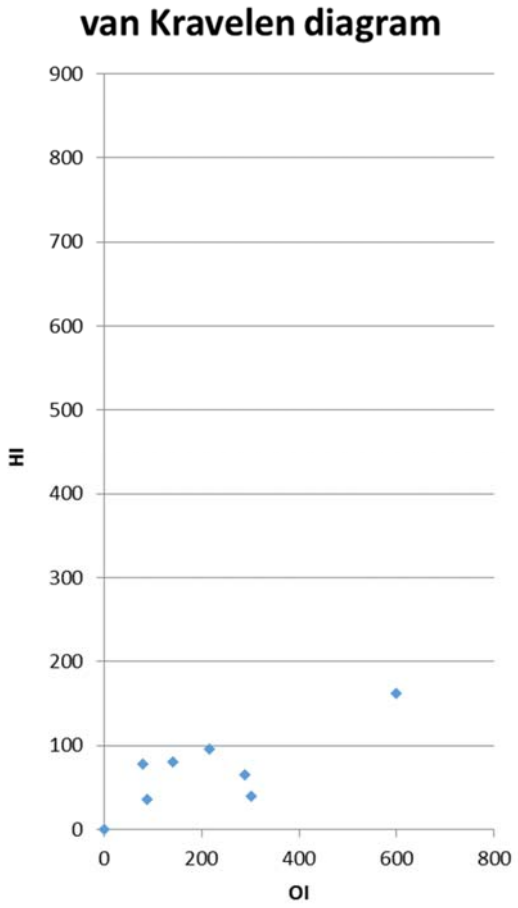

Appendix 8 – Example of clay-fraction XRD analysis

TDP 9

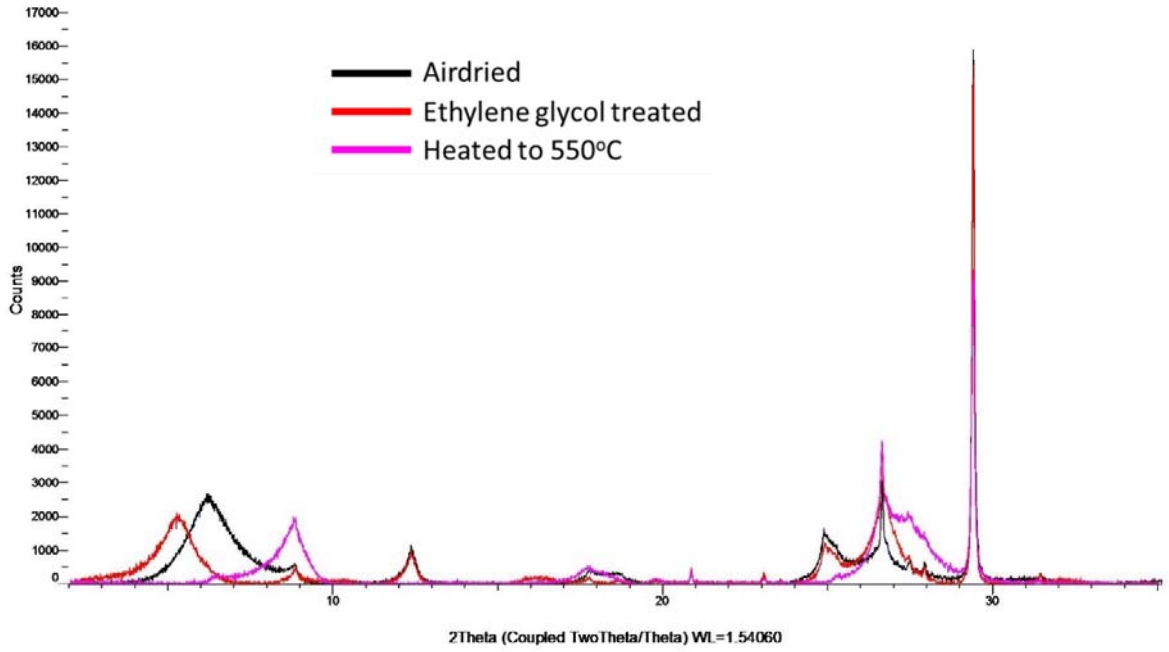

TDP 7B

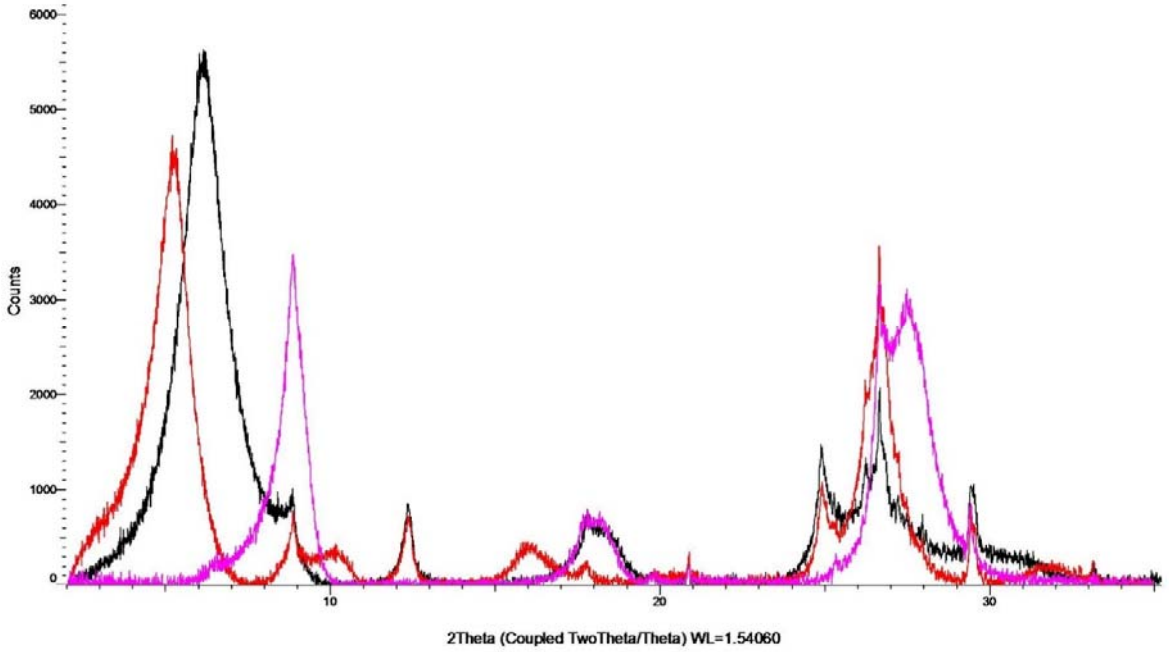

TDP 2

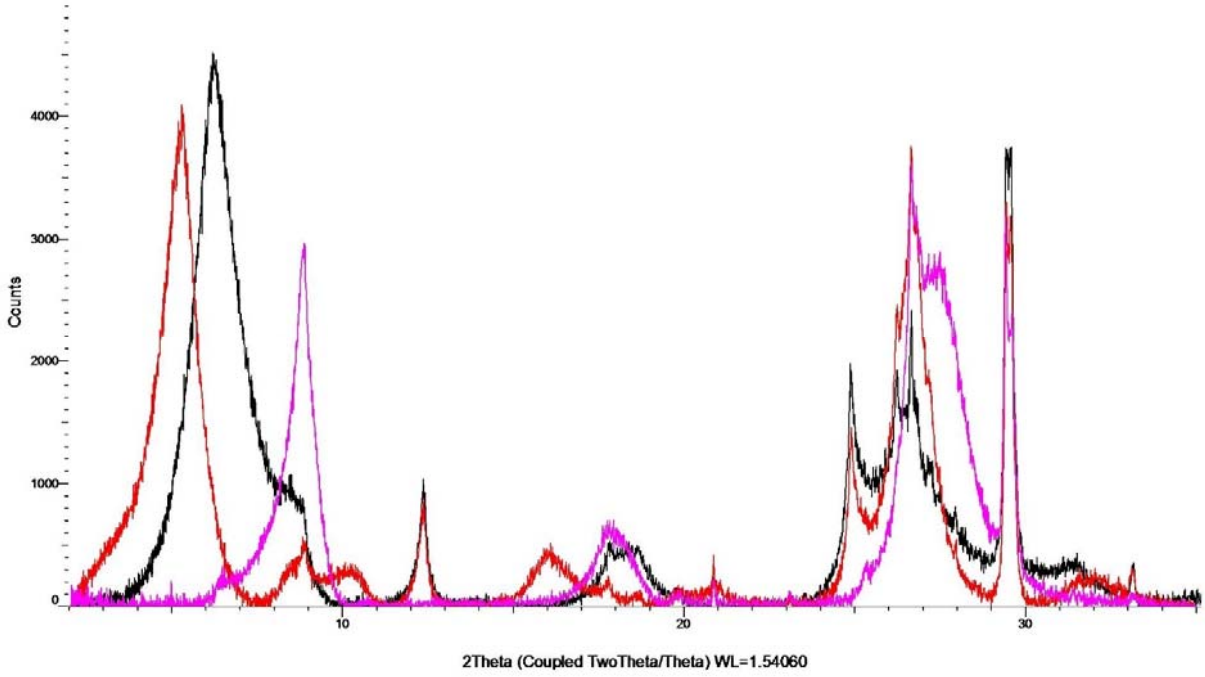
Counts
4000
3000
2000
1000
0
10
20
30
2Theta (Coupled TwoTheta/Theta) WL=1.54060

TDP 1

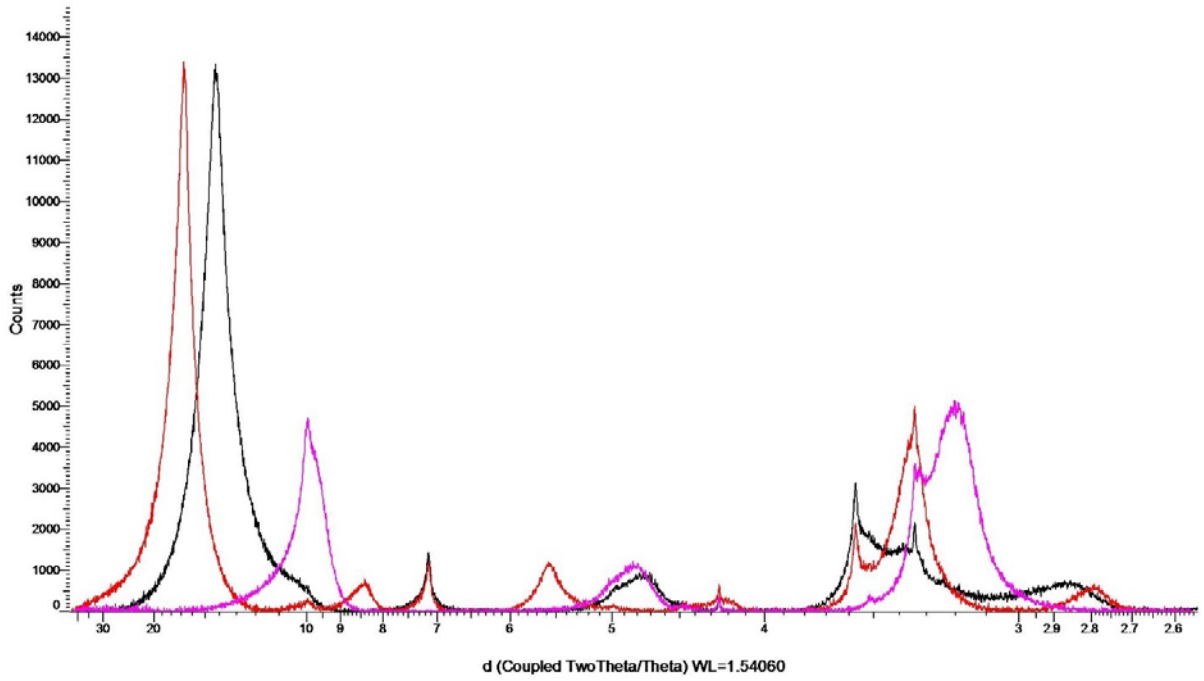
Counts
14000
13000
12000
11000
10000
9000
8000
7000
6000
5000
4000
3000
2000
1000
0
30
20
10
9
8
7
6
5
4
3
2.9
2.8
2.7
2.6
d (Coupled TwoTheta/Theta) WL=1.54060

Appendix 9 –

Fibrous calcite observed in thin sections (TDP 7B)

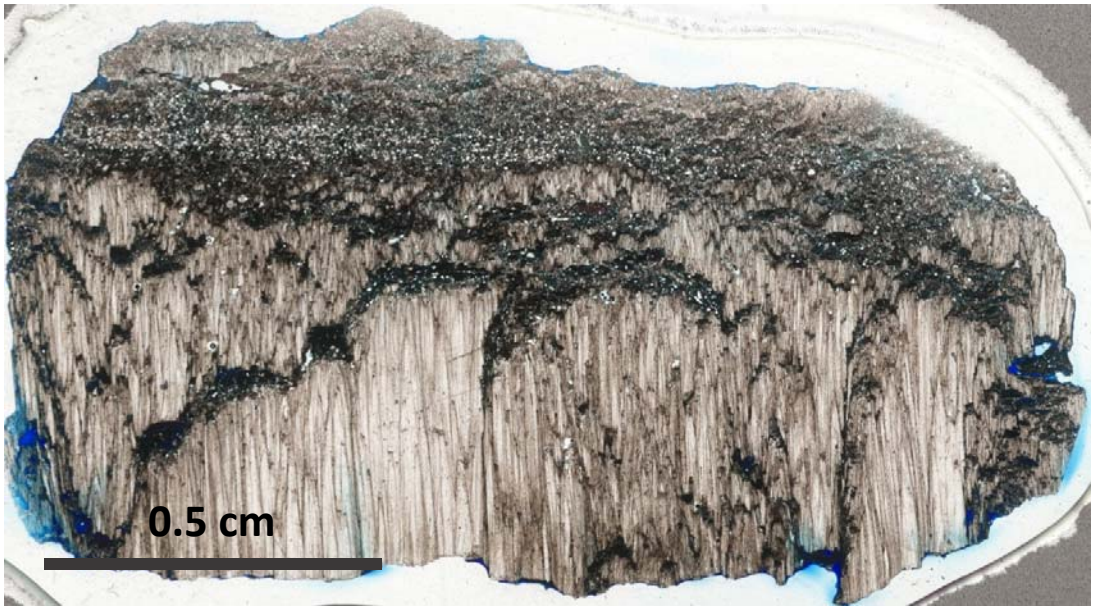

Sample c7B_54.14

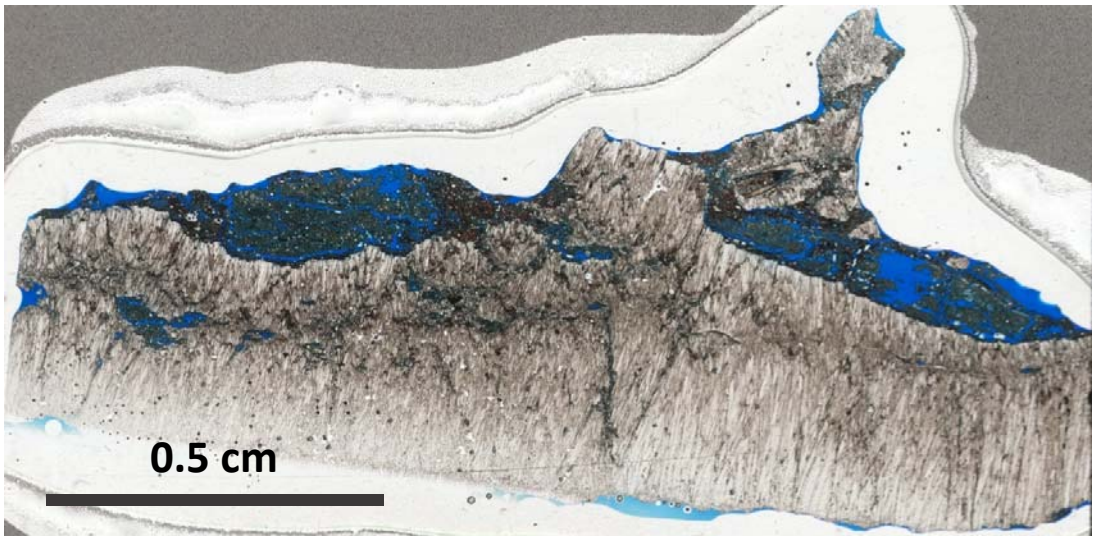

Sample c7B_25.14

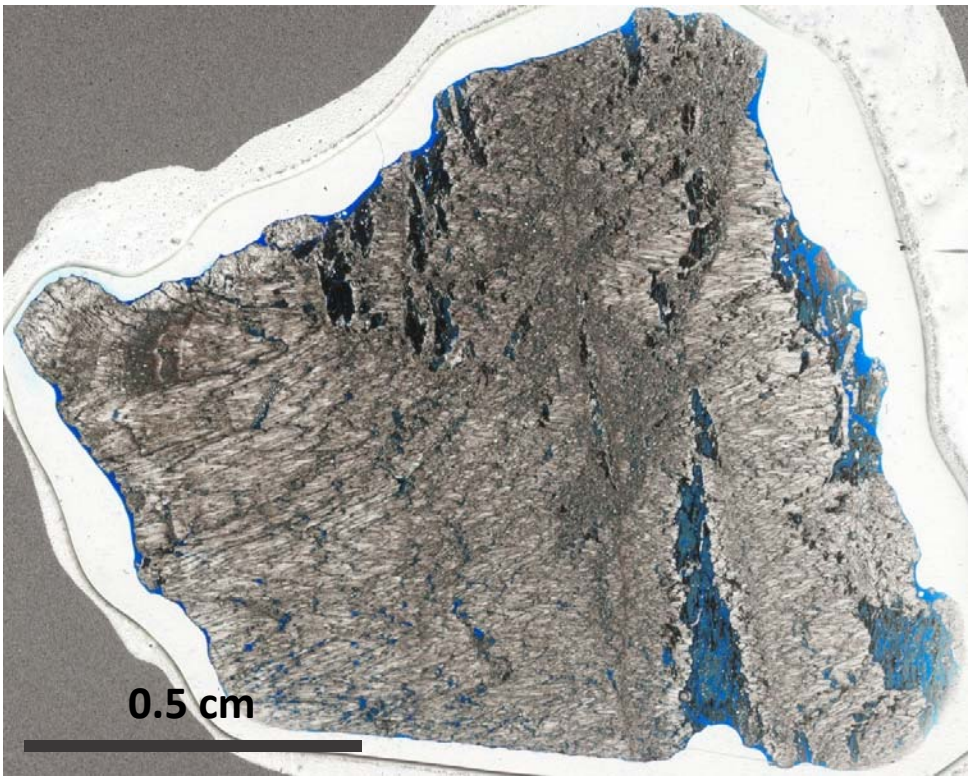

Sample c7B_80.10

Asante.